UNIVERSITÀ della CALABRIA
Facoltà di Ingegneria
Dipartimento di Meccanica

Scuola di Dottorato "Pitagora" in Scienze Ingegneristiche

Dottorato di Ricerca in Ingegneria Meccanica XXI Ciclo

SETTORE SCIENTIFICO DISCIPLINARE: ING-IND/14

Tesi di Dottorato

Development of static and dynamic techniques
for the elastic characterization
of isotropic and composite materials

Coordinatore del Dottorato
Prof. Sergio Rizzuti

Supervisore
Prof. Leonardo PAGNOTTA

Candidato
Ing. Giambattista STIGLIANO

CONTENTS

Chapter 6

INTRODUCTION

The elastic properties of solids play a fundamental role in both scientific and technological fields. Their measurement provides information regarding the forces exchanged among the atoms or ions that compose a solid, thus helping to characterise the nature of the links. It also allows us to describe the mechanical behaviour of the material which is fundamental for the structural design and experimental stress analysis. Moreover, the possibility of measuring the elastic constants of materials, fast and accurately, during the manufacturing cycle of a product could help with quality control. As a result there are many methodologies for the elastic characterization of materials. Today there is still great interest in this subject especially in the context of the development of new and more complex materials for which the classic methods of characterization appear time-consuming, expensive and, in some cases, unsuitable.

The increasing use of composite and ceramic materials in engineering has led to the development of new methodologies of characterization. Among these methodologies, the most promising are those identifying the elastic constants through a process that minimizes the difference between the dynamic or static response of the real structure (measured response) and the response of the same structure predicted by an analytical or numerical model (virtual response). These methods, known as mixed numerical-experimental techniques (MNET), update iteratively the values of the elastic constants of material in the model, until the virtual response (usually, the first natural frequencies in dynamic approaches or the field of superficial displacements or strains in static approaches) approximates as closely as possible the real response measured by means of experimental observations. The values of the constants used in the last iteration are the elastic properties of the material. The identification of all the elastic constants can take place simultaneously, with a single experiment and without damaging the specimen.

Although such methodologies have been mainly devoted to the elastic characterization of anisotropic materials, where many elastic parameters are involved, they can certainly be used for the analysis of isotropic materials where only two parameters have to be identified. Indeed, many authors proved the effectiveness of their methodologies by analysing samples of isotropic materials with conventional geometrical shapes. However, there is no reason to think that the approach is unsuitable for characterizing specimens of different shape. Such a possibility could be very useful when the production of proper bulk specimens is not feasible or when the material sample must not be damaged or processed by a conventional testing geometry and therefore should be tested as it is.

The aim of the present work is the development of identification procedures to determine the elastic properties of isotropic and composite materials. The dissertation has been split into two part: the dynamic approach and the static approach. Due to the simplicity and the potentiality of the dynamic technique, in literature there are many works based on it, but, still today no one checked the feasibility and limits of its application to characterise isotropic plates (a more simple problem with only two elastic parameters) with geometry different from the standardised shapes. More specifically, the original contributions of this thesis to the dynamic field is the development and the application of the MNET to characterise isotropic plates of irregular shapes and layered materials. In particular, the Young modulus and Poisson ratio in a FE model of the specimen are updated until the corresponding first four natural frequencies match the experimental ones as closely as possible. For this purpose, different optimization methods and error functions have been compared in order to select the best combination of them. Furthermore, a numerical approach has been proposed to see the existence of a minimum in case of plates with a particularly complex shape. In addition, the dissertation suggests instrumentation and equipment for developing a cheaper and efficient measuring system. In the present thesis, the static way for the elastic characterization has been taken into account. As well as for the dynamic technique, a MNET has been applied to identify the elastic properties of isotropic or anisotropic materials. In this case, instead of the natural frequencies, the method makes use of the full-field measurement of the surface displacements of a plate of generic form under suitable flexural loads. The main advantage of the present identification method with respect to the traditional

methodologies used for the characterization of unidirectional laminates is that all the elastic constants are determined from one static test. The original contributions of this thesis, in the static field, is the development of a correlation-based method to find the more suitable load and constrain configurations for any-shaped plates. This method is of great help in checking the feasibility of a specimen geometries for solving the elastic inverse problem by the full-field technique.

The thesis is composed of three main parts. The first part (chapters 1 and 2) gives an introduction to the elastic constant and to the standardised test methods present in literature. The second part (chapters 3 and 4) is related to the dynamic characterization; in particular the third chapter presents the theoretic aspects and the fourth ones provides the experimental validation and the practical aspects of the technique. The last part (chapter 5 and 6) is related to the static characterization: the fifth chapter provides a general overview of the proposed technique while the sixth chapter reports the experimental validation of the method.

1 LINEAR ELASTICITY

1.1   The Generalized Hooke's Law

The stress-strain relation that describes the linear elastic behaviour of a material can be expressed by matrices. The matrices take the name of compliance (**S**) or stiffness (**C**) matrices. The stiffness matrix is the inverse of the compliance matrix. The linear elastic stress-strain relation is given by the generalised Hooke's law:

$$
\begin{aligned}
&= \mathbf{C} \\
&= \mathbf{S}
\end{aligned}
\tag{1.1}
$$

in which   and   represent the engineering stress and strain vector respectively, expressed in a coordinate system parallel to the principal material axes. The stiffness matrix is used to find the stress field from the strain field, while the compliance matrix is used to find the strain field from the stress field. Since both   and   are vector with nine elements, the stiffness matrix S has to be 9×9 elements. This implies the need of 81 parameters to describe a material's elastic stress-strain relation. In general, for a three dimensional anisotropic object the independent constants of the compliance matrix (**S**) are 21, while the non-zero elements of the matrices of elasticity are 36 (Gibson, 1994); this is due to the various symmetry conditions that simplify the equations. Both stresses and strains are symmetric due to equilibrium of an infinitesimal element, so that there are only six independent stress components and six independent strain components (minor symmetry). Furthermore, due to the existence of the strain energy density, the stiffness and compliance matrices are symmetric (main symmetry). Fortunately all the materials have some form of symmetry that can reduce the independent constants that describe the linear elastic behaviour, however, no known material is completely anisotropic (Gibson, 1994). For example, a

monoclinic material has one plane of material property symmetry and so the number of independent moduli is reduced to 13. The orthotropic material has three orthogonal planes of material property symmetry, and in this case the number of independent elastic constants is reduced to 9. In this case, if the used coordinate system is not aligned with the principal material directions (the directions parallel to the intersection of the three orthogonal symmetry planes) the elastic matrices have 36 non-zero elements and the materials is called *generally orthotropic*. If the used coordinate system is aligned with the principal material directions (it is called principal or in-axis coordinate system) the elastic matrices have 12 non-zero elements and the materials is called *specially orthotropic*. In this last case the stiffness matrix becomes:

$$\mathbf{C} = \begin{bmatrix} C_{11} & C_{12} & C_{13} & 0 & 0 & 0 \\ & C_{22} & C_{23} & 0 & 0 & 0 \\ & & C_{33} & 0 & 0 & 0 \\ & & & C_{44} & 0 & 0 \\ & \text{SYM} & & & C_{55} & 0 \\ & & & & & C_{66} \end{bmatrix} \qquad (1.2)$$

There is another kind of material symmetry that is important in the study of composites. In most composite materials the fiber-packing arrangement is statistically random in nature, so that the properties are nearly the same in any direction perpendicular to the fibers and the materials is called *transversely isotropic*. In this last case the stress-strain behaviour can be described by 12 nonzero elastic moduli but only 5 are independent:

$$\mathbf{C} = \begin{bmatrix} C_{11} & C_{12} & C_{12} & 0 & 0 & 0 \\ & C_{22} & C_{23} & 0 & 0 & 0 \\ & & C_{22} & 0 & 0 & 0 \\ & & & (C_{22}-C_{23})/2 & 0 & 0 \\ & \text{SYM} & & & C_{66} & 0 \\ & & & & & C_{66} \end{bmatrix} \qquad (1.3)$$

where the 23 plane and all parallel planes are assumed to be planes of isotropy, and so that $C_{12}=C_{13}$, $C_{22}=C_{33}$ and $C_{55}=C_{66}$ and C_{44} is a function of the other constant.

If the material has an infinite number of symmetry planes, the material is said to be isotropic. In the case of an isotropic material the stress-strain behaviour can be described by 12 nonzero elastic moduli where only 2 are independent, in fact $C_{11}= C_{22}= C_{33}$, $C_{12}= C_{23}= C_{13}$, $C_{44}=C_{55}= C_{66}=(C_{11}-C_{12})/2$ and the relation becomes:

$$\mathbf{C} = \begin{bmatrix} C_{11} & C_{12} & C_{12} & 0 & 0 & 0 \\ & C_{11} & C_{12} & 0 & 0 & 0 \\ & & C_{11} & 0 & 0 & 0 \\ & & & (C_{11}-C_{12})/2 & 0 & 0 \\ & \text{SYM} & & & (C_{11}-C_{12})/2 & 0 \\ & & & & & (C_{11}-C_{12})/2 \end{bmatrix} \quad (1.4)$$

Table 1.1 reports the elastic coefficients in the stress-strain relationships for different materials and coordinate system.

Table 1.1 – Summary of the material symmetries.

Material and coordinate system	Number of nonzero coefficients	Number of independent coefficients
Three-dimensional case		
Anisotropic	36	21
Generally Orthotropic (nonprincipal coordinates)	36	9
Specially Orthotropic (principal coordinates)	12	9
Specially Orthotropic Transverely isotropic	12	5
Isotropic	12	2
Two-dimensional case		
Anisotropic	9	6
Generally Orthotropic (nonprincipal coordinates)	9	4
Specially Orthotropic (principal coordinates)	5	4
Isotropic	5	2

Until now three-dimensional cases have been considered. Often some tension component can be neglected and so a two-dimensional cases can be obtained. In this case other simplification can be carried out and the matrices of elasticity become 3x3. If the material is anisotropic, the nonzero elements in the elastic matrices are 9 while the independent moduli are 6. If the material is

orthotropic and the off-axis coordinate system is considered, the nonzero elements are 9, while the independent moduli are 4. If an in-axis coordinate system is considered the nonzero elements become 5. For isotropic materials there are still 5 non zero elastic constants, but only 2 are independent

1.2   Engineering Constants

1.2.1   Isotropic Materials

In practice, elastic material properties are usually characterised with a set of engineering constants like generalised Young's moduli, shear moduli and Poisson's ratios instead of the coefficients (C_{ij} or S_{ij}) of the elasticity matrices. The engineering constants are also widely used in analysis and design because they are easily defined and interpreted in terms of simple states of stress and strain (Timoshenko, Gere, 1997).

The assumption of the elasticity leads to the existence of a strain energy (U). For isotropic materials no preferential directions exist and so the stress-strain relation is independent of the coordinate system adopted for stress and strain description; in the elastic case this leads to the dependence of the strain energy (U) on the invariants (Corradi Dell'Acqua, 1992):

$$U(\varepsilon_{ij}) = \int_0^{\varepsilon_{ij}} \sigma_{ij} d\varepsilon_{ij} = U(I_1, I_2, I_3) \tag{1.5}$$

with:

$$\begin{aligned}
I_1 &= \varepsilon_I + \varepsilon_{II} + \varepsilon_{III} \\
I_2 &= \varepsilon_I \varepsilon_{II} + \varepsilon_{II} \varepsilon_{III} + \varepsilon_{III} \varepsilon_I \\
I_3 &= \varepsilon_I \varepsilon_{II} \varepsilon_{III} = det(\ )
\end{aligned} \tag{1.6}$$

where I_1, I_2 and I_3 are the linear, quadratic and cubic invariants, while ε_I, ε_{II}, ε_{III} are the principal strains. In the linear case U has quadratic form, so that cubic invariant does not exist in the energy expression:

$$U = aI_1^2 + bI_2 \tag{1.7}$$

where a and b are the constitutive parameters. Only two parameters are needed to describe the elastic linear stress-strain relation. The previous equation often is written using the Lamè constant (λ and G):

$$a = (\lambda + 2G)$$
$$b = -2G$$
(1.8)

Using Eq. (1.8) and Eq. (1.7) the expression of the strain energy became:

$$U = \frac{1}{2}(\lambda + 2G)I_1^2 - 2GI_2$$
(1.9)

From the definition of the strain energy it is possible to obtain the following expression:

$$\sigma_{ij} = \frac{\partial U}{\partial \varepsilon_{ij}}$$
(1.10)

and so, using Eq. (1.9) and Eq. (1.10) it's possible to write:

$$\sigma_{ij} = (\lambda + 2G)I_1 \frac{\partial I_1}{\partial \varepsilon_{ij}} - 2G \frac{\partial I_2}{\partial \varepsilon_{ij}}$$
(1.11)

Unfortunately the Lamè's constants are not easily defined and interpreted in terms of simple states of stress and strain. As highlighted, usually, the elastic coefficients are expressed as a function of the so-called "engineering constants", which are more easily defined and interpreted in terms of simple states of stress and strain:

$$E = G\frac{3\lambda + 2G}{\lambda + G}$$
$$v = \frac{\lambda}{2(\lambda + G)}$$
(1.12)

where E is the Young modulus (or modulus of elasticity), v is the Poisson ratio and G is the shear modulus (or modulus of rigidity). Young's modulus involves the longitudinal elongation of a material when it is subjected to a tension or compression test and it is defined as the ratio between the normal stress and the normal strain. The shear modulus implies the angular distortion undergone by the material when subjected to pure shear and it is defined as the ratio between the shear stress and the shear strain. Finally, Poisson's ratio describes the lateral (or radial) contraction or expansion of the material when it is subjected to a longitudinal normal stress and is defined by the ratio between the strain in the lateral or radial direction and the strain in the longitudinal or axial direction.

Inverting the Eq. (1.12) it's possible to obtain:

$$\lambda = E \frac{\nu}{(1+\nu)(1-2\nu)} \tag{1.13}$$

$$G = \frac{E}{2(1+\nu)} \tag{1.14}$$

Often the stress-strain relationship is written in terms of the three moduli E, ν and G but, it should be noted that, only two elastic constants are independent.

1.2.2 Orthotropic Materials

An orthotropic material can be characterised in three orthogonal directions by twelve engineering constants. Considering a stress state where $_{ii}$ is the only non-zero stress component, the Young's modulus in the i-direction is defined as:

$$E_i = \frac{\sigma_{ii}}{\varepsilon_{ii}}, \qquad i = 1,2,3 \tag{1.15}$$

while the Poisson's ratio for transverse strain in the j-direction when the material is stressed in the i-direction is defined as:

$$\nu_{ij} = -\frac{\varepsilon_{jj}}{\varepsilon_{ii}}, \quad i,j = 1,2,3, \;\; i \neq j \tag{1.16}$$

Note that, as with isotropic materials, a negative sign mast be used in the definition of Poisson's ratio.

The shear modulus in the ij-plane is defined as:

$$G_{ij} = \frac{\tau_{ij}}{\gamma_{ij}}, \qquad ij = 12,32,31 \tag{1.17}$$

considering a stress state where τ_{ij} is the only non-zero stress component.

Since the engineering constants are defined for uni-axial stress conditions, it is much easier to express them in terms of compliance than in terms of stiffness. The combination of the definitions in Eqs. (1.15-1.17) with the strain-stress relations of an orthotropic material leads to the following compliance matrix:

$$\mathbf{S} = \begin{bmatrix} \dfrac{1}{E_1} & -\dfrac{21}{E_2} & -\dfrac{31}{E_3} & 0 & 0 & 0 \\[2mm] -\dfrac{12}{E_1} & \dfrac{1}{E_2} & -\dfrac{32}{E_3} & 0 & 0 & 0 \\[2mm] -\dfrac{13}{E_1} & -\dfrac{23}{E_2} & \dfrac{1}{E_3} & 0 & 0 & 0 \\[2mm] 0 & 0 & 0 & \dfrac{1}{G_{23}} & 0 & 0 \\[2mm] 0 & 0 & 0 & 0 & \dfrac{1}{G_{31}} & 0 \\[2mm] 0 & 0 & 0 & 0 & 0 & \dfrac{1}{G_{12}} \end{bmatrix}$$

(1.18)

The matrix shows 12 elastic constant. Due to the symmetry properties, only 9 moduli are independent, in fact it is possible to write:

$$\frac{v_{ij}}{E_i} = \frac{v_{ji}}{E_j}$$

(1.19)

which means that there are only three independent Poisson's ratios.

1.3   Constraints on the Engineering Constants

The elastic material parameters cannot take any value, they are restricted by a number of physical limits (Jones, 1999). The considered restrictions are the so-called thermodynamic constraints which are based on the principle that the total work done by all the stress components must be positive in order to avoid the creation of energy. The work done by a stress component is given by the product of the stress component with the corresponding strain component. The work of the stress components will only be positive, if the stiffness and compliance matrices are positive-defined.

1.3.1   Isotropic Materials

To have a positive work from the product of the tension and the longitudinal elongation, *i.e.* the Young modulus defined positive, the following inequality is necessary:

$$v > -1$$

(1.20)

In the same way, if an isotropic material is subject to hydrostatic pressure (p), the volumetric deformation is:

$$\theta = \varepsilon_x + \varepsilon_y + \varepsilon_z = \frac{p}{E/3(1-2\nu)} = \frac{p}{B} \qquad (1.21)$$

Where B is the Bulk modulus. To define B>0 the following relation are necessary:

$$E > 0 \qquad (1.22)$$

$$\nu < \frac{1}{2} \qquad (1.23)$$

1.3.2   Orthotropic Materials

The restrictions on the orthotropic material parameters can be established using the same thermodynamic considerations as in the previous section: the total work done by all the stress components must be positive in order to avoid the creation of energy. It is possible to demonstrate (Jones, 1999) that this restriction, in the plane case, can be expressed by the following inequality:

$$E_1 > 0, \, E_2 > 0, \; G_{12} > 0$$
$$1 - \nu_{12}\nu_{21} > 0 \qquad (1.24)$$

Using Eq. (1.19) it is possible to obtain:

$$|\nu_{12}| < \sqrt{\frac{E_1}{E_2}} \; \; or \; \; |\nu_{21}| < \sqrt{\frac{E_2}{E_1}} \qquad (1.25)$$

1.4   Elastic Properties for an Arbitrary Orientation

For plate-like structures, the stress analysis is usually carried out under the Kirchhoff assumptions. For a structure parallel to the 12-plane, the Kirchhoff assumptions result in plane stress state ($_3 = 0$, $_{23} = 0$, $_{31} = 0$). Accepting the Kirchhoff assumptions, the general strain-stress relation for specially orthotropic materials reduces to the following in-plane strain-stress relation:

$$\left\{\begin{array}{c}\varepsilon_1 \\ \varepsilon_2 \\ \gamma_{12}\end{array}\right\} = \left[\begin{array}{ccc}S_{11} & S_{12} & 0 \\ S_{21} & S_{22} & 0 \\ 0 & 0 & S_{66}\end{array}\right]\left\{\begin{array}{c}\sigma_1 \\ \sigma_2 \\ \tau_{12}\end{array}\right\} \tag{1.26}$$

where the compliance coefficients S_{ij} and the engineering constants are related to each other by the following equations:

$$S_{11} = \frac{1}{E_1}, \quad S_{22} = \frac{1}{E_2},$$

$$S_{12} = S_{21} = -\frac{v_{12}}{E_1} = -\frac{v_{21}}{E_2}, \quad S_{66} = \frac{1}{G_{12}} \tag{1.27}$$

The lamina stresses in terms of tensor strains are given by:

$$\left\{\begin{array}{c}\sigma_1 \\ \sigma_2 \\ \tau_{12}\end{array}\right\} = \left[\begin{array}{ccc}Q_{11} & Q_{12} & 0 \\ Q_{21} & Q_{22} & 0 \\ 0 & 0 & Q_{66}\end{array}\right]\left\{\begin{array}{c}\varepsilon_1 \\ \varepsilon_2 \\ \gamma_{12}\end{array}\right\} \tag{1.28}$$

where the stiffness coefficients Q_{ij} are referred to the plane stress-reduced stiffness because they are obtained from C_{ij}. They are related to the engineering constants in the following manner:

$$Q_{11} = \frac{S_{22}}{S_{11}S_{22} - S_{12}^2} = \frac{E_1}{1 - v_{12}v_{21}}$$

$$Q_{12} = -\frac{S_{12}}{S_{11}S_{22} - S_{12}^2} = \frac{v_{12}E_2}{1 - v_{12}v_{21}} = C_{21}$$

$$Q_{22} = \frac{S_{11}}{S_{11}S_{22} - S_{12}^2} = \frac{E_2}{1 - v_{12}v_{21}}$$

$$Q_{66} = \frac{1}{S_{66}} = G_{12} \tag{1.29}$$

The properties described in Eq. (1.26) are defined in the directions of the principal material axes. These on-axis properties describe the behaviour of the material when subjected to a stress field that is aligned with the principal material axes (1-2), but this behaviour can vary with the orientation of the considered load. As with isotropic materials, a normal stress induces only normal strains, and all shear strains are equal to zero. This lack of shear/normal interaction is observed only for the principal material coordinate system. For any other set of coordinates the so-called "shear-coupling" effect is present. The off-axis properties describe the material behaviour when subjected to a stress field with an

12

arbitrary orientation (x-y). Consider a load with an arbitrary orientation and a global axis system x-y which is aligned with the principal directions of this load. In this local axis system, the stress-strain relation can be expressed as:

$$\{\overline{\sigma}\} = [\overline{C}]\{\overline{\varepsilon}\} \tag{1.30}$$

$$\begin{Bmatrix} \sigma_x \\ \sigma_y \\ \tau_{xy} \end{Bmatrix} = \begin{bmatrix} \overline{Q}_{11} & \overline{Q}_{12} & \overline{Q}_{16} \\ \overline{Q}_{12} & \overline{Q}_{22} & \overline{Q}_{26} \\ \overline{Q}_{16} & \overline{Q}_{26} & \overline{Q}_{66} \end{bmatrix} \begin{Bmatrix} \varepsilon_x \\ \varepsilon_y \\ \gamma_{xy} \end{Bmatrix} \tag{1.31}$$

where the overbars indicate that the quantities are expressed in local coordinates (off-axis properties). The transformed stiffness matrix $[\overline{C}]$ contains the off-axis properties. The off-axis properties can be obtained starting from the on-axis properties in the following way:

$$[\overline{Q}] = [T]^{-1}[Q][T] \tag{1.32}$$

where [T] is the transformation matrix defined as (Tsai and Hahn, 1980):

$$\mathbf{T} = \begin{bmatrix} \cos^2\theta & \sin^2\theta & 2\cos\theta\sin\theta \\ \sin^2\theta & \cos^2\theta & -2\cos\theta\sin\theta \\ -\cos\theta\sin\theta & \cos\theta\sin\theta & \cos^2\theta - \sin^2\theta \end{bmatrix} \tag{1.33}$$

where θ is the angle between the x- and 1-axis, as shown in Figure 1.1.
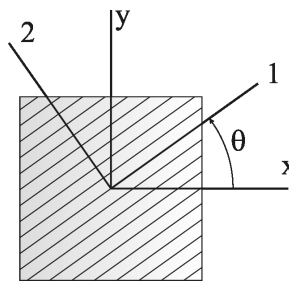

Figure 1.1 - Definition of the orientation angle .

Note that, for an arbitrary value of the orientation angle , the transformed compliance matrix has nine non-zero elements. However, the elastic behaviour is still fully characterized by only four independent material constants.

It is possible to obtain the same relation for the compliance when a global axis system x-y is considered:

$$\{\bar{\varepsilon}\} = [\bar{S}]\{\bar{\sigma}\} \tag{1.34}$$

$$\begin{Bmatrix} \varepsilon_x \\ \varepsilon_y \\ \gamma_{xy} \end{Bmatrix} = \begin{bmatrix} \bar{S}_{11} & \bar{S}_{12} & \bar{S}_{16} \\ \bar{S}_{12} & \bar{S}_{22} & \bar{S}_{26} \\ \bar{S}_{16} & \bar{S}_{26} & \bar{S}_{66} \end{bmatrix} \begin{Bmatrix} \sigma_x \\ \sigma_y \\ \tau_{xy} \end{Bmatrix} \tag{1.35}$$

where the $\bar{S}_{ij}$ are the components of the transformed lamina compliance matrix which are defined as follows:

$$\bar{S}_{11} = S_{11}\cos^4 + S_{22}\sin^4 + (2S_{12} + S_{66})\sin^2 \cos^2$$

$$\bar{S}_{12} = \frac{1}{8}[S_{11} + 6S_{12} + S_{22} - S_{66} - (S_{11} - 2S_{12} + S_{22} - S_{66})\cos4]$$

$$\bar{S}_{22} = S_{11}\sin^4 + S_{22}\cos^4 + (2S_{12} + S_{66})\sin^2 \cos^2$$

$$\bar{S}_{16} = \frac{1}{2}[S_{11} - S_{22} + (S_{11} - 2S_{12} + S_{22} - S_{66})\cos2]\sin2 \tag{1.36}$$

$$\bar{S}_{26} = \frac{1}{2}[S_{11} - S_{22} - (S_{11} - 2S_{12} + S_{22} - S_{66})\cos2]\sin2$$

$$\bar{S}_{66} = \frac{1}{2}[S_{11} - 2S_{12} + S_{22} + S_{66} - (S_{11} - 2S_{12} + S_{22} - S_{66})\cos4]$$

The lamina engineering constants can also be transformed from the principal material axes to the off-axes coordinates. For example, the modulus of elasticity associated whit uniaxial loading along the x direction is defined as:

$$E_x = \frac{\sigma_x}{\varepsilon_x} = \frac{\sigma_x}{\sigma_x \bar{S}_{11}} = \frac{1}{\bar{S}_{11}} \tag{1.37}$$

where the strain ε_x in the denominator has been found by substituting the stress condition σ_x 0, $\sigma_y = \tau_y = 0$. By replacing $\bar{S}_{11}$ and using Eq. (1.27) it is possible to write:

$$E_x = \frac{1}{\frac{1}{E_1}\cos^4\theta + \left[-\frac{2v_{12}}{E_1} + \frac{1}{G_{12}}\right]\cos^2\theta \sin^2\theta + \frac{1}{E_2}\sin^4\theta} \tag{1.38}$$

Similar transformation equations may be found for other off-axis engineering constants such as v_{xy} and G_{xy} (Gibson, 1994) replacing the $\bar{S}_{ij}$ in the following equations:

14

$$E_x = \frac{\sigma_x}{\varepsilon_x}\bigg|_{\sigma_y=\tau_{xy}=0} = \frac{1}{\overline{S}_{11}} \qquad E_y = \frac{\sigma_y}{\varepsilon_y}\bigg|_{\sigma_x=\tau_{xy}=0} = \frac{1}{\overline{S}_{22}}$$

$$\nu_{xy} = -\frac{\varepsilon_y}{\varepsilon_x}\bigg|_{\sigma_y=\tau_{xy}=0} = \frac{\overline{S}_{12}}{\overline{S}_{11}} \qquad \nu_{yx} = -\frac{\varepsilon_x}{\varepsilon_y}\bigg|_{\sigma_x=\tau_{xy}=0} = \frac{\overline{S}_{12}}{\overline{S}_{22}} \qquad (1.39)$$

$$G_{xy} = \frac{\tau_{xy}}{\gamma_{xy}}\bigg|_{\sigma_x=\sigma_y=0} = \frac{1}{\overline{S}_{66}}$$

The variation of these properties with lamina orientation for a fiber-reinforced composite (E_1=100 GPa, E_2=10 GPa, G_{12}=6 GPa and ν_{12}=0.3) is shown graphically in Figure 1.2. As intuitively expected, E_x varies from a maximum at θ= 0° to a minimum at θ = 90° for this particular material.
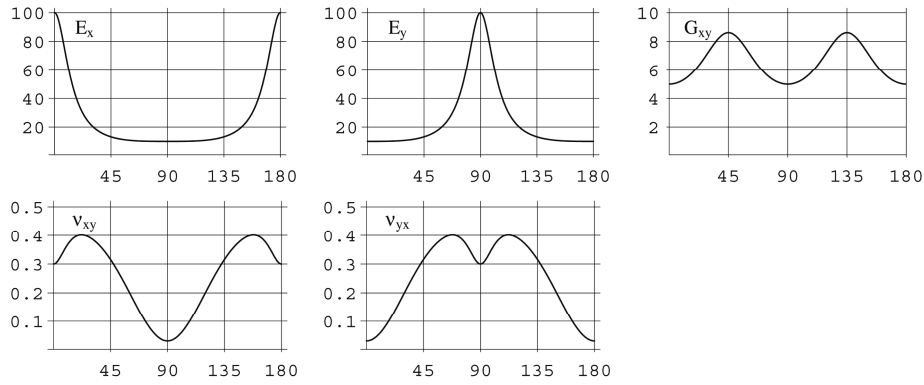
Figure 1.2 – Variation of lamina engineering constant with lamina orientation.

The shear-coupling effect has been described previously as the generation of shear strains by off-axis normal stresses and the generation of normal strains by off-axis shear stresses. To quantify the degree of shear coupling a dimensionless shear-coupling ratio may be defined (Halpin, 1984). There are two ways to define it. For example, when the state of stress is defined as $\sigma_x \neq 0$, $\sigma_y=\tau_y=0$, the ratio

$$\eta_{x,xy} = \frac{\gamma_{xy}}{\varepsilon_x} = \frac{\overline{S}_{16}}{\overline{S}_{11}} \qquad (1.40)$$

is a measure of the amount of shear strain generated in the *xy* plane per unit normal strain along the direction of the applied normal stress σ_x.

Other shear-coupling ratios can be defined for different states of stress. For example, when the stresses are $\tau_y \neq 0$, $\sigma_y= \sigma_x =0$, the ratio

$$\eta_{xy,y} = \frac{\varepsilon_y}{\gamma_{xy}} = \frac{\overline{S}_{26}}{\overline{S}_{66}} \tag{1.41}$$

characterizes the normal strain response along the y direction due to a shear stress in the *xy* plane.

In the same way, other shear-coupling ratios can be defined as:

$$\eta_{y,xy} = \frac{\gamma_{xy}}{\varepsilon_y} = \frac{\overline{S}_{26}}{\overline{S}_{22}} \tag{1.42}$$

$$\eta_{xy,x} = \frac{\varepsilon_x}{\gamma_{xy}} = \frac{\overline{S}_{16}}{\overline{S}_{66}} \tag{1.43}$$

As shown in Figure 1.3, $\eta_{x,xy}$ strongly depends on orientation and has its maximum value at some intermediate angle.
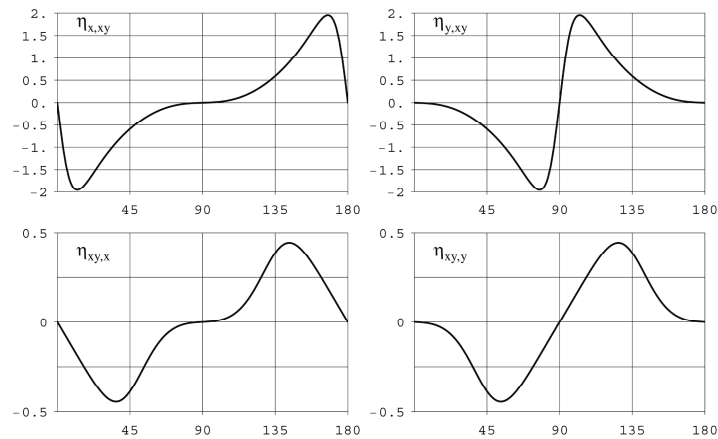
Figure 1.3 – Variation of the shear-coupling ratios.

1.5 The classical laminated plate theory

In general, the composite materials are manufactured in the form of thin sheets, called laminae or layers. These sheets present a low stiffness. In order to increase the stiffness of the component, laminae are bonded together to form a laminate. In composite manufacturing exist a number of design parameters like:

1. layer materials
2. layer orientation
3. number of layers
4. layer thickness

that give a wide number of solutions for component property design.

16

In most applications, the thickness of a laminate is small compared to the planar dimensions, so that two-dimensional theories can be used to analyse composite laminates. Two-dimensional theories are obtained from the three-dimensional elasticity theory by making assumptions concerning the variation of displacements and/or stresses through thickness of the laminate. The classical laminated plate theory (CLPT) is an extension of the classical plate theory to laminated plates. In this theory, the in-plane displacements are assumed to vary linearly through the thickness and the transverse displacement is assumed to be constant through the thickness (i.e., transverse normal strain is zero). The classical laminated plate theory is found to be adequate for most applications where the thickness of the laminate is two orders of magnitude smaller than the in-plane dimensions. When the classical laminated plate theory is not applicable, a refined theory is used. A refinement to the classical laminate theory is provided by the first-order shear deformation plate theory (FSDT) (Reddy, 1992).
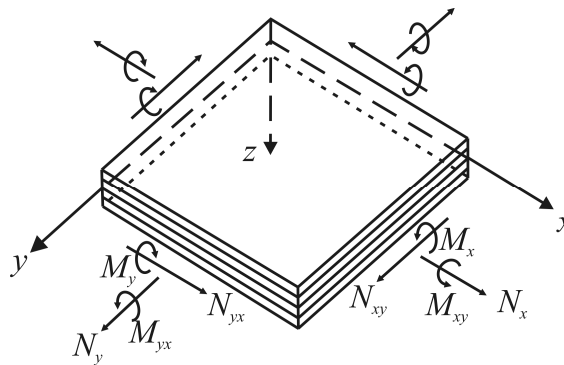
Figure 1.4 – Coordinate system and stress resultants for laminated plate

Although the laminate is made up of multiple laminae, it is assumed that the individual laminae are perfectly bonded together so as to behave as a unitary, nonhomogeneous, anisotropic plate. Interfacial slip is not allowed and the interfacial bonds are not allowed to deform in shear, which means that displacements across lamina interfaces are assumed to be continuous. These assumptions mean that the deformation hypothesis from the classical homogeneous plate theory can be used for the laminated plate. Figure 1.4 defines the coordinate system to be used in developing the laminated plate analysis. The xyz coordinate system is assumed to have its origin on the middle surface of the plate, so that the middle surface lies in the xy plane. The displacements at a point

in the x, y, z directions are u, v, and w, respectively. The basic assumptions relevant to the present static analysis are (Gibson, 1994):

1. The plate consists of orthotropic laminae bonded together, with the principal material axes of the orthotropic laminae oriented along arbitrary directions with respect to the *xy* axes;

2. The thickness of the plate, *t*, is much smaller than the lengths along the plate edges *a* and *b*;

3. The displacements *u*, *v*, and *w* are small compared with the plate thickness.

4. The in-plane strains $_x$, $_y$, and $_{xy}$ are small compared with unity;

5. Transverse shear strains $_{xz}$ and $_{yz}$ are negligible;

6. Tangential displacements u and v are linear functions of the *z* coordinate;

7. The transverse normal strain $_z$ is negligible;

8. Each ply obeys Hooke's law;

9. The plate thickness *t* is constant;

10. Transverse shear stresses $_{xz}$ and $_{yz}$ vanish on the plate surface defined by z = ±*t*/2.

Assumption 5 is a result of the assumed state of plane stress in each ply, whereas assumptions 5 and 6 together define the Kirchhoff deformation hypothesis that normals to the middle surface remain straight and normal during deformation. According to the previous assumptions, the displacements can be expressed as:

$$
\begin{aligned}
u &= u_0(x, y) - z \frac{\partial w}{\partial x} \\
v &= v_0(x, y) - z \frac{\partial w}{\partial y} \\
w &= w_0(x, y)
\end{aligned}
\tag{1.44}
$$

from which it is possible to find the strain:

$$
\begin{aligned}
{}_x &= {}_x^0 + z \, {}_x = \frac{\partial u_0}{\partial x} - z \frac{\partial^2 w}{\partial x^2} \\
{}_y &= {}_y^0 + z \, {}_y = \frac{\partial v_0}{\partial y} - z \frac{\partial^2 w}{\partial y^2} \\
{}_{xy} &= {}_{xy}^0 + z \, {}_{xy} = \frac{\partial u_0}{\partial y} + \frac{\partial v_0}{\partial x} - 2z \frac{\partial^2 w}{\partial x \partial y}
\end{aligned}
\tag{1.45}
$$

where u_0, v_0 and w_0 are the displacements of the middle surface, κ_x is a bending curvature associated with bending of middle surface in the xz plane and κ_y is a bending curvature associated with bending of middle surface in the yz plane. κ_{xy} is a twisting curvature associated with out-of-plane twisting of the middle surface which lies in the xy plane before deformation.

Using Eq. (1.45) and Eq. (1.31) it is possible to find the stress along arbitrary xy axes in the k-th lamina of a laminate:

$$\begin{Bmatrix} \sigma_x \\ \sigma_y \\ \tau_{xy} \end{Bmatrix}_k = \begin{bmatrix} \overline{Q}_{11} & \overline{Q}_{12} & \overline{Q}_{16} \\ \overline{Q}_{12} & \overline{Q}_{22} & \overline{Q}_{26} \\ \overline{Q}_{16} & \overline{Q}_{26} & \overline{Q}_{66} \end{bmatrix}_k \begin{Bmatrix} \varepsilon_x^0 + z\kappa_x \\ \varepsilon_y^0 + z\kappa_y \\ \gamma_{xy}^0 + z\kappa_{xy} \end{Bmatrix} \tag{1.46}$$

From this equation it is possible to note the shear-coupling effect due to the anisotropic behaviour of the off-axis lamina.

In the laminated plate analysis Eq. (1.46) for lamina stress is of limited practical use because the curvatures are not generally known and are difficult to measure. Thus, the midplane strains and curvatures can be related to applied forces and moments by static equilibrium equations in order to make these equations more useful. In the laminated plate analysis, however, it is convenient to use forces and moments per unit length rather than forces and moments. The forces and moments per unit length shown in Figure 1.4 are also referred to as stress resultants.

For example, the force per unit length, N_{ij}, and the moment per unit length M_{ij} are given by:

$$N_{ij} = \int_{-\frac{t}{2}}^{\frac{t}{2}} {}_{ij} dz = \sum_{k=1}^{N} \int_{z_{k-1}}^{z_k} \left({}_{ij} \right)_k dz$$

$$M_{ij} = \int_{-\frac{t}{2}}^{\frac{t}{2}} {}_{ij}\, z\, dz = \sum_{k=1}^{N} \int_{z_{k-1}}^{z_k} \left({}_{ij} \right)_k z\, dz$$

(1.47)

where N is the number of layers in the laminate, and (z_k,z_{k+1}) are the thickness coordinates of the bottom and top of the k-th layer.

Using Eq. (1.46) and Eq. (1.47) it is possible to write:

$$\begin{Bmatrix} \mathbf{N} \\ \cdots \\ \mathbf{M} \end{Bmatrix} = \begin{Bmatrix} N_x \\ N_y \\ N_{xy} \\ M_x \\ M_y \\ M_{xy} \end{Bmatrix} = \begin{bmatrix} A_{11} & A_{12} & A_{13} & B_{11} & B_{12} & B_{13} \\ A_{12} & A_{22} & A_{23} & B_{12} & B_{22} & B_{23} \\ A_{13} & A_{23} & A_{33} & B_{13} & B_{23} & B_{33} \\ B_{11} & B_{12} & B_{13} & D_{11} & D_{12} & D_{13} \\ B_{12} & B_{22} & B_{23} & D_{12} & D_{22} & D_{23} \\ B_{13} & B_{23} & B_{33} & D_{13} & D_{23} & D_{33} \end{bmatrix} \begin{Bmatrix} \varepsilon^0_x \\ \varepsilon^0_y \\ \varepsilon^0_{xy} \\ k_x \\ k_y \\ k_{xy} \end{Bmatrix} \tag{1.48}$$

where the elements of the matrix **A**, **B** and **D** are defined as:

$$\begin{aligned} A_{ij} &= \int_{-t/2}^{t/2} (\overline{Q}_{ij})_k \, dz = \sum_{k=1}^{N} (\overline{Q}_{ij})_k (z_k - z_{k-1}) \\ B_{ij} &= \int_{-t/2}^{t/2} (\overline{Q}_{ij})_k \, z \, dz = \frac{1}{2} \sum_{k=1}^{N} (\overline{Q}_{ij})_k (z_z^2 - z_{z-1}^2) \\ D_{ij} &= \int_{-t/2}^{t/2} (\overline{Q}_{ij})_k \, z^2 \, dz = \frac{1}{3} \sum_{k=1}^{N} (\overline{Q}_{ij})_k (z_z^3 - z_{z-1}^3) \end{aligned} \tag{1.49}$$

From Eq. (1.48) it is possible to note that the extensional stiffness matrix **A** relates the in-plane forces {N} to the midplane strains $\{\varepsilon^\circ\}$ and the bending stiffness matrix **D** relates the moments {M} to the curvatures {k}. The coupling stiffness matrix **B** couples the in-plane forces {N} with the curvatures {k} and the moments {M} with the midplane strains $\{\varepsilon^\circ\}$. A laminate having nonzero B_{ij} will bend or twist under in-plane loads. Such a laminate will also exhibit midplane stretching under bending and twisting moment loading. It can be easily shown that laminate geometric and material property symmetry with respect to the middle surface leads to the condition that all $B_{ij} = 0$ and that asymmetry about the middle surface leads to nonzero B_{ij}. Note that there are two types of coupling: the lamina shear coupling, that it is a result of anisotropic material behaviour, and the laminate shear coupling, that it is due to geometric and/or material property asymmetry with respect to the middle surface and is unrelated to material anisotropy.

The laminate Force-Deformation equation described by the matrices **A**, **B** and **D** can be inverted. The inverted equations are described by other three matrices **A'**, **B'** and **D'**. When the coefficient of the matrix **B'** are zero, **A'** is also used in the derivation of the effective laminate engineering constants:

$$E_x = \frac{1}{h\,A'_{11}} \qquad E_y = \frac{1}{h\,A'_{22}}$$

$$_{xy} = -\frac{A'_{12}}{A'_{11}} \qquad _{yx} = -\frac{A'_{12}}{A'_{22}}$$

$$G_{xy} = \frac{1}{h\,A'_{33}}$$

Using similar derivation, effective laminate flexural moduli may be expressed in terms of the flexural compliances (D_{ij}'):

$$E_{fx} = \frac{12}{h^3 D'_{11}} \qquad E_{fy} = \frac{12}{h^3 D'_{22}}$$

$$_{fxy} = -\frac{D'_{12}}{D'_{11}} \qquad _{fyx} = -\frac{D'_{12}}{D'_{22}} \ .$$

$$G_{fxy} = \frac{12}{h^3 D'_{33}}$$

1.6   Bibliography

Corradi Dell'Acqua, L., 1992. Meccanica delle strutture. McGraw-Hill libri, Italia

Gibson, R.F., 1994. Principles of Composite Material Mechanics. McGraw Hill, Singapore.

Halpin J.C., 1984. Primer on composite materials: analysis. Technomic Publishing Co., Lancaster.

Jones R. M., 1999. Mechanics of Composite Materials, Taylor & Francis, Philadelphia.

Reddy, J.N., OCHOA, O.O., 1992. Finite Element Analysis of Composite Laminates. Kluwer Academic Publishers, London.

Timoshenko S.P., Goodier J.N., 1970. Theory of Elasticity. McGraw Hill, New York.

Timoshenko S.P., Gere J.M., 1997. Mechanics of Materials, PWS Publishing Company, Boston.

Tsai S.W., Hahn H.T., 1980. Introduction to Composite Materials. Technomic Publishing Co., Lancaster.

2 STANDARD TEST METHODS FOR THE ELASTIC CHARACTERIZATION OF MATERIALS

2.1 Introduction

The knowledge of the elastic properties of materials is very important for both structural design and engineering applications and the possibility of measuring them, fast and accurately and during the production process, could be a valid improvement for quality control. Because of such importance, the great number of methodologies developed and presented in the scientific literature is not surprising. Still today, the argument gives rise to a wide interest among researchers, especially in the context of the development of new and more complex materials, for which the classical methods of characterization appear slow, expensive and not always suitable.

The methods for determining the elastic properties of a materials can be classified into two big categories: static methods and dynamic methods. Static methods are generally based on direct measurement of strains and stress components of a suitable specimen subject to mechanical test (tensile, compressive, flexural, torsional, etc.). Young and shear moduli are determined from the slope of the linear region of the stress–strain curve, while Poisson's ratio is determined from the ratio between transverse and longitudinal strains of a specimen loaded by a uniaxial load (Carlsson and Pipes, 1997). The elastic moduli influence the dynamic behaviour of the material (for example, its mechanical resonant frequencies or the sound velocity); so that, such properties can be used in order to characterise a suitable test specimen. Dynamic methods are generally based on this principles. In the present chapter a review of both the basic static and dynamic standard test for determining the elastic constant of materials are discussed.

2.2 Dynamic procedures

Starting from 1935, when the first dynamic characterization applications have been carried out, the dynamic technique have grown into valid tools for measuring the elastic moduli of isotropic materials. In standardised resonant methods, Young's modulus, shear modulus, and Poisson's ratio can all be computed from the resonant frequencies of prismatic bars, rods, or slabs. There are several ASTM standards that cover the determination of elastic properties of specific materials by measuring resonance frequencies by sonic resonance or by impulse excitation of vibration. All these test methods may differ from each other in several areas (e.g., sample size, dimensional tolerances, sample preparation).

The ASTM C848 ("Young's Modulus, Shear Modulus, and Poisson's Ratio For Ceramic Whitewares by Resonance") allows to obtain the elastic properties of ceramic materials using the sonic resonance. In fact, this test method measures the resonance frequencies of test bars of suitable geometry by exciting them at continuously variable frequencies. Mechanical excitation of the specimen is provided through a transducer that transforms an initial electrical signal into a mechanical vibration (see Figure 2.1). Another transducer senses the resulting mechanical vibrations of the specimen and transforms them into an electrical signal that can be displayed on the screen of an oscilloscope to detect resonance. In the end, the resonance frequencies, the dimensions, and the mass of the specimen are used to calculate Young's modulus and the shear modulus.
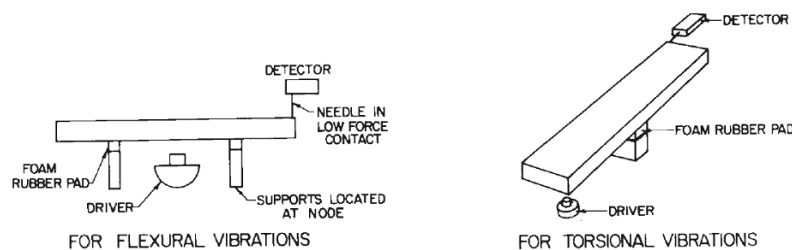
Figure 2.1 – Specimen Positioned for Measurement of Flexural and Torsional Resonance Frequencies Using "Tweeter" Exciter (extracted from the ASTM C848)

ASTM C1198 describes a test method for determining the dynamic elastic module of advanced ceramics. It is a clone of two earlier ASTM standards (C848 and C623) and, rather than using the tables and graphs (like in the previous standards), uses the original equations for relating the elastic constants to the resonance frequencies. Although recommended sizes for flat and round specimens

are given, the equations are sufficiently general, so that a wide size range can be used. The equations include the conventional polynomial correction factors to reflect the finite specimen thicknesses, but simplified equations are also provided for instances where the length-to-thickness ratio of the specimens is greater than 20. ASTM standards C1198 and C1259 form the basis for two ASTM standards: ASTM E1875 ("Standard Test Method for Dynamic Young's Modulus, Shear Modulus, and Poisson's Ratio by Sonic Resonance") and ASTM E1876 ("Standard Test Method for Dynamic Young's Modulus, Shear Modulus, and Poisson's Ratio by Impulse Excitation"). These two standards are identical versions of C1198 and C1259, which are generic and are not confined to ceramic materials, but are applicable to all elastic materials. The ASTM standard C1259 allows to derive the elastic properties of homogeneous isotropic materials measuring the resonant frequencies of beam-shaped specimen with rectangular cross-section by exciting it mechanically by a singular elastic strike with an impulse tool (instead of using the sonic resonance as in the C1198 and in the E1875). A transducer (for example, a contact accelerometer or a non-contacting microphone) senses the resulting mechanical vibrations of the specimen and transforms them into electric signals (see Figure 2.2). Specimen supports, impulse locations, and signal pick-up points are selected to induce and measure specific modes of the transient vibrations. The signals are analyzed, and the fundamental resonant frequency is measured.
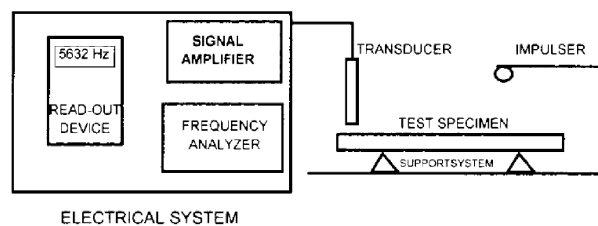
Figure 2.2 – Block Diagram of Typical Test Apparatus
(extracted from the ASTM C1259)

The appropriate fundamental resonant frequencies, dimensions, and mass of the specimen are used to calculate dynamic moduli. In particular, the elastic modulus can be derived from the fundamental out-of-plane flexural vibration mode using the following equation:

$$E = 0.9465 \frac{m f_f^2}{b} \frac{L^3}{t^3} T_1 \tag{2.1}$$

where b, L, t are the width, the length and the thickness of the beam, while f_f is the fundamental natural frequencies and m is the mass. T_1 is a correction factor defined as:

$$T_1 = 1 + 6.585(1 + 0.0752\nu + 0.8109\nu^2)\left(\frac{t}{L}\right)^2 - 0.868\left(\frac{t}{L}\right)^4$$
$$- \left[\frac{8.340(1 + 0.2023\nu + 2.173\nu^2)\left(\frac{t}{L}\right)^4}{1.00 + 6.338(1 + 0.1408\nu + 1.536\nu^2)\left(\frac{t}{L}\right)^2} \right] \tag{2.2}$$

The shear modulus can be obtained using the following equation

$$G = \frac{4mLf_t^2}{bt} \frac{B}{1+A} \tag{2.3}$$

where f_t is the torsional vibration frequency, while A and B are given as follows:

$$A = \frac{\left[0.5062 - 0.8076\left(\frac{b}{t}\right) + 0.3504\left(\frac{b}{t}\right)^2 - 0.0078\left(\frac{b}{t}\right)^3 \right]}{\left[12.03\left(\frac{b}{t}\right) + 9.892\left(\frac{b}{t}\right)^2 \right]} \tag{2.4}$$

$$B = \frac{\left[\frac{b}{t} + \frac{t}{b} \right]}{\left[4\left(\frac{t}{b}\right) - 2.52\left(\frac{t}{b}\right)^2 + 0.21\left(\frac{t}{b}\right)^3 \right]} \tag{2.5}$$

When $L/t \geq 20$ Eq. (2.2) can simplified to the following form:

$$T_1 = 1 + 6.585\left(\frac{t}{L}\right)^2 \tag{2.6}$$

Therefore from Eqs. (2.3) and (2.5) is possible to calculate both E and G. If $L/t < 20$, the elastic modulus has to be calculated with an estimation of the Poisson ratio and an iterative procedure.

In the ASTM E1876 there is an annex that covers the evaluation of the frequencies of disc geometry specimens for the determination of the dynamic elastic properties of elastic materials at ambient temperatures. With a disc-shaped

specimen, the Poisson's ratio is determined using the first two resonant frequencies. The dynamic Young's modulus and dynamic shear modulus are then calculated using the Poisson's ratio, the experimentally-determined fundamental resonant frequencies, and the specimen dimensions and mass.

The fundamental equation defining the relationship between the natural resonant frequency, the material properties, and the specimen dimensions can be found on the ASTM standards and is defined as:

$$f_i = \frac{K_i}{2\pi r}\sqrt{\frac{A}{\rho h}} \tag{2.7}$$

where f_i is the resonant frequency of interest, K_i is the geometric factor for that resonant frequency, r is the radius of the disc, ρ is the density of the disc and A is the plate constant defined as:

$$A = \frac{Eh^3}{12(1-v^2)} \tag{2.8}$$

where t is the disc thickness, E is Young's modulus and v is the Poisson's ratio for the disc material. This is a general equation which is valid for both the first and the second natural vibrations. Poisson's ratio can be determined directly from the experimental values of the first and the second natural resonant frequency by the use of suitable tables present on the ASTM E1876. The value for Poisson's ratio is interpolated from the table using the ratio of the second natural resonant frequency to the first natural resonant frequency (f_2/f_1) correlated with the ratio of the specimen thickness to the specimen radius (t/r). For the Young's modulus of a disc, two calculations of E (E_1 and E_2) are made independently from the two resonant frequency measurements, and then a final value E is determined by averaging the two calculated values:

$$E_1 = \frac{37.699 f_1^2 D^2 m(1-v^2)}{K_1^2 t^3}$$

$$E_2 = \frac{37.699 f_2^2 D^2 m(1-v^2)}{K_2^2 t^3} \tag{2.9}$$

$$E = \frac{E_1 + E_2}{2}$$

Unfortunately all these dynamic standards cannot be applied to the orthotropic materials and an extension seems not easy to carry out. This is due

mainly to the difficulty of finding a fundamental equation that describes the dynamic behaviour of these materials.

2.3   Static procedures

Considering the stress state imposed to the specimen, the static methods can be classified in the following groups:

- Tension Test Methods
- Compressive Test Methods
- Flexure Test Methods
- Shear Test Methods

In theory, to characterise an isotropic material only the stress-strain state in a point of the sample is necessary; the simplest way to develop this is to test the sample in tension with a known load and measuring the strain by one or more strain-gages. The physics of composites testing may appear to be similar to the physics of testing isotropic materials, but the differences are significant. Determination of the mechanical behaviour is influenced by several factors that include metallurgical/material variables, test methods, and the nature of the applied stresses. The properties of a test sample made of composite materials are often significantly different in different directions; consequently, special testing methods may be required (ASM Vol. 21). For example, uniaxial mechanical tests never produce a pure uniaxial stress state throughout an entire test specimen; three dimensional stresses always exist at discontinuities and loading points. Many isotropic materials are created as bulk material and later formed into the end product. However, most composites are consolidated into the final material form at the same time that the end product is produced. This can introduce additional process variations into the basic material.

The tension test is one of the most commonly used tests for evaluating materials. In its simplest form, the tension test is carried out by gripping opposite ends of a sample within the load frame of a test machine. A tensile force is applied by the machine, resulting in the gradual elongation and eventual fracture of the sample. During this process the force-extension data are monitored and recorded. When properly conducted, the tension test provides force extension data that can quantify several important mechanical properties of a material like the

elastic deformation properties (such as the modulus of elasticity and Poisson's ratio), the yield strength, the ultimate tensile strength and the ductility properties (such as elongation). The ASTM E111 describes the method for the determination of Young's modulus, tangent modulus, and chord modulus of isotropic materials by tension test. The tangent modulus is the slope of the stress-strain curve at a specified value of stress or strain while the chord modulus is the slope of the chord drawn between any two specified points on the stress-strain curve, below the elastic limit of the material. These two moduli are used for materials that follow nonlinear elastic stress-strain behaviour. Furthermore the standards give the recommendation on the preparation of specimens, the temperature control, the speed of testing, the alignment of the sample into the test machine etc. In ASTM E132 the value of Poisson's ratio is obtained from the longitudinal and the transverse strains resulting from uniaxial stress only at room temperature. This test method is limited to specimens of rectangular section and to materials in which creep is negligible compared to the strain produced immediately upon loading.

The general concept of tensile properties is very similar for metallic and non-metallic materials, but there are also some differences in their behaviour and so in the required test procedures. Ceramics materials are brittle materials that are extremely sensitive to bending strains, besides the hard surface of ceramics reduces the effectiveness of frictional gripping devices; so that tension testing of ceramics requires more attention to alignment and gripping of the sample in the test machine. The procedure to apply tension testing to monolithic ceramics at room temperature is described in ASTM standard C1273 ("Test Method for Tensile Strength of Monolithic Advanced Ceramics at Ambient Temperatures"), while the standard method for continuous fiber-reinforced advanced ceramics at ambient temperatures is described in C1275 ("Test Method for Monotonic Tensile Behaviour of Continuous Fiber-Reinforced Advanced Ceramics with Solid Rectangular Cross-Section Test Specimens at Ambient Temperature"). Plastic materials are viscoelastic materials that exhibit time-dependent deformation during force application and so the tension depend more strongly on the strain rate and on the temperature. Thus, control of temperature and strain rates are more critical than for metals. The ASTM standard D638 ("Test Method for Tensile Properties of Plastics") describes the tension test for unreinforced and reinforced

plastic materials and includes the option of determining Poisson's ratio at room temperature; for tensile properties of resin-matrix composites reinforced with oriented continuous or discontinuous high modulus (more than 20GPa) fibers, tests shall be made in accordance with Test Method D3039/D3039M ("Standard Test Method for Tensile Properties of Polymer Matrix Composite Materials"). The standard reports all the recommendations for the specimen design tolerances, control of test machine-induced misalignment and bending, measurement of thickness, selection of transducers and calibration of instrumentation, description of failure modes and the definition of elastic property calculation. The Test Method ISO 527 is substantially based on ASTM D3039, but this last standard offers better control of testing details that may cause variability and, for this reason, is the preferred method. By changing the sample configuration, the tensile test methods are able to evaluate different material configurations, including unidirectional laminates, woven materials, and general laminates. However, some sample-material configuration combinations are less sensitive to specimen preparation and testing variations than others. Perhaps the most dramatic example is the unidirectional specimen. Fiber versus load axis misalignment in a 0° unidirectional specimen, which can occur due to either specimen preparation or testing problems or both, can reduce strength as much as 30% due to an initial 1° misalignment (ASM Vol. 21). Furthermore, bonded end tabs can actually cause premature failure of the sample (even in nonunidirectional case) if not applied and used properly. The characterization of composite is not easy due to the mentioned problem and similar issues.
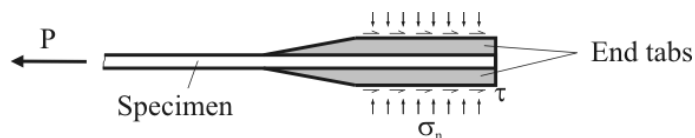
Figure 2.3 – End tabs used in tension test

In each of the previous test methods, a tensile stress is applied to the specimen through a mechanical shear interface at the ends of the specimen, normally by either wedge or hydraulic grips. If used, the end tabs are intended to distribute the load from the grips to the specimen with a minimum of stress concentration. Tabs should be made from [±45°] or [0/90°] glass/epoxy or woven fabric composites and they are bonded on each side of the specimen. The load is

transferred into the specimen test section through shear (see Figure 2.3). The material response is measured in the gage section of the coupon by either strain gages or extensometers, subsequently determining the elastic material properties. In Figure 2.4 a typical specimen is reported, while in Table 2.1 the recommended specimen dimensions are reported.

Figure 2.4 Tension test specimen

Table 2.1 –Tensile specimen geometry recommendations (ASTM D3039)

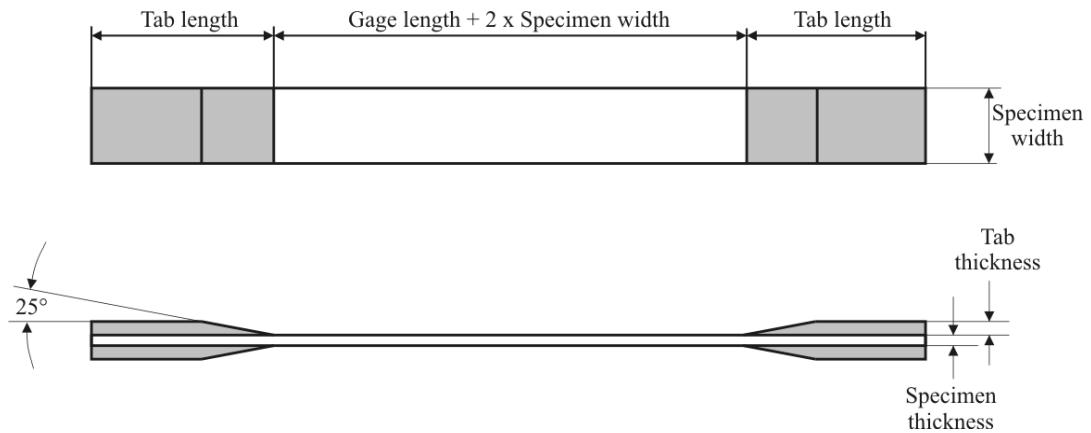| Fiber Orientation	Width	Overall Length	Thickness	Tab Length	Tab Thickness
	[mm]	[mm]	[mm]	[mm]	[mm]
0° unidirectional	15	250	1.0	56	1.5
90° unidirectional	25	175	2.5	25	1.5
balanced and symmetric	25	250	2.5	emery cloth	—
random-discontinuous	25	250	2.5	emery cloth	—

To characterize the tensile response of unidirectional lamina, 0° and 90° specimens are employed to determine longitudinal and transverse properties. The [±45°] laminate tension test measures shear properties of the lamina. If Poisson's ratio is desired, a 0/90° strain gage rosette should be bonded in the center-gage-section region of the specimen. The properties obtained from tension tests on composite materials are effective (average) properties. The test method applies to unidirectional composites but can also be performed on laminates, woven fabrics, or discontinuous fiber composites. For asymmetric and/or unbalanced laminates, extension/bending coupling and extension/shear coupling effects produce nonuniform stress states in the test section. Obviously, under these conditions, effective properties cannot be accurately determined from the tensile test.

The compression test is conducted on composite materials, using appropriate instrumentation, to determine compressive modulus, Poisson's ratio, ultimate compressive strength or strain-at-failure. These properties are determined through the use of test fixturing that is typically designed to be as simple to use and fabricate as possible, to minimize stress concentrations, to minimize specimen volume, and to introduce a uniform state of uniaxial stress in the specimen test section. Several compression test methods emerged during the past twenty years, and much confusion exists on their relative virtues. The numerous compression test methods available can be broadly classified into three groups based on load introduction and specimen design: shear loading, end-loading, and sandwich beam specimen testing (see Figure 2.5).
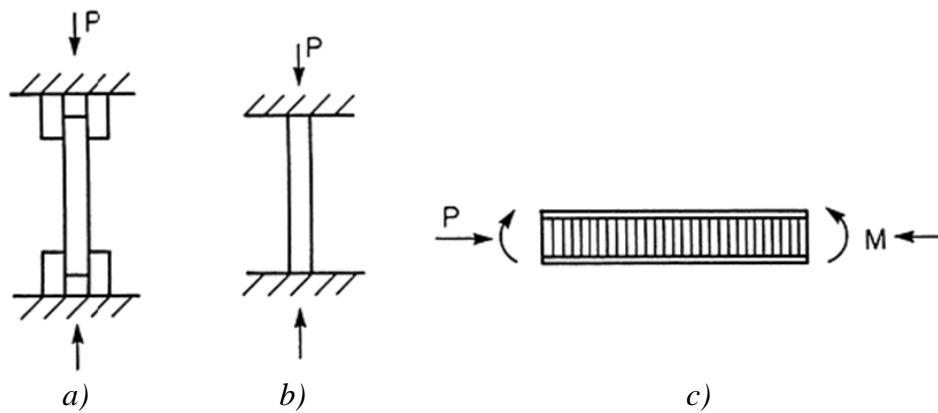
Figure 2.5 - Generic types of compression test methods. (a) Shear loaded. (b) End-loaded. (c) Sandwich beam (extracted from the ASM Vol. 8)

The measured compression strength for a single material system has been shown to differ when determined by different test methods. Variation in results can usually be attributed to fabrication practices, control of fiber alignment, improper specimen preparation and machining, improper placement of samples in testing machines, and improper use of test equipment. Sufficient restraint must be provided to inhibit undesirable failure modes, such as column buckling of the sample. However, if excessive restraint is used, the resulting failure strengths may be artificially high. Buckling and kinking of the fibers within the composite are features regarded as representative for the material and should not be inhibited. To avoid buckling instability, relatively short gage lengths are necessary, but short gage lengths generally tend to amplify sensitivities to clamping. Thus, for very short gage lengths, the apparent compressive strength tends to decrease.

The ASTM D3410 ("Test Method for Compressive Properties of Polymer Matrix Composite Materials with Unsupported Gage Section by Shear Loading") covers the determination of the in-plane compressive properties of polymer matrix composite materials reinforced by high-modulus fibers. The composite material forms are limited to continuous-fiber or discontinuous-fiber reinforced composites for which the elastic properties are specially orthotropic with respect to the test direction. This test procedure introduces the compressive force into the specimen through shear at wedge grip interfaces. Since the compressive load is introduced in the specimen through shear via tabs, there are stress concentrations in the regions at the ends of the end tabs at the beginning of the gage section. Consequently, failures are commonly observed close to the ends of the end tabs, but, such failures are difficult to avoid and are commonly accepted. In Figure 2.6 an example of common failure modes are reported.

Acceptable Failure Modes   Unacceptable Failure Modes
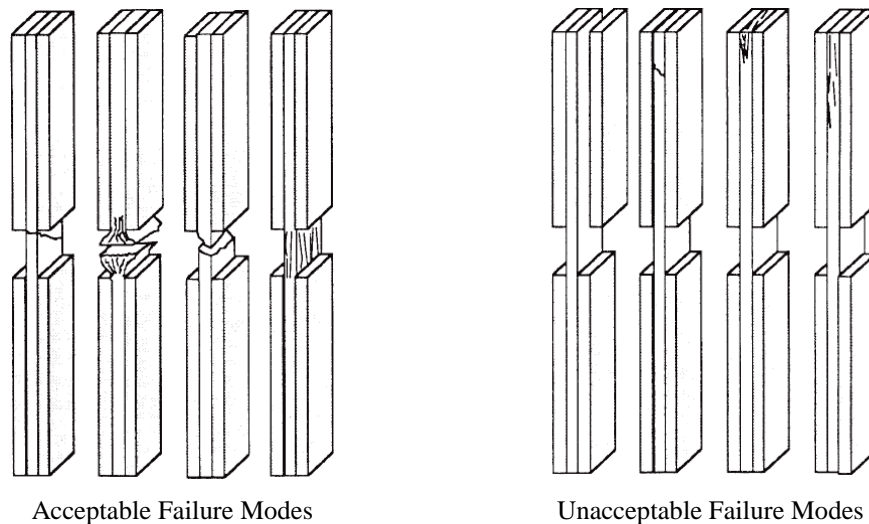
Figure 2.6 - Sketch of the specimen failure (extracted from ASTM D3410)

The ASTM D695 ("Standard Test Method for Compressive Properties of Rigid Plastics") covers the determination of the mechanical properties of unreinforced and reinforced rigid plastics, including high-modulus composites, when loaded in compression at relatively low uniform rates of straining or loading. This test procedure introduces the compressive force into the specimen by end-loading.

The ASTM D6641/D6641M ("Determining the Compressive Properties of Polymer Matrix Composite Laminates Using a Combined Loading Compression

(CLC) Test Fixture") method establishes a procedure for determining the compressive strength and stiffness properties of polymer matrix composite materials using a combined loading compression or comparable test fixture. The compressive force is introduced into the specimen by combined end- and shear-loading. This test method is applicable to general flat laminates that are balanced and symmetric and contain at least one 0° ply. Unidirectional (0° ply orientation) composites can be tested to determine unidirectional composite modulus and Poisson's ratio.

The ASTM D5467 ("Compressive Properties of Unidirectional Polymer Matrix Composites Using a Sandwich Beam") uses a honeycomb-core sandwich beam that is loaded in four-point bending, placing the upper face-sheet in compression (see Figure 2.7). The upper sheet is loaded in compression and is usually a six-ply unidirectional laminate. The lower face-sheet is typically the same material, but twice thicker in order to drive failure into the compressive face-sheet. The two face-sheets are separated by and bonded to a deep honeycomb core (usually aluminium). Failure of the compressive face-sheet enables measurement of compression strength, compression modulus, and strain-at-failure if strain gages or extensometers are employed. This procedure is applicable primarily to laminates made from prepreg or similar product forms. Other product forms may require deviations from the test method.
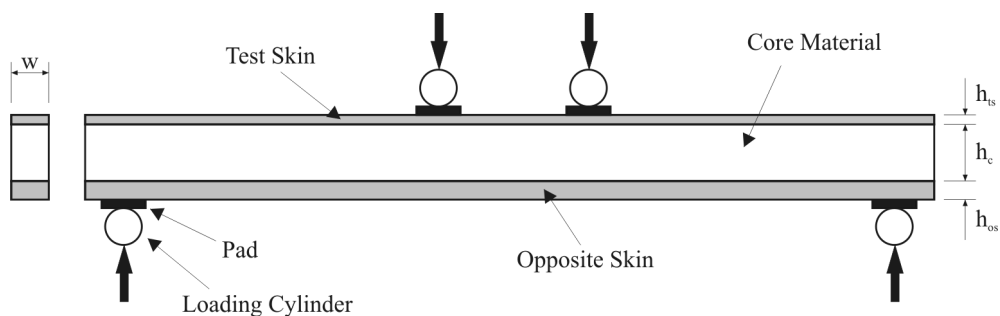
Figure 2.7 - Longitudinal compression sandwich beam test specimen.

ASTM C393 ("Flexural Properties of Flat Sandwich Constructions") is one of a series designed to test sandwich constructions, and covers the determination of the properties of flat, sandwich constructions subjected to flatwise flexure in the same manner as ASTM D5467. ASTM C393 expands on the properties measured by ASTM D5467, and provides a methodology to determine the flexural

and shear stiffness of the entire sandwich, the shear modulus and shear strength of the core, or the compressive or tensile strength of the facesheets. There are no limitations on the core or skin materials for this test method.

The Flexure Testing is one of the most commonly used tests for evaluating ceramics and polymer materials. Bend test eliminates the gripping problems associated with the tension testing of the specimen. Flexure testing have emerged because they demand a very simple specimen preparation and testing. The method is applicable for purposes of material development, and sometimes design. However, for design purposes, tension testing is generally preferred (ASM Vol. 8). Flexure tests are not recommended for determination of design data because deformation and failure of the material occur under a combined stress state, and stress concentrations at loading points and supports may lead to failure. Therefore, the flexural moduli and strength are combinations of the corresponding tensile and compressive properties of the material. Flexure tests are most commonly used to generate flexural modulus and strength for the purpose of quality control. Proper testing and data reduction may render the test data of more value than just a quality check. Great care is needed in flexure testing because significant errors (>5%) can occur from twisting, misalignment, and frictional constraints. Flexure testing of continuous-fiber, ceramic matrix composites must be viewed with considerable caution because the failure mode could be tension fracture, shear fracture, compression failure, or buckling. It is generally limited to unidirectional materials with the fibers aligned parallel or perpendicular to the beam axis.

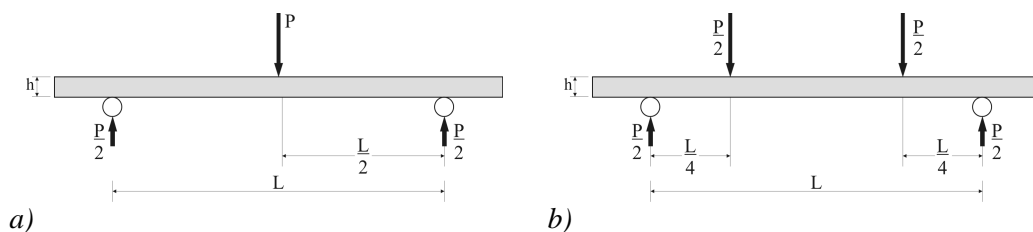*Figure 2.8 - Scheme of flexure tests: a) Three-point loading. b) Four-point loading.*

Flexure testing can be applied using the three-point or four-point methods. For three-point loading, the strain gage is placed on the tension side centered directly under the central loading pin. For four-point loading, the strain gage may be on either the top (compression) or bottom (tension) surface. The flexural stress

at the specimen surface at beam midspan is calculated from the applied load (P), the span (L), the specimen width and the specimen thickness (h). The elastic moduli can be evaluated from the initial slope of the curve obtained by plotting the stress versus the strain gage readings.

The test methods ASTM C1161 ("Standard Test Method for Flexural Strength of Advanced Ceramics at Ambient Temperature") and ASTM C1211 ("Standard Test Method for Flexural Strength of Advanced Ceramics at Elevated Temperature") cover the determination of flexural properties of ceramic materials at ambient and elevated temperature respectively. The European standard test UNI EN843-1 ("Monolithic Ceramics, Mechanical Properties at Room Temperature") is similar to the ASTM C1161. D790 ("Flexural Properties of Unreinforced and Reinforced Plastics and Electrical Insulating Materials") and D6272 ("Test Method for Flexural Properties of Unreinforced and Reinforced Plastics and Electrical Insulating Materials by Four-Point Bending") utilize a three and four point loading system, respectively, for the determination of flexural properties of unreinforced and reinforced plastics, including high-modulus composites and electrical insulating materials in the form of rectangular bars. The European standard test UNI EN14125 ("Fibre-reinforced plastic composites: Determination of flexural properties") is equivalent to the ASTM D6272 and ASTM D790.

The shear tests are carried out to determine shear modulus and shear strength of a material. The response of a composite material subjected to shear is commonly nonlinear, and full characterization requires the entire stress-strain curve (ASM Vol.8). The ideal shear test method should provide a region of pure, uniform shear stress. It is also required that the shear stress and strain can be straightforwardly evaluated from the applied load and deformation measurements. The major difficulty in designing shear tests for composite materials is attaining a uniform state of pure shear stress in the test section. Up to now many shear test methods have been developed, but more studies are still necessary.

The ASTM E0143 ("Test Method for Shear Modulus at Room Temperature") covers the determination of shear modulus of structural materials. This test method is limited to materials in which creep is negligible compared to the strain produced immediately upon loading. The cylindrical or tubular test specimen is loaded by applying an external torque, as to cause a uniform twist within the gage length. The Shear modulus can be computed by the slope of the

shear stress-strain curve, which may be derived from the torque value, the geometry and the angle of twist of the sample. The torsion tube test is especially suited for in-plane shear testing of filament-wound structural parts, and has been recognized as an excellent shear test. The specimen, however, is difficult to fabricate from prepreg and can obviously not be used to test materials in the form of flat sheets. The ASTM D1043 ("Standard Test Method for Stiffness Properties of Plastics as a Function of Temperature by Means of a Torsion Test") test method covers the determination of the stiffness characteristics of plastics over a wide temperature range by direct measurement of the apparent modulus of rigidity.

The test method ASTM D3518/D3518M ("Test Method for In-Plane Shear Response of Polymer Matrix Composite Materials by Tensile Test of a ±45° Laminate") determines the in-plane shear response of polymer matrix composite materials reinforced by high-modulus fibers. The material and laminate form is limited to fully balanced and symmetric ±45° materials. A uniaxial tension test of a ±45° laminate is performed in accordance with test method ASTM D3039. Using expressions derived from laminated plate theory, the in-plane shear stress in the material coordinate system is directly calculated from the applied axial load, and the related shear stress is determined from longitudinal and transverse normal strain data obtained by transducers. These data are used to create an in-plane shear stress-shear strain curve and to evaluate the shear moduli. It is not acceptable for thin specimen.

In the test method ASTM D5379 ("Shear Properties of Composite Materials by the V-Notched Beam Method"), also called as the Iosipescu shear test, a material coupon in the form of a rectangular flat strip with symmetrical, centrally located V-notches is loaded in a mechanical testing machine by the fixture shown in Figure 2.9. Analysis of the specimen under compressive loading reveals that a state of relatively uniform shear stress exists in the center of the notched specimen. The notch makes the distribution more uniform than would be seen without it. The test can be used to characterise laminated and woven composites.
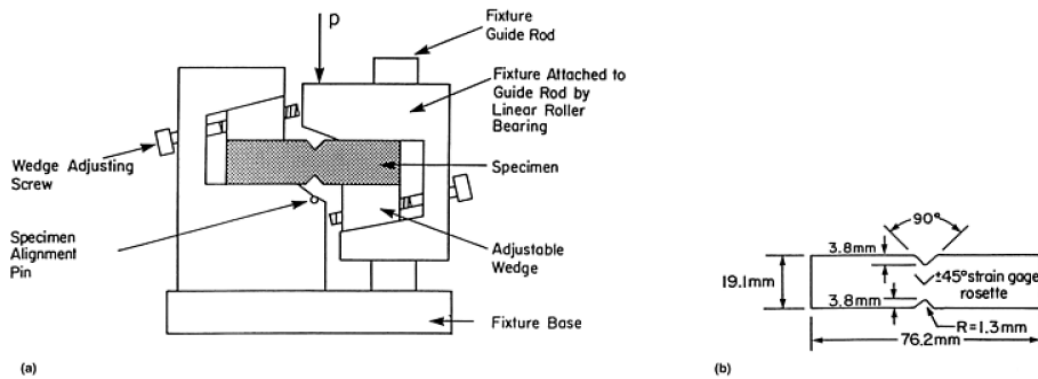
Figure 2.9 – Iosipescu shear test: a) Testing configuration. b) Specimen
(extracted from the ASTM D5379)

The ASTM D4255 describes the test known as "rail shear test". The in-plane shear properties are determined by imposing edgewise shear loads on the specimen using a fixture consisting of two pairs of tensile loaded rails (Method A) or a fixture consisting of three pairs of rails in tension or compression loading (Method B). Figure 2.10 reports the two load configurations used in the ASTM standard. Usually the specimen is bolted to the rails, but slippage is common at increasing loads for some composites. To find the shear moduli the specimens is instrumented with ±45° strain gage rosettes as indicated in Figure 2.10. For ±45° angle-ply laminates difficulties may occur because a uniform state of shear is not attained for this orientation. In this case the Test Method D3518/D 3518M is recommended.

Figure 2.10 – Rail shear test: a) Two-rail configuration. b) Three-rail configuration.
(extracted from the ASTM D4255)

37

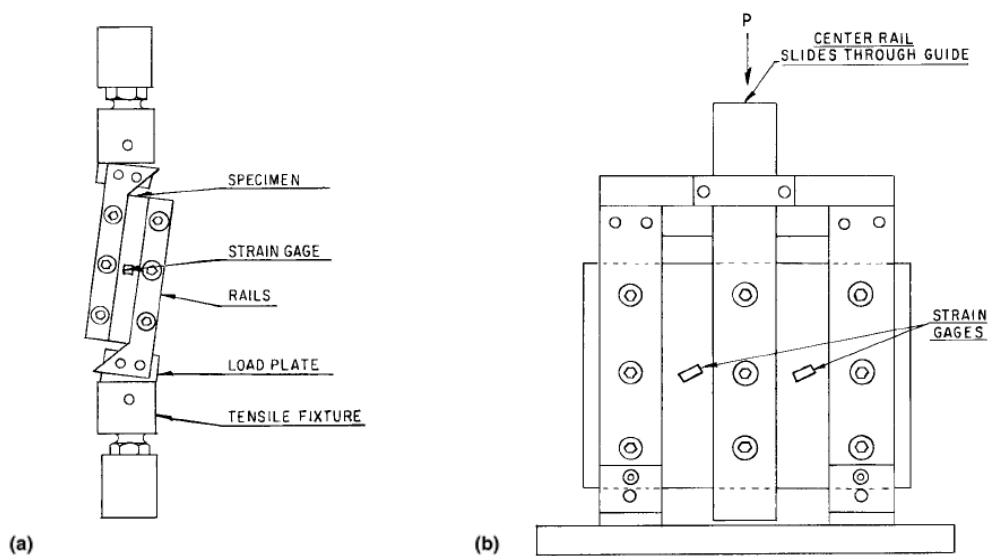In the static tests it's possible to include the hardness testing. It is a very common mechanical test applied to materials. Hardness testing is used extensively in quality control, where data can be collected that relate the mechanical properties of a given material, its microstructure, and processing methods. Over the years, many researchers have endeavored to relate hardness values obtained from mechanical testing to the properties of the material. This has proved to be difficult because the shape of the indenters, loads, and rate of loading interact with each material in a different manner.

2.4　Bibliography

ASM Metals Hand Book. 2000. Mechanical Testing and Evaluation. Vol. 8. ASM International Materials Park, OH.

ASM Metals Hand Book. 2000. Composites. Vol. 21. ASM International Materials Park, OH.

ASTM Standard C0393 Flexural Properties of Flat Sandwich Constructions.

ASTM Standard C0623 Test Method for Young's Modulus, Shear Modulus, and Poisson's Ratio for Glass and Glass-Ceramics by Resonance.

ASTM Standard C0848 Young's Modulus, Shear Modulus, and Poisson's Ratio For Ceramic Whitewares by Resonance.

ASTM Standard C1161 Standard Test Method for Flexural Strength of Advanced Ceramics at Ambient Temperature.

ASTM Standard C1198 Test Method for Dynamic Young's Modulus, Shear Modulus, and Poisson's Ratio for Advanced Ceramics by Sonic Resonance.

ASTM Standard C1211 Standard Test Method for Flexural Strength of Advanced Ceramics at Elevated Temperature.

ASTM Standard C1259 Test Method for Dynamic Young's Modulus, Shear Modulus, and Poisson's Ratio for Advanced Ceramics by Impulse Excitation of Vibration.

ASTM Standard C1273 Test Method for Tensile Strength of Monolithic Advanced Ceramics at Ambient Temperatures.

ASTM Standard C1275 Test Method for Monotonic Tensile Behavior of Continuous Fiber-Reinforced Advanced Ceramics with Solid Rectangular Cross-Section Test Specimens at Ambient Temperature.

ASTM Standard D0638 Test Method for Tensile Properties of Plastics.

ASTM Standard D0695 Standard Test Method for Compressive Properties of Rigid Plastics.

ASTM Standard D0790 Flexural Properties of Unreinforced and Reinforced Plastics and Electrical Insulating Materials.

ASTM Standard D1043 Standard Test Method for Stiffness Properties of Plastics as a Function of Temperature by Means of a Torsion Test.

ASTM Standard D3039/D3039M Standard Test Method for Tensile Properties of Polymer Matrix Composite Materials.

ASTM Standard D3410 Test Method for Compressive Properties of Polymer Matrix Composite Materials with Unsupported Gage Section by Shear Loading.

ASTM Standard D3518/D3518M Test Method for In-Plane Shear Response of Polymer Matrix Composite Materials by Tensile Test of a ±45° Laminate.

ASTM Standard D4255 Test Method for In-Plane Shear Properties of Polymer Matrix Composite Materials by the Rail Shear Method.

ASTM Standard D5379 Shear Properties of Composite Materials by the V-Notched Beam Method.

ASTM Standard D5467 Compressive Properties of Unidirectional Polymer Matrix Composites Using a Sandwich Beam.

ASTM Standard D6272 Test Method for Flexural Properties of Unreinforced and Reinforced Plastics and Electrical Insulating Materials by Four-Point Bending.

ASTM Standard E0111 Test Method for Young's Modulus, Tangent Modulus, and Chord Modulus.

ASTM Standard E0132 Test Method for Poisson's Ratio at Room Temperature.

ASTM Standard E0143 Test Method for Shear Modulus at Room Temperature.

ASTM Standard E1875 Standard Test Method for Dynamic Young's Modulus, Shear Modulus, and Poisson's Ratio by Sonic Resonance.

ASTM Standard E1876 Standard Test Method for Dynamic Young's Modulus, Shear Modulus, and Poisson's Ratio by Impulse Excitation.

Carlsson, L.A., Pipes, B.R., 1997. Experimental characterization of advanced composite materials. Technomic Publishing Company Inc., Lancaster Basel.

ISO 527 Determination of tensile properties.

ISO 6721 Determination of dynamic mechanical properties.

ISO 14129 Fibre-reinforced plastic composites: Determination of the in-plane shear stress/shear strain response, including the in-plane shear modulus and strength, by the plus or minus 45 degree tension test method.

ISO 14125 Fibre-reinforced plastic composites: Determination of flexural properties.

UNI EN843-1 Monolithic Ceramics: Mechanical Properties at Room Temperature.

3 NUMERICAL-EXPERIMENTAL METHODOLOGIES FOR THE MATERIALS CHARACTERIZATION BY VIBRATIONAL TESTING

3.1 State of the art and focus of the research

Dynamic methods for the elastic characterization of the materials can be generally classified into two groups: pulse and resonant methods. Pulse techniques are based on measuring the time-of-flight, that is the time spent for the ultrasonic pulse to travel through the specimen from the transmitting to the receiving transducer. The Young and shear moduli of the material can be calculated from a knowledge of the dimensions and density of the samples and the

transit time for longitudinal and transversal ultrasonic waves. Resonant methods consist of making a specimen vibrate mechanically in one or more vibration resonant modes (sonic and/or ultrasonic). The elastic constants of the material can then be determined from a knowledge of the vibration modes, natural frequencies, dimensions and mass of the samples. According to the function of the model used for the calculation of the natural frequencies, the resonant techniques, present in literature, can be grouped in analytical approaches, i.e. Rayleigh-Ritz (Deobald, Gibson, 1988; Lai, Lau, 1993; Pedersen, Frederiksen, 1992; Sol, 1986; De Wilde et al., 1984, 1986) or Rayleigh (Ayorinde, Gibson, 1993), and numerical approaches, e.g. finite element method (Fällström, Jonsson, 1991; Alfano et al., 2007; Hwang, Chang, 2000; Maletta, Pagnotta, 2004; Pedersen, 1989; Qian et al., 1997; Rikards et al., 2001; Mota Soares et al., 1993). Due to the simplicity and the inexpensiveness of the vibrational tests, the use and the study of these techniques is growing. Until today many works, about the elastic characterization of isotropic and orthotropic materials, have been carried out; the methods differ according to the optimization methodology and/or experimental technique used to acquire the dynamic response. Förster (1937) and Ide (1935) have been among the first reporting about the possibility to determine the elastic constant of a materials by a vibrational test. They used the Euler beam theory to find the elastic modulus of a beam-shaped specimen from the first flexural frequency. In 1945 Pickett (Pickett, 1945) made use of the approximate solution of the Timoshenko beam equations (developed by Goens') to improve the dynamic elastic characterization of beam-shaped specimen with rectangular or circular section (Timoshenko, 1970). The ASTM resonant beam test procedure (ASTM Standard E1875), which standardised material testing based on analytical vibration models, are established on the work of Spinner and Teft (Spinner and Teft, 1961); they have completed Pickett's work taking into account torsional frequencies to identify the shear modulus too. Deobald and Gibson (1988) used a Rayleigh-Ritz model on an orthotropic rectangular plate and measured resonance frequencies to obtain estimated values for the plate rigidities of composite plates. Furthermore they have examined a thin plate with different boundary conditions and have showed as the plate with all boundaries free can obtain better results than that with one or more clamped edges. Subsequently, Ayorinde and Gibson (1993) made use of the classical lamination theory and an optimized three-mode Rayleigh formulation to

obtained the four independent elastic constants (considering free-free boundary conditions) of two rectangular thin orthotropic plates with two different orthotropy ratios (E_1/E_2= 1 and 13) and two plate aspect ratios (width/ length = 1 and 2). Lai and Lau (1993) extended the approach to a generic orthotropic plates. Fällström and Jonsson (1991) and Fällström (1991) used a real-time TV-holography system to determine frequencies and shapes of the first five modes of vibration of plates with free-free boundary conditions. In order to determine all the five independent elastic constants of transversely isotropic materials, thick plates are used because the effects of outplane shear modulus are more evident in these plates. Frederiksen (1995) used single-layer plate theory to analyse the vibration of thick symmetrically laminated rectangular plates with free-free boundary conditions: in this type of theory the three-dimensional elasticity theory is reduced to a two-dimensional one by replacing the laminated plate by an equivalent homogeneous anisotropic plate and introducing a global displacement approximation in the thickness direction. Ayorinde (1995) incorporated the shear and rotatory inertia effect into the model to obtain the three-dimensional elastic constants of a completely free orthotropic plate from experimental plate vibration data. Subsequently Frederiksen (1997) used a numerical model based on a higher-order shear deformation theory (Reddy, 1984) to identified the elastic constants of thick orthotropic plates by the consideration of higher mode natural frequencies. Hwang and Chang (2000) presented a combination method of finite element analysis and optimum design to obtain the out-of-plane shear modulus by using less number of higher frequencies. They shown, also, that for aluminium plates the boundary conditions with all edges free can obtain better results, and seeking two elastic constants is a fast and accurate way for isotropic materials. Furthermore they showed that for carbon/epoxy plates the elastic constants have no clear dependency on the specimen dimensions and the stacking sequences. Sol (1986) in his PhD thesis has found a relation to maximise the sensitivity of the natural frequencies of a composite plate to the elastic constants. Subsequently Sol et al. (1997) presented a Mixed Numerical/Experimental Technique (MNET) for the nondestructive identification of the stiffness properties of fibre reinforced composite materials using a Finite Element Analysis (FEA) and an optimization tools. The method requires the measurement of the first five resonant frequencies of freely suspended rectangular test plates. Mota Soares et al. (1993) proposed a

similar method to characterise composite plates using a MNET. In their work they have formulated the laminate analysis in terms of non-dimensional material parameters. They showed also the limitations of the model to predict the required quantities and its range of application and accuracy. Subsequently, Araújo et al. (2002) proposed a discrete finite element model, associated to an inverse method using experimental vibration data to carry out the identification of electromechanical properties in composite plate specimens with surface bonded piezoelectric patches or layers. Muthurajana et al. (2004) have presented the determination of elastic constants, through vibration testing, of thin specially orthotropic plates with free boundary conditions; they have introduced a influence coefficients evaluated by FEA in order to improve the accuracy of the Rayleigh–Ritz method. Caillet et al. (2007) proposed a direct elastic characterization method, it relies on the identification of the first twenty modal shapes and the natural frequencies of clamped (or supported) rectangular orthotropic plate. In this case the harmonic vibratory field is measured by nearfield acoustic holography techniques. In the meantime many authors have proposed different MNET for elastic characterization of orthotropic rectangular plates using natural frequencies. The works differ mainly on the optimization tools used in the characterization. For example, in Maletta and Pagnotta a Genetic Algorithm (GA) has been proposed while in Rikards et al. (2001), Bledzkia et al. (1999) and Hwang et al. (2000) a different approach has been used; in these works, instead of direct minimization of the identification function, experimental design is used, by which response surfaces of the function to be minimised are obtained. The response surface approximations are obtained by using information on the behaviour of a structure in the reference points of the experiment design. In these case the finite-element modelling of the structure is performed only in the reference points. Qian, et al. (1997) have presented a work in which they use mode shapes and complex eigenfrequencies for determining elastic and damping properties of composite. An original method allowing the direct determination of the flexural stiffness from natural frequencies and modal shape measurements of plate specimens of any shape, which does not require initial estimates of the stiffness nor iterative computations, is proposed in Grediac et al. (Grediac and Paris, 1996a; Grediac et al., 1996b). This methodology has the disadvantage (differently from the proposed technique) of requiring complicated techniques to measure the modal shapes.

Similar methodologies, some already in commerce, have been proposed for small samples. They are identified with RUS that is the acronym of: Resonant Ultrasound Spectroscopy (Leisure, Willis, 1997; Migliori, Darling, 1996; Yaoita et al., 2005). Cubic, spherical or cylindrical specimens can be characterized with these methods by measuring an elevated number of natural frequencies in the ultrasonic field.

The main objective of the present research has been the development of a vibration-based identification procedure to determine the elastic properties of the materials by test specimens of irregular shape. This technique meet the requirements to characterise sample of "not-standardised" shape. In fact, all the mentioned techniques make use of specimen like beams or rectangular plates. In particular, the work has been focused on the development of an iterative technique (also known as MNET) to characterise isotropic materials using specimen like plate of irregular shape; moreover a comparison with direct technique suitable just for test specimens like rectangular isotropic plates is reported. Moreover the MNET has been used to characterise a layered materials. Also in this case a comparison with the direct technique has been reported.

3.2   Methodologies for characterizing isotropic materials

The applicability of a resonant test method depends on a knowledge of the frequency equations relating the natural frequencies of a suitable test specimen to the elastic properties of the material of which it is made. These relations can be obtained by solving a differential equation which generally depends on the boundary conditions and on the shape of the specimen in a very complicated way. Theoretical solution are for this reason limited to simple geometry and boundary conditions. Solution for free edge test specimens like slender bars, rods and circular plates are recommended in ASTM standards for the elastic characterization of homogeneous isotropic materials. Approximate solution for rectangular isotropic plate are given in Alfano and Pagnotta (2007). In the following this technique will be showed and indicated as "Direct Methods". Furthermore, the developed iterative method, indicated as mixed numerical-experimental techniques, will be presented. This technique is necessary when the

frequency equation, or an approximate solution, is not known, due to sample geometry or to the boundary condition.

3.2.1 Direct Methods

A way to determine the elastic constants from frequency measurements, without iteration or optimization processes consists of using suitable relationships relating natural frequencies and elastic properties. Alfano and Pagnotta (2007) made use of FEM calibration to improve the approximate frequency equation, reported in Warburton (1953), on rectangular thin plates subjected to free transverse vibration and with free boundary conditions.

A frequency equation suitable for determining the elastic properties of the plate could be obtained by solving the following differential equation of motion:

$$D\nabla^2\nabla^2 w + \rho h \frac{\partial^2 w}{\partial t^2} = 0 \qquad (3.1)$$

where w is the displacement field, $D=Eh^3/[12(1-\nu^2)]$ is the flexural stiffness of the plate, ρ is the density of the material and h is the thickness. Unfortunately, it is not possible to find a suitable form for the displacement field w that simultaneously satisfies both the boundary conditions and the differential equation of motion. Therefore, to seek practical solutions, many researchers have resorted to various approximate analytical methods. Classical analytical methods have been used in the past to deal with the flexural vibrations of thin rectangular isotropic plates with different edge conditions. Warburton (1953) used characteristic beam vibration functions in Rayleigh's method in order to obtain, for any boundary conditions and for each mode of vibration, very useful, simple and approximate formulae expressing natural frequencies in terms of dimensions of the plate, density and elastic constants of the material. Such formulae assume the following form:

$$f = \frac{\pi}{2}\sqrt{\frac{D}{\rho h}}\frac{\lambda}{a^2} \qquad (3.2)$$

where a is the length of the plate, f is the natural frequency while λ is a non-dimensional factor (the "frequency factor") that, for a given aspect ratio a/b

(where b is the width of the plate) depends only on ν if one or more edges of the plate are free. In principle, by inverting Eq. (3.2) one is able to determine the elastic properties if the natural frequencies, the dimensions and the mass of the plate are measured. Nevertheless, the accuracy of the frequency values calculated using Eq. (3.2) is excellent for plates without free edges, otherwise it can decrease significantly. In order to improve the accuracy of the Warburton formulas Alfano and Pagnotta (2007) have used a Finite Element Method calibration. In Alfano and Pagnotta (2007) the case of thin rectangular plates with free edges has been explored for various modes of flexural vibration and for different a/b ratios. The values of the frequency factors versus ν have been reported in the form of graphs for different values of a/b (i.e., 1.0, 1.5, 2.0 and 2.5).

Table 3.1 - First four modal shapes for rectangular isotropic steel thin plates with different aspect ratio a/b (ν=0.3).

a/b	Mode I	Mode II	Mode III	Mode IV
1.0	(1,1)	((0,2) – (2,0))	((0,2) + (2,0))	(1,2)
1.5[c]	(1,1)	(0,2)	(1,2)	(2,0)
2.0[d]	(0,2)	(1,1)	(1,2)	(0,3)
2.5	(0,2)	(1,1)	(0,3)	(1,2)

c: for ν<0.13 the modal sequence became: (0,2), (1,1), (2,0), (1,2)
d: for ν<0.24 the modal sequence became: (0,2), (1,1), (0,3), (1,2)

In table 3.1 the first four modes of vibration of a rectangular isotropic steel thin plate (ν=0.3) with free edges are illustrated. The values in brackets (i,j) denote the modal designations by the numbers of nodal lines in the two directions approximately parallel to the edges of the plate. It is well known that non-parallel patterns can be observed for a free-edged square plate. In this case, in fact, if i=j or i-j = ±1; ±3; ±5; ... the normal modes of vibration are of the type (i,j) with nodal lines approximately parallel to the edges, while, when i-j= ±2; ±4; ±6; ...,

the normal modes are of the type $((i,j) \pm (i,j))$, with patterns that do not consist of lines parallel to the edges of the plate but is the overlapping of two patterns. Note that the sequence and precise details of mode shapes depend on the particular values of elastic constants and geometrical dimensions. Nevertheless their knowledge is of critical concern for the experimental activities (*i.e.*, measurement of the natural frequencies).

A knowledge of the corrected relations between λ and ν for each of the first four modes of vibration allows for the elastic characterization to be carried out: Poisson's ratio can be determined by the frequency ratio f_i/f_j between the frequencies of two of the first four resonant modes i and j. In fact, as can be deduced from Eq. (3.2), the frequency ratio $f_{ij} = f_i/f_j$ is equal to the frequency factors ratio $\lambda_{ij} = \lambda_i/\lambda_j$ that depends only on ν. Therefore the Poisson's ratio can be obtained simply by solving the equation $f_{ij=} \lambda_{ij}(\nu_{ij})$. The variations of ν with frequency factor ratios, for all the possible combinations of the first four modes of vibration of a square plate, are illustrated in Fig. 3.1.
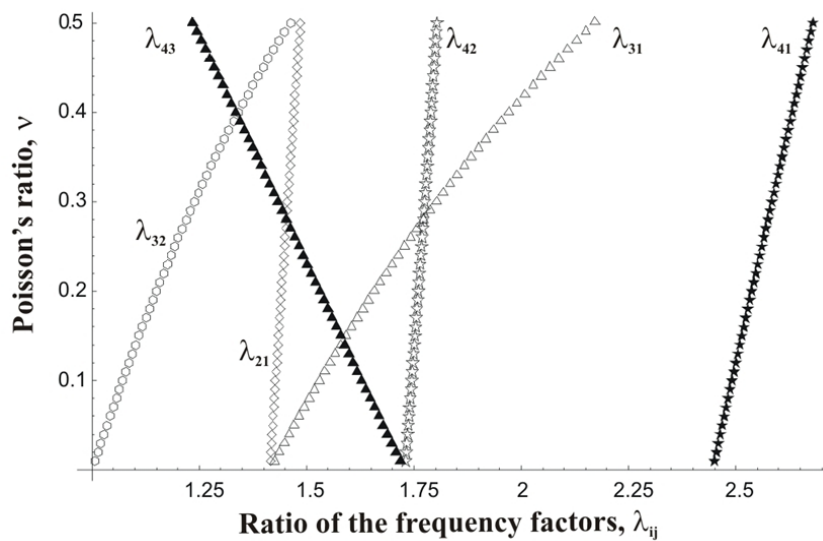

Figure 3.1 - Variation in ν with the ratio of the frequency factors for a/b=1

The value of ν could be obtained by any of the curves of Figure 3.1 but, practically, measurement errors on frequencies propagate on frequency ratios and then on the calculated value of ν. For this reason the sensitivity of ν to the changes in frequency parameter ratio, represented by the slope of the curve considered, should be taken into account.
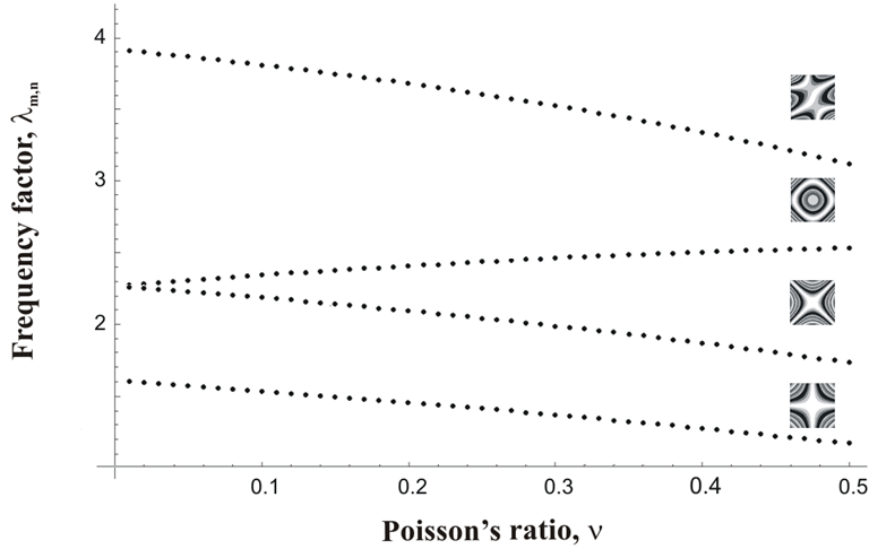
Figure 3.2 - Variation in the frequency factors with ν for a/b= 1

The value of ν can be used to evaluate λ_i and then the Young's modulus. The variation of the frequency factor with the Poisson's ratio are reported in Figure 3.2. Inverting Eq. (3.2) and introducing the mass m of the specimen, Young's modulus can be expressed as

$$(E_{ij})_i = \frac{48}{\pi^2}\left[\frac{f}{\lambda_i(\nu)}\right]^2 \frac{ma^3(1-\nu_{ij}^2)}{bh^3} \tag{3.3}$$

where f_i is one of the two resonant frequencies considered. However, in order to average the effects of the error in frequency measurement, Young's modulus could be determined as the mean of the values obtained using both the natural frequencies f_i and f_j, that is $E_{ij}=[(E_{ij})_i+(E_{ij})_j]/2$.

In the present dissertation a validation of above illustrated technique has been done (in the next chapter are reported the experimental results). The method is accurate enough to be used in a procedure for determining the Poisson ratio (ν) and Young modulus (E) of isotropic materials. As will be evidenced in the experimental section, the procedure is very easy and fast to implement. The negative aspect of the method is the necessity of making a thin rectangular plate sample with an exact aspect ratio (a/b). In fact, for validating the method an ad *hoc* calibration has been necessary for each plate because its aspect ratio is different from the nominal value (1.0, 1.5, 2.0, 2.5) and a high sensitivity to it has

been shown by the results. When it is not possible or it is too expensive to obtain a "standardised sample" (like ASTM shape-sample or thin rectangular plate sample with exact aspect-ratio) a numerical-experimental technique is preferable.

3.2.2 Mixed numerical-experimental techniques

Recently, mixed numerical -experimental techniques for the characterization of both isotropic and anisotropic materials have received a lot of attention. In these techniques, unknown material parameters (elastic constant) in a numerical model of the specimen are updated until the dynamic response (generally, the values of the first natural frequencies) matches the experimental observations as closely as possible. The values of the parameters used in the last computation are the results of the identification procedure and yield the elastic properties. In principle, the approach makes possible to identify all the elastic constants simultaneously from a single experiment without damaging the specimen. In any case, a limit of applicability of all the above mentioned methodologies is the geometry of the specimens. The possibility of characterizing specimens with irregular geometries could be of remarkable usefulness in both industrial and scientific fields. Today, the availability of several commercial finite element codes able to carry out, quickly and accurately, the dynamic analysis of complex structures makes possible to extend the field of applicability of the methodologies to plate with contours of any shape.

The identification of the elastic moduli of a material is an inverse problem and, therefore, it can be formulated and resolved as a typical optimization problem (Liu, Han, 2003). In particular, the procedure proposed in the present dissertation allows to identify the elastic moduli minimizing an error function (φ) defined as the difference between the numerically determined resonance frequencies of a free plate and the real one measured experimentally. The values of the resonant frequencies of free plates with the same geometry, dimensions and material density depend, in fact, exclusively on the elastic moduli of the material. As regarding isotropic material, the resonant frequencies depend just on two elastic moduli (Young's modulus and Poisson's ratio), so that $= $ (E,). Therefore, the identification of E and can be carried out, by searching among a set of possible solutions for the one that, introduced in a model able to predict the

dynamic behaviour of the modelled plate, gives resonant frequencies as near as possible to the resonant frequencies of the real plate.

3.2.2.1 MNET formulation

A flow diagram is reported in Figure 3.3 showing the procedure for the elastic characterization of a material. The procedure has been developed on a personal computer in MATLAB$^{\circledR}$ environment and recalls the finite element code MSC/Nastran$^{\text{TM}}$ for the dynamic analysis of the plate. In input, the procedure requires material density, real resonant frequencies and the finite element model of the plate. All these data can be obtained by means a measurement process carried out in a preliminary experimental phase where the measurement of material density, resonance frequencies, shape and thickness of the plate under examination are performed. Among the various commercial codes available for constructing a finite element model of the plate from the measured geometric dimensions, in the work presented here, the pre and post processor MSC/Patran$^{\text{TM}}$ has been used.

At the start, the process calculates the error function corresponding to each initial solution (trial values of the elastic constants). The type of minimization process employed determines the number of such solutions. It can vary from a minimum of one solution for the more traditional algorithms to an entire population of solutions for non conventional algorithms like the genetic algorithms. The values of the trial solutions can be imposed arbitrarily by the user based on his own experience or can be chosen randomly.

During the pre-processing stage, the values of the elastic constants are included (by modifying the MAT1 bulk data entry which defines the isotropic stress-strain relationship) inside the input file of Nastran$^{\text{TM}}$ code which contains the topology of the model. After that, the normal modal analysis for predicting modal frequencies of the plates has been carried out by using "Solution 103", neglecting the damping and using the method of extraction of Lanczos. In the post-processing stage, the desired first non-zero natural frequencies extracted from the output file of results are stored (the first six rigid body modes for the free edge condition have zero frequency). Moreover, all the files generated from the FEM code are removed in order to release the memory of the computer.
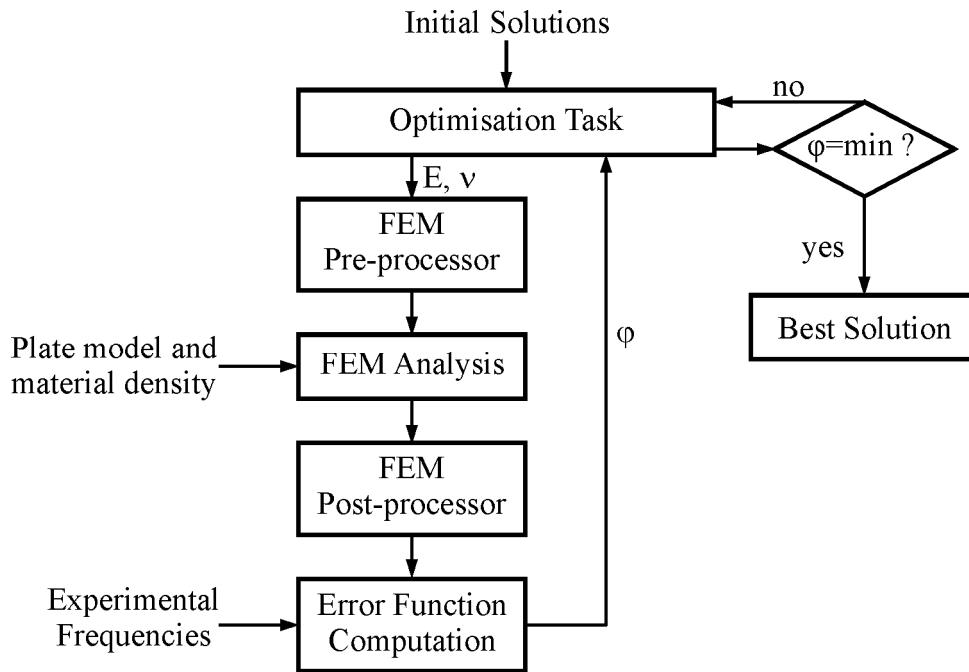
Figure 3.3 - Flow-chart of the MNET formulation.

At this point, using the experimental data, the value of the error function is calculated and saved, then the cycle restarts with a new solution. Finally, a convergence test is performed. This test could consist in controlling if, after a fixed number of successive iterations, the differences between the values of both elastic constants remain inside a prefixed range. When, such a condition is verified, the best solution is reached and the procedure is stopped.

3.2.2.2 The error function

In an optimization procedure a correct selection of the error function is of fundamental importance. Finding the minimum is faster and more accurate if it is unique and easy to identify inside the domain of existence of the function. The type of considered function influences the choice of the procedure to be used for the minimum identification. Among the wide variety of potential error functions, in the following, attention has been focused on some of the more commonly used error functions. In equations (3.4)-(3.7), the expressions of the examined functions are reported. Among these, the well known norms L_1 and L_2 (Liu, Han, 2003), in Eq. (3.4) and Eq. (3.7), can be recognised. They represent, respectively, the sum of the absolute values of the errors and the sum of the squares of the errors. In

those equations, $\overline{f_i}$ is the i-th resonant frequency measured during the vibrational test, f_i is the i-th frequency calculated with the theoretical model, and n is the number of the modes used in order to define the error function. The functions φ_2 and φ_3 instead, represent the square root of the sum of the absolute values of the relative errors and the square root of the sum of the squares of the relative errors, respectively. They proffer the interesting characteristic of reducing the influence of the greater errors in the experimental measures of the higher frequencies.

$$\varphi_1 = \sum_{i=1}^{n} \left| f_i - \overline{f_i} \right| \tag{3.4}$$

$$\varphi_2 = \sqrt{\sum_{i=1}^{n} \left| \frac{f_i - \overline{f_i}}{\overline{f_i}} \right|} \tag{3.5}$$

$$\varphi_3 = \sqrt{\sum_{i=1}^{n} \left(\frac{f_i - \overline{f_i}}{\overline{f_i}} \right)^2} \tag{3.6}$$

$$\varphi_4 = \sum_{i=1}^{n} \left(f_i - \overline{f_i} \right)^2 \tag{3.7}$$

Figure 3.4 reports the graphs of Eqs. (3.4) - (3.7) versus E and ν (for an aluminium square thin plate with $E = 70.0$ GPa, $= 0.33$, side $l = 100$ mm and thickness $h = 1$ mm), obtained considering the first four frequencies of resonance. Note that into the figure the error function is divided by its maximum value (φ_{max}) and so it is dimensionless. The graphs have been reconstructed using the results of an extended series of finite element analysis.

The choice of the most suitable error function depends on a compromise between high convergence speed and accuracy. With regards to the number of natural frequencies to use in the equations of the error function, note that in order to avoid indeterminate or ill-conditioned problems that would make the inverse problem insoluble, a number of frequencies equal to or greater than the number of the unknowns of the problem has to be used.
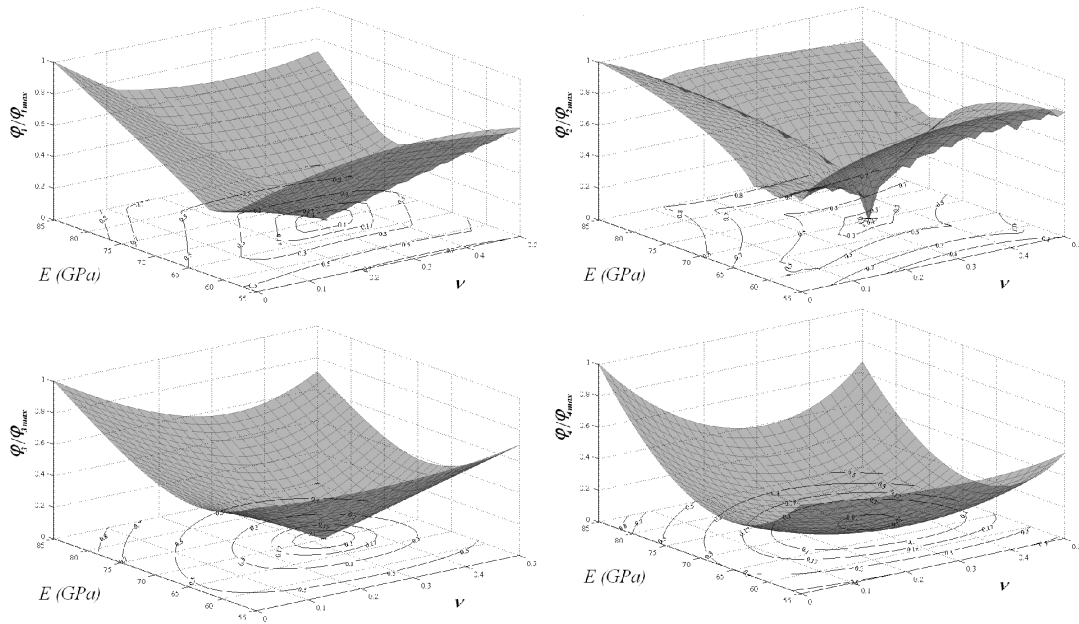
Figure 3.4 - A comparison of different error functions.

In Figure 3.5a the contour plot of the function φ_3/φ_{3max} for n=1 (the first resonant frequency for a square plate) is reported. The condition of minimum, in this case, leads undoubtedly to a situation in which the solution is indeterminate. That situation changes when one of the two elastic constants is known. Although, a similar behaviour is verified for many other frequencies, it cannot, unfortunately, be generalized to all frequencies. For example, Figure 3.5b illustrates the contour plot of the error function for the eighth frequency. In this case, the value of E can be identified if the value of ν is known, but it is not possible to identify ν unequivocally if E is known.
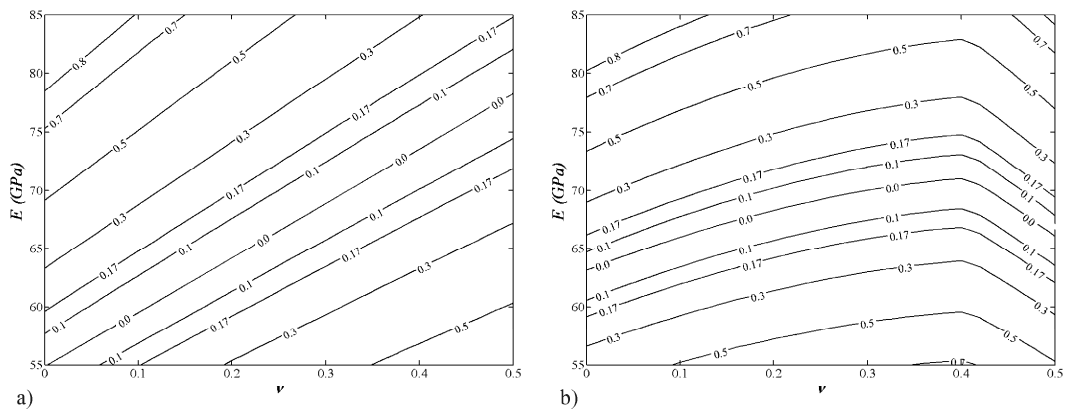

Figure 3.5 - Contour plot of φ_3/φ_{3max} *with n=1: a) first frequency; b) eighth frequency.*

In conclusion, the choice of the vibration mode to be considered in the error function is essential to solving the inverse problem. From the above observations,

it is possible to conclude that for estimating both the elastic constants two resonant frequencies have to be known, and also that such a condition would not be sufficient if the vibration modes are not well chosen.

For example, in Figure 3.6a the variation in the ratio φ_3/φ_{3max} calculated using the first two frequencies (n=2) is reported. It can be seen that the minimization of such a ratio is an ill-conditioned problem, while the variation in the same ratio calculated using the first and the third resonant frequencies (see Figure 3.6b) presents a unique minimum identifying only one well distinguished solution.
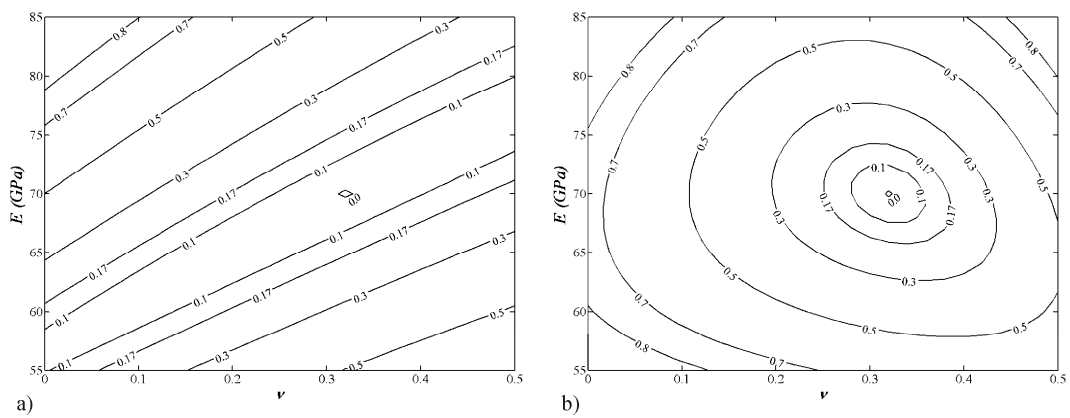

Figure 3.6 - Contour plot of φ_3/φ_{3max} with n=2:
a) first and second frequencies; b) first and third frequencies.

In order to avoid the situations illustrated above, that if not recognized could lead to solutions that are completely wrong, a number of resonant frequencies always larger than or equal to the number of unknowns is recommended.

The results of an extensive series of numerical analyses, carried out on isotropic plates of various shape and dimension, have shown that a minimum of four frequencies (generally, the first four) have to be used to accurately determine the two unknown elastic moduli. Table 3.2 and Table 3.3 reports the contour plot of the error function for different geometry of plates. Same variations have been observed even when considering a number of frequencies greater than four (e.g. n=10). Moreover, negligible variations have been noted when the resonance frequencies are not taken in sequence. That can be very useful, especially when, because of experimental difficulties, the measured values of some frequencies are not available or are unreliable and must be excluded.

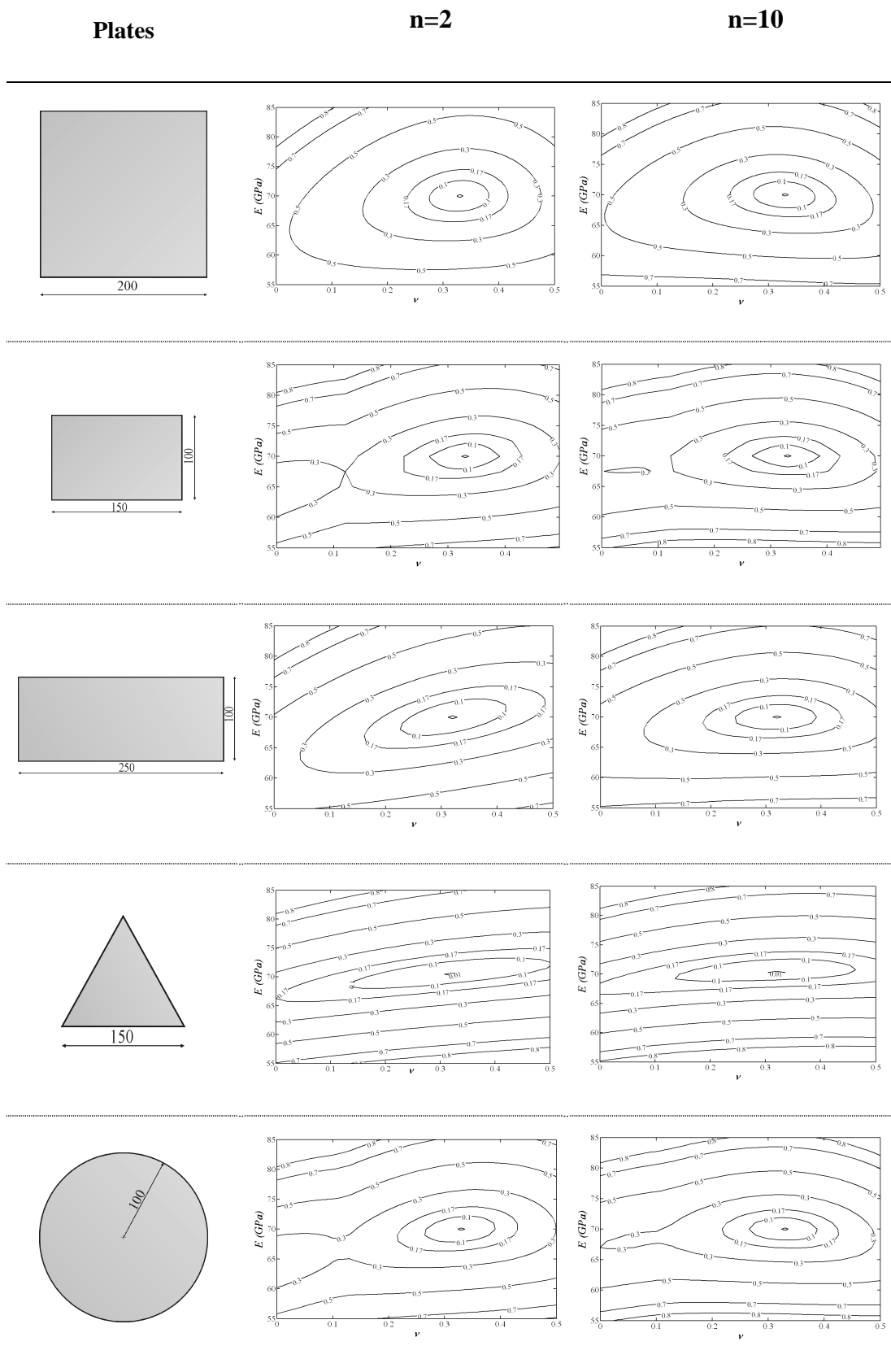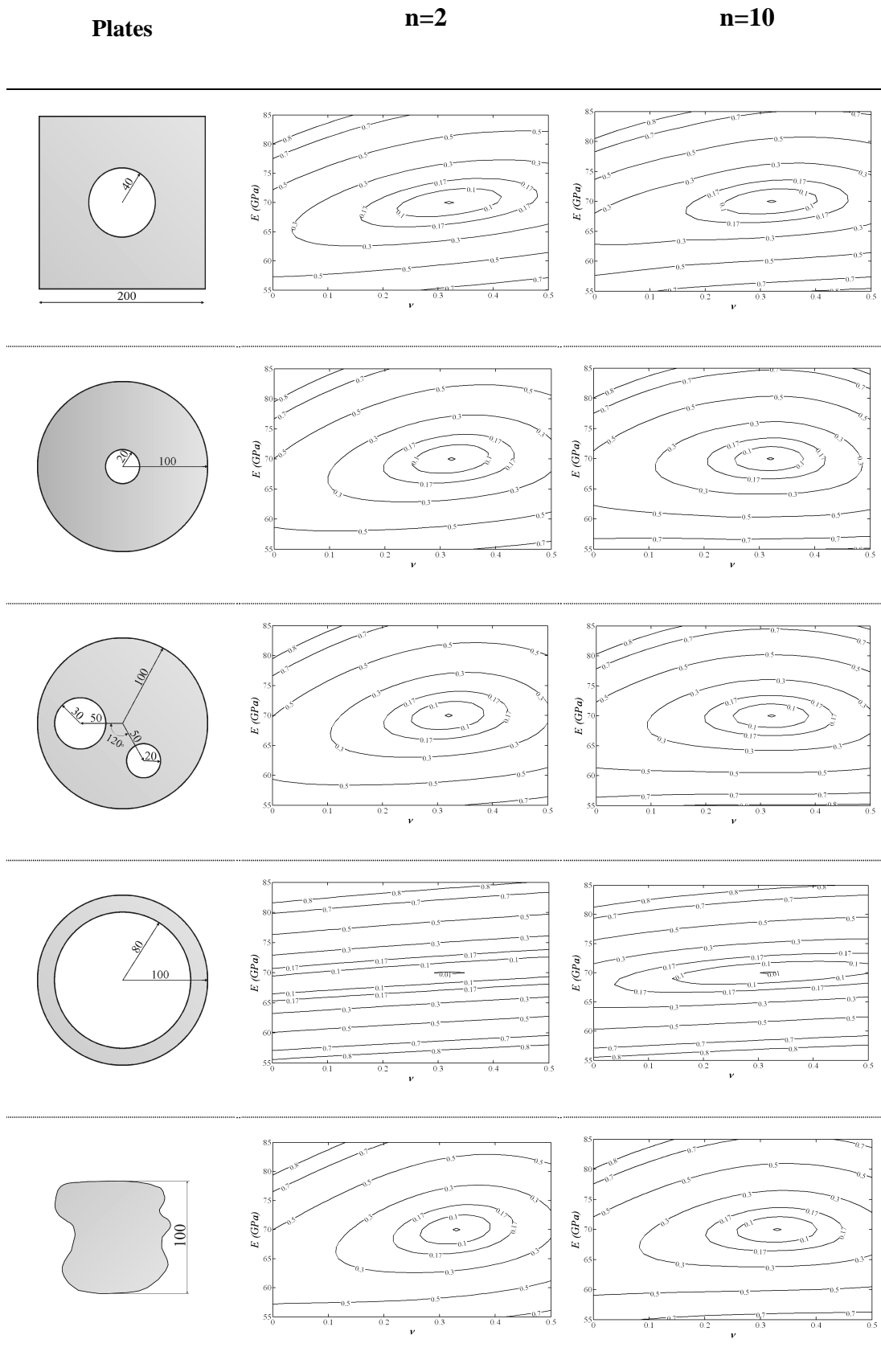**Table 3.2 - Contour plot of the error functions ($\varphi_3/\varphi_{3\max}$) for different plates.**

Plates	**n=2**	**n=10**

Table 3.3 - Contour plot of the error functions ($\varphi_3/\varphi_{3\max}$) for different plates.

Plates	n=2	n=10

The proposed procedure can be successfully applied even to pierced plates. Apart the thin ring, all the functions have, in fact, a well distinguished minimum. Thin ring represents an exception. In that case, the error function is practically insensitive to the Poisson ratio if four frequencies are take into account, and therefore this plate is not well suited for the determination of both the elastic constants. If this or similar cases are not recognized, unreliable or completely wrong results can be obtained. Thus, in suspect cases, it is always recommended to carefully examine the variation in the error function before starting a material characterization process.

The method works well also when the frequencies of two modes are very close or coincide or even when two couples of very close frequencies are encountered (as, for example, in the case of the rectangular plate with length to width ratio equal to 1.5), and no correspondence with modal shape order seems necessary. However, in some cases (like in this last plate) it could happen that the error function presents a local minimum in addition to global minimum and, if the initial guess point is not wisely chosen, the "classical" optimization methods can fail, getting trapped at the local minimum. To overcome the problem, the user could run the procedure more times starting from different guess points or/and take a number of frequencies greater than four. A better approach could be to choose four not sequential suitable frequencies to remove the local minimum. Alternatively, a different optimization method could be used (genetic algorithms are suitable).

3.2.2.3 Selection of the error function and minimization method

If the error function is defined properly, the procedure for the identification of the elastic constants can be, in principle, achieved by using any of the many methods for finding the absolute minimum value of a two variable function. Comparing their efficiency in terms of the rapidity with which the solution is reached, the more suitable method can be chosen. In Table 3.4, the convergence speeds of the procedure achieved using different minimization methods and error functions are compared. The results reported in that table have been obtained from the analysis of a thin square plate with the same dimensions and elastic properties as the plate considered in the previous section. Similar results have also been

obtained for other geometries. In each case, the first four resonant frequencies obtained numerically in a preliminary phase (for the vibrational modes and the relative frequencies see Table 3.5) have been assumed.

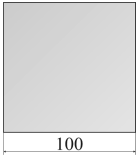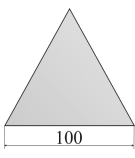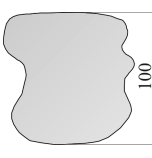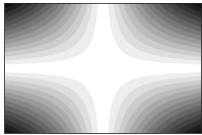**Table 3.4 - Comparison of the number of FEM code runs.**

Optimization method	Error function			
	φ_1	φ_2	φ_3	φ_4
Simplex	63	*	60	64
Gradient	*	*	164	*
Least-squares	-	-	-	21
Genetic Algorithm	441	630	469	351

(* attainment of convergence depends on the initial attempt solution)

Convergence speed is inversely proportional to the number of times that the FEM code runs until the difference between the values in the calculated elastic constants and the nominal ones is less than 0.1%. The following methods of minimization have been employed: simplex method (Nelder and Mead algorithm), gradient method (Broyden-Fletcher-Goldfarb-Shanno algorithm), the least-squares method (according to Gauss-Newton), a genetic algorithm (see Appendix B). The procedure calls the first three methods through the library functions of MATLAB: "fminsearch", "fminunc", and "lsqnonlin" (optimization toolbox of MATLAB).

For the same minimization method and error function, the number of iterations for converging to a solution depends on the trial solution. Therefore, in order to take this into account, for every case, a series of analyses has been carried out assuming different trial solutions (solutions have been chosen inside a rectangular region of the elastic domain of ± 25% of the value of each elastic constant) and in Table 3.4 the mean numbers of iterations are reported. In the case of the genetic algorithm, various initial populations have been considered, each constituted from individuals randomly extracted inside a rectangular region of the elastic domain of ± 25% of each elastic constant value. Also in this case, the number reported in the table is the average of the FEA for converging to the solution.

Table 3.5 - Modal shapes and resonant frequencies of some of the examined plates.

Square	Rectangular	Triangular	Irregular
100 ‑ 100	100 ‑ 150	100	100
1600 element Quad8	2400 element Quad8	1200 element Quad8	2535 element Quad8
f_1: 325.7 Hz	f_1: 216.1 Hz	f_1: 845.5 Hz	f_1: 476.4 Hz
f_2: 477.2 Hz	f_2: 233.5 Hz	f_2: 873.2 Hz	f_2: 677.9 Hz
f_3: 604.7 Hz	f_3: 500.3 Hz	f_3: 873.9 Hz	f_3: 871.4 Hz
f_4: 846.2 Hz	f_4: 548.4 Hz	f_4: 2075.9 Hz	f_4: 1193.7 Hz
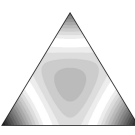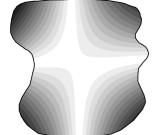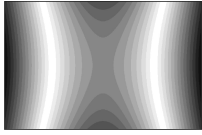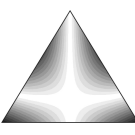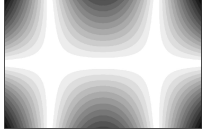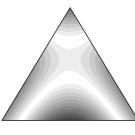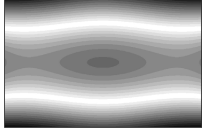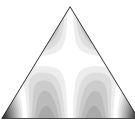
From Table 3.4 the least-squares method appears the fastest (requiring an average of 21 iterations); it must be noted that it is usable only in conjunction with the function error φ_4. Simplex and gradient methods follow. These methods can be, in theory, used with any type of error function if it does not present local minima, otherwise the convergence largely depends on the trial solution. The genetic algorithm (an ARGA, Adaptive Range Genetic Algorithm, working with populations of 20 individuals: Pagnotta, Stigliano, 2006) always finds the

solution, whatever the error function, confirming the main feature of this type of optimization method that consists in being able to find the global minimum even when the function has more local minima. Unfortunately, it has the drawback of requiring a very low convergence speed compared with the other methodologies and therefore it is not competitive for solving a problem with two unknowns.

It is necessary to underline that, although the results of Table 3.4 indicate that for reaching the highest convergence speed the least-squares method coupled to the function φ_4 have to be used, ulterior analyses (discussed in the next section), taking into account the influence of the measurement errors, have shown that the simplex method coupled with φ_3 can represent a valid alternative.

3.2.2.4 Numerical application and sensitivity analysis

The effectiveness of the procedure has been verified numerically, simulating the process of elastic characterization for a wide number of thin plates with various geometries, shapes, dimensions and materials. In the first stage, every plate has been modelled, meshed and then numerically processed for the calculation of the first four resonant frequencies. Successively, using experimental data, simulated by the values of the resonant frequencies previously calculated, the identification process has been carried out. In Table 3.5, some of the tested typologies (square, rectangular, triangular and irregular plate) are illustrated. Every plate has been meshed using eight node quadrangular elements of NASTRAN library and the number of elements used is reported in the table. In the same table, the first four vibrational modes and the resonant frequencies of each plate are also indicated. Such results have been obtained considering aluminium plates having the following elastic properties E = 70.0 GPa; = 0.33, material density = 2.7 g/cm^3, and thickness t = 1 mm.

The material characterization process has been carried out using both least-squares and simplex methods, assuming the following trial values for the elastic constants E = 80 GPa, = 0.30. In all the cases the solution has been reached, within a margin of error of 0.1%, in less than 50 iterations.

In order to investigate the influence of the experimental errors affecting the measured frequencies on the solution, a series of numerical tests has been carried out. The uncertainties of the solutions have been estimated analysing samples of

20 series of "experimental measurements". Each series included the values of the first four frequencies. The value of each single experimental frequency has been obtained by extracting a real number from a normal distribution with a mean value equal to the value of the calculated frequency and standard deviation equal to a prefixed percentage of the calculated frequency.

In Table 3.6 - Table 3.8 the mean values and standard deviations of the normal distributions of the results, for every examined plate and for the three levels of noise, 0.5%, 1.0% and 1.5%, respectively, are reported. In particular, the results obtained by the least-squares method and by the simplex method coupled to the objective function φ_1 and φ_3 are reported in the tables. Despite the fact that from the tests carried out without measurement errors (Table 3.4) the least-squares method turned out to be the fastest, the tests in the presence of errors has shown negligible differences between the convergence speeds of the two solution methods (on average about 45 iterations against the 42 iterations of the simplex method, the tests being stopped after five successive iterations without any improvement in the solution).

An analysis of data reported in Table 3.6-Table 3.8 indicates that the solutions obtained with both methods are stable and sufficiently accurate for the examined noise levels. The observation of the error function contour also shows, in all the cases, a noticeable sensitivity of the Poisson ratio to the experimental errors.

Table 3.6 - Sensitivity analysis results obtained by the simplex method using φ_1

Gaussian Noise			Plates			
			Square	Rectangular	Triangular	Irregular
0.0%	$\bar{x}$ ($_x$%)	E	70.0 (0.0%)	70.0 (0.0%)	70.0 (0.0%)	70.0 (0.0%)
		ν	0.330 (0.0%)	0.330 (0.0%)	0.330 (0.0%)	0.330 (0.0%)
0.5%	$\bar{x}$ ($_x$%)	E	70.0 (0.6%)	69.9 (0.5%)	69.9 (0.6%)	69.9 (0.6%)
		ν	0.331 (2.3%)	0.329 (3.8%)	0.331 (3.8%)	0.327 (4.5%)
1.0%	$\bar{x}$ ($_x$%)	E	70.1 (1.1%)	69.6 (1.2%)	70.0 (1.4%)	70.0 (1.3%)
		ν	0.332 (4.0%)	0.325 (6.5%)	0.332 (8.2%)	0.333 (10.2%)
1.5%	$\bar{x}$ ($_x$%)	E	70.4 (1.4%)	70.0 (1.3%)	70.0 (1.7%)	70.0 (1.9%)
		ν	0.329 (6.3%)	0.327 (12.8%)	0.322 (11.5%)	0.333 (14.6%)

Table 3.7 - Sensitivity analysis results obtained by the simplex method using φ_3

Gaussian Noise			Plates			
			Square	Rectangular	Triangular	Irregular
0.0%	$\bar{x}\ (\ _x\%)$	E	70.0 (0.0%)	70.0 (0.0%)	70.0 (0.0%)	70.0 (0.0%)
		ν	0.330 (0.0%)	0.330 (0.0%)	0.330 (0.0%)	0.330 (0.0%)
0.5%	$\bar{x}\ (\ _x\%)$	E	70.0 (0.5%)	70.0 (0.5%)	70.0 (0.5%)	70.1 (0.5%)
		ν	0.331 (2.2%)	0.332 (3.8%)	0.329 (2.7%)	0.331 (2.3%)
1.0%	$\bar{x}\ (\ _x\%)$	E	70.1 (1.1%)	70.1 (1.1%)	69.9 (1.2%)	70.2 (0.9%)
		ν	0.332 (4.1%)	0.325 (6.6%)	0.328 (8.1%)	0.329 (4.6%)
1.5%	$\bar{x}\ (\ _x\%)$	E	70.2 (1.3%)	69.4 (1.6%)	70.2 (1.6%)	70.0 (1.6%)
		ν	0.329 (6.2%)	0.325 (8.5%)	0.333 (10.3%)	0.333 (7.0%)

Table 3.8 - Sensitivity analysis results obtained by the least-squares method

Gaussian Noise			Plates			
			Square	Rectangular	Triangular	Irregular
0.0%	$\bar{x}\ (\ _x\%)$	E	70.0 (0.0%)	70.0 (0.0%)	70.0 (0.0%)	70.0 (0.0%)
		ν	0.330 (0.0%)	0.330 (0.0%)	0.330 (0.0%)	0.330 (0.0%)
0.5%	$\bar{x}\ (\ _x\%)$	E	70.0 (0.8%)	70.0 (0.5 %)	69.9 (0.7%)	70.1 (0.6%)
		ν	0.330 (2.4%)	0.327 (4.4%)	0.327 (3.6%)	0.331 (2.8%)
1.0%	$\bar{x}\ (\ _x\%)$	E	70.3 (1.1%)	69.7 (1.5%)	69.8 (1.5%)	70.1 (1.1%)
		ν	0.330 (4.6%)	0.323 (5.4%)	0.326 (9.7%)	0.333 (5.9%)
1.5%	$\bar{x}\ (\ _x\%)$	E	70.1 (1.9%)	70.0 (1.3%)	70.5 (1.7%)	69.5 (2.0%)
		ν	0.331(6.4%)	0.330 (12.9%)	0.339 (12.4%)	0.338 (6.5%)

Table 3.9 - Effect of the number of frequencies on the sensitivity in square plate

Gaussian Noise			Number of frequencies	
			n=4	n=10
0.0%	$\bar{x}\ (\ _x\%)$	E	70.0 (0.0%)	70.0 (0.0%)
		ν	0.330 (0.0%)	0.330 (0.0%)
0.5%	$\bar{x}\ (\ _x\%)$	E	70.0 (0.5%)	70.0 (0.3%)
		ν	0.331 (2.2%)	0.329 (2.3%)
1.0%	$\bar{x}\ (\ _x\%)$	E	70.1 (1.1%)	70.0 (0.8%)
		ν	0.332 (4.1%)	0.328 (3.7%)
1.5%	$\bar{x}\ (\ _x\%)$	E	70.2 (1.3%)	69.8 (1.1%)
		ν	0.329 (6.2%)	0.329(5.5%)

Although the simplex method coupled to the objective function φ_3 obtained results slightly more accurate than the least-squares method, it can, however, be concluded that, in general, both methods are suitable for the elastic characterization of a material. The results of the simplex method coupled to the objective function φ_2 are not reported because the attainment of convergence depends on the initial attempt solution.

In Table 3.9 the results of the numerical simulations carried out on a square plate using four and ten frequencies to compute the objective function φ_3 are reported. The results indicate that a number of ten frequencies gives better results in terms of standard deviation, this is due to the error compenzation on all the frequencies. A number of four frequencies gives good results too. In experimental stage a high number of frequencies is preferred, but often it is not easy to acquire all the desired frequencies.

3.3   Methodologies for characterizing orthotropic materials

As it was show in the first chapter the behaviour of an orthotropic thin plate can be described by four independent elastic moduli (E_{11}, E_{22}, G_{12} and ν_{12}). For the elastic characterization of composites materials the same procedure used for isotropic materials can be carried out. Obviously, more natural frequencies are needed to have a well-posed problem. In literature more authors have proposed methods for identifying the elastic moduli using this procedure. Unfortunately, some problems exist in the sensitivity of the natural frequencies to all the elastic moduli. In fact, such methodology can only yield good results if the experimental data (the natural frequencies for the proposed methodology) change significantly for a variations of each of the elastic moduli. For instance, the bending and torsion frequencies are sensitive to a variation of Young's and shear moduli respectively; but these frequencies are insensitive to changes of Poisson's ratio. This constant describes the lateral contraction (or expansion) of the material when it is subjected to a longitudinal normal stress. Therefore, to achieve a high sensitivity to Poisson's ratio a mode that has a deformation component in both x and y directions needs to be used. In order to obtain modes that are appreciable sensitive to the Poisson ratio, rectangular plate-shaped specimens with a particular length to

width ratio have to be used (Sol, 1986). In order to give a tool to find the optimal aspect ratio of the sample, in terms of Poisson's ratio sensitivity, the following equation has been proposed:

$$\frac{length}{width} = \sqrt[4]{\frac{E_2}{E_1}} \qquad\qquad (3.8)$$

The equation can be obtained matching the resonant frequencies of the first flexural mode in the x- and y-direction. A plate whose length-to-width ratio complies with (3.8) is called "Poisson plate" due to the high Poisson ratio sensitivity. It must be noted that the aspect ratio of the tested plate depends on the parameters to be determined and so that if a new material has to be characterised a previous evaluation of the elastic moduli needs to carry out. From these consideration, it's possible to deduce that the elastic characterization of orthotropic plates of any shape using only the natural frequencies seems to be arduous.

3.4 Methodologies for characterizing layered material

Today the use of ceramic and/or metallic coatings as protective layers to improve the surface properties of substrate materials is growing. The basic properties of a coated system, for instance the adhesion strength or its thermo-mechanical behaviour, mainly depend on the elastic modulus. Therefore, coatings development demands an efficient, reliable and convenient technology for its measurement. Up to now, there is an extensive literature on the identification of the elastic properties of layered materials; the most widespread methods are based on conventional quasi-static tests. These are based on the direct measurement of strains undergone by suitable coated specimens subjected to mechanical loads, *i.e.* tensile, bending or torsion tests. In particular, specimens are gradually loaded and the deformation is measured at various load levels, then the elastic properties are deduced by means of suitable equations (Mencik, 1996). In the case of free-standing coatings the conventional standards for monolithic materials can also be used (ASTM E132; ASTM E111; ASTM E143; ASTM C1273; ASTM C1161).

Another noteworthy static procedure is represented by indentation (Mencik, 1996; Oliver and Pharr, 1992). It allows to determine the modified Young's

modulus, *i.e.* $E/(1-v^2)$, of a sample from the analysis of the initial part of the unloading curve obtained with a spherical indenter in the elastic range. The elastic modulus in the out of plane direction is then obtained assuming a value of the Poisson ratio *a priori*. Alternative static methodologies have been recently proposed. For instance, in Furgiuele *et al.* (1997), Pagnotta (2007) and Bruno *et al.* (2002) the Young's modulus and Poisson ratio are determined from the analysis of the surface displacement field of suitable specimens subjected to static loads. These procedures have been demonstrated on metallic as well as on ceramic specimens. Even if the indentation and the static techniques are currently used in order to obtain the elastic properties of layered materials (Kim and Kweon, 1999; Beghini *et al.*, 2001a, b; Chudoba *et al.*, 2002; Antunes *et al.*, 2007; Liu and Wang, 2007), they are cumbersome and, therefore, too tedious for a routine application in production. As an alternative, the use of dynamic test methods has increased in the last decades. In particular, resonant methods are currently widespread (Atri *et al.*, 1999; D'evelyn and Taniguchi, 1999; D'evelyn and Zgonc, 1997; Radovic and Lara-Curzio, 2004; Radovic *et al.*, 2004; Schmidt *et al.*, 2005). In particular, frequencies measurement is achieved by continuous variable excitation, generally of sinusoidal or random stationary type, or by Impulse Excitation Technique (IET). IET has the advantage of being simple, fast and accurate and requires inexpensive experimental equipment and can certainly be used for rapid production process monitoring. In addition, it allows to determine the in-plane elastic moduli subjecting the specimen to lower strains so that they are measured nearly at the origin of the stress-strain curve and fracture is prevented. In the following a "direct method" and the proposed mixed numerical-experimental techniques used to characterise layered samples by natural frequencies are described. In particular the direct method is an extension of the Förster's formulation, while the MNET is an extension of the procedure proposed for isotropic materials.

3.4.1 Analytical Method

The methodologies described in paragraph 3.2.1 are not suited for layered materials. For this class of materials the resonant method has been extended in Chiu and Case (1991). Starting from the well known Bernoulli-Euler equation, which describes the transverse (i.e. flexural) motion of a homogeneous isotropic

linear elastic beam, they have founded an implicit form for the frequency equation. In particular, considering a bi-layered sample (see Figure 3.7) with free end conditions and neglecting shear and rotary inertia effects, a frequency equation suitable for the elastic characterization can be written as follows:

$$f_1 = \frac{k_1^2}{2\pi} \left\{ \frac{E_c I_c + E_s I_s}{\rho_c A_c + \rho_s A_s} \right\}^{1/2}$$

(3.9)

where k_1 is a constant equal to $k_1=4.73004/L$, E_i represents the in-plane elastic modulus, A_i is the cross sectional area, ρ_i the mass density, I_i the second moment of area of the cross section with respect to the neutral axis, L is the length of the composite beam while the subscript c and s refer to the coating and the substrate, respectively.
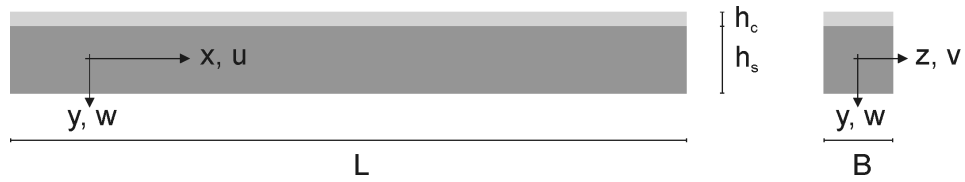
Figure 3.7. Schematic representation of a bi-material beam.

The in-plane elastic modulus of the coating can be obtained using Eq.(3.9). As it is in implicit form an iterative procedure should be used, however, in the present work, the function *Solve* available in the software package *Mathematica*® (Wolfram, 2006) has been used to obtain an explicit form:

$$E_c = \frac{1}{L^4} \left(\begin{array}{l} -2.0\,E_s h_c^3 h_s - 3.0\,E_s h_c^2 h_s^2 - 2.0\,E_s h_c h_s^3 + \\ 0.4732\,f_1^2 L^4 (h_c^2{}_c + h_c h_s{}_s) + \\ \sqrt{-994580\,E_s h_c^4 h_s (248645\,E_s h_s^3 - 235344\,f_1^2 L^4 (h_c{}_c + h_s{}_s)) + } \\ h_c^2 (E_s h_s (1.492 \times 10^6 \, h_c h_s + 994580 (h_s^2 + h_c^2)) \\ -235344\,f_1^2 L^4 (h_c{}_c + h_s{}_s))^2 \end{array} \right)$$

(3.10)

From the equation it is possible to see that, in order to find the coating Young's modulus, the property of the substrate have to be known. This is the main drawback of the technique. Moreover it is not possible to find Poisson's ratio by this equation because only the Young modulus affect the flexural

frequencies. To find Poisson's ratio a Mixed Numerical-Experimental Technique is necessary.

3.4.2 Assessment of the MNET for characterizing layered materials

In the case of layered beam-like samples there are no equations available that connect both the elastic moduli to frequencies. In the present dissertation, the possibility of using MNET to take into account also the Poisson ratio has been investigated. The procedure implemented for characterizing layered materials is the same of that for the isotropic materials; in fact only a change of the FE model was necessary. Also for these procedure, in order to find the elastic moduli of the coating materials the elastic moduli of the substrate materials have to be known.

3.4.2.1 Error function and sensitivity analysis

As for isotropic materials, the inverse problem for layered materials is very sensitive to the choice of the error function. For this case, the error function (φ_3) described in Eq. (3.6) has been used. In Figure 3.8 the contour plots of the error function φ_3, adimensionalized by the maximum value versus E- calculated considering the first frequency (a) or the first and the second frequencies (b) of a layered beam are reported.
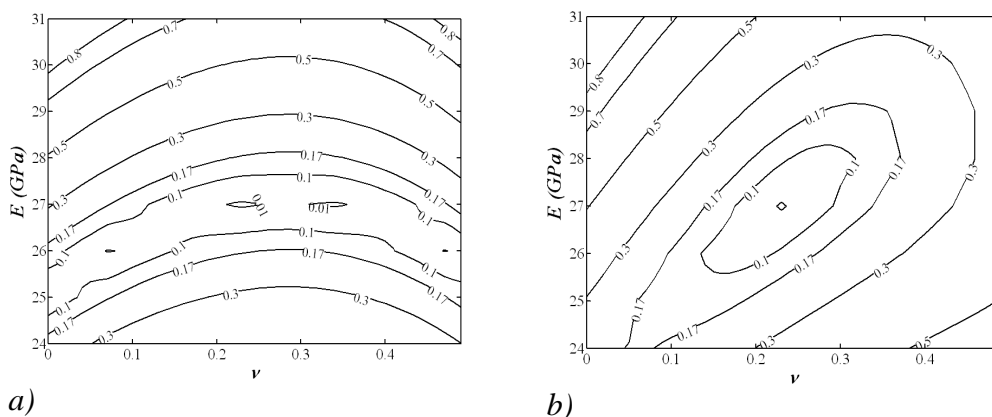

a)
b)

Figure 3.8 - Contour plot of φ_3/φ_{3max} of layered beam considering:
a) first frequency; b) first and second frequencies.

For the numerical simulations, the following model parameters have been used: L=100 mm, B=25 mm, h_s=4 mm, h_c=0.4, E_s=210 GPa, E_c=27 GPa ,ν_s=0.30,

$\nu_c=0.22$, $\rho_s= 7.8$ Kg/dm^3, $\rho_c=5.4$ Kg/dm^3. If the Poisson's ratio (or the shear modulus) is requested, a minimum of two frequencies is necessary. In fact, as it is possible to see from Figure 3.8, only the Young modulus can be found by the first frequency (if the Poisson's ratio is fixed a priori or if approximated results are allowed).

a)   b)
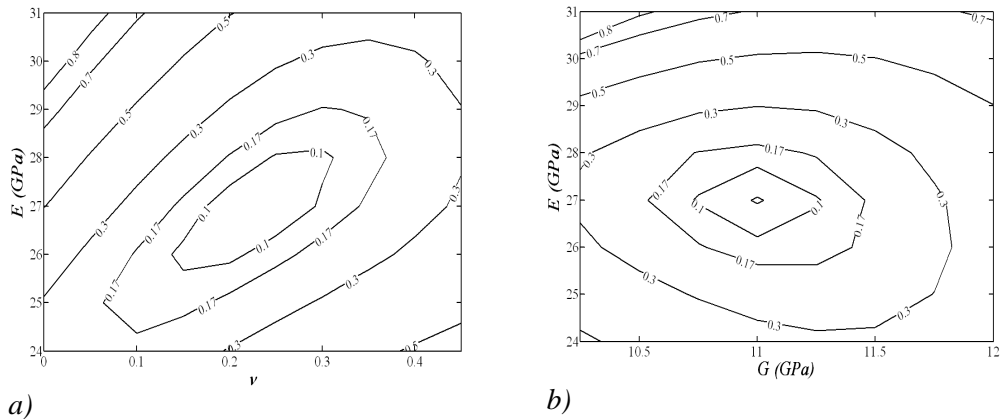
Figure 3.9 - Contour plot of φ_3/φ_{3max} of layered beam:
a) φ_3 versus E-ν b) φ_3 versus E-G function.

In Figure 3.9 the contour plots of the error function φ_3/φ_{3max} versus E- (a) and versus E-G (b) calculated considering the first four frequencies of a layered beam are reported while the first four natural modal shapes and resonant frequencies of the examined beam are reported in Table 3.10.

Table 3.10 - Modal shapes and resonant frequencies of the examined beam (free-free condition).

| *f$_1$: 2101.0 Hz* | *f$_2$: 4859.8 Hz* |

| *f$_3$: 5749.3 Hz* | *f$_4$: 9993.3 Hz* |
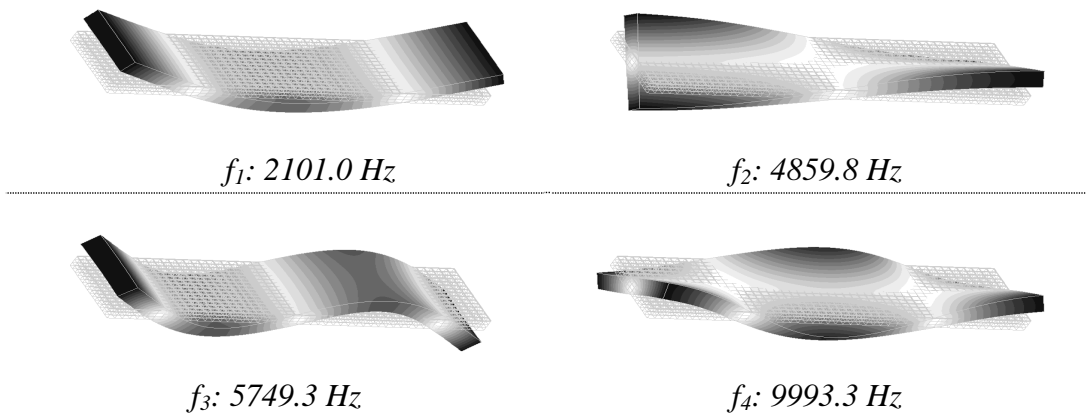
In coated beams the sensibility of the frequencies to Poisson's ratio is low. The Young's and shear moduli have bigger influence on the first two frequencies

(flexural and torsional respectively). In an iterative process, the use of the Young's and shear moduli makes the problem well-conditioned. As for isotropic plates, to decrease the experimental noise, four frequencies are preferred to two.

The effectiveness of the procedure has been verified numerically, by simulating the process of elastic characterization for a layered sample. The characterization process has been carried out only for the coating properties; the substrate moduli have been taken as known values. In the first stage, the sample has been modelled, meshed and then numerically processed for the calculation of the first four resonant frequencies. Successively, using the same finite element model and the values of the resonant frequencies previously calculated as simulated experimental data, the identification process has been carried out. To simulate the experimental errors, three level of Gaussian noise (0.5%, 1.0% and 1.5%) have been added to the numerical frequencies. The sample has been meshed using twenty node CHEXA elements of NASTRAN library. Such results have been obtained considering two layered beam having the same properties used in the previous analysis. The material characterization process has been carried out using the simplex method, assuming the following trial values for the elastic constants: E_c=50 GPa, ν_c=0.3 or G_c=16 GPa. In order to show the sensitivity of the optimization to the elastic parameters two series of analyses have been carried out; in the first series the Young's modulus and Poisson's ratio have been considered unknown values of the iterative process, in the second one the shear modulus has been considered instead of the Poisson's ratio.

Table 3.11 Sensitivity analysis results obtained using φ_3

Gaussian Noise		1st series Optimization variables		2nd series Optimization variables	
		E_c [GPa]	ν_c	E_c [GPa]	G_c [GPa]
0.0%	$\bar{x}$	40.0	0.220	40.0	16.0
	$_x\%$	0.0%	0.0%	0.0%	0.0%
0.5%	$\bar{x}$	40.2	0.210	39.6	16.7
	$_x\%$	9.0%	30.3%	8.2%	8.4%
1.0%	$\bar{x}$	39.5	0.220	38.9	15.9
	$_x\%$	13.5%	45.6%	16.7%	16.7%
1.5%	$\bar{x}$	38.5	0.218	40.5	15.5
	$_x\%$	18.7%	51.3%	18.9%	22.3%

In Table 3.11 the mean values and mean standard deviations of the normal distributions of the results for the two series, for the three levels of noise, 0.5%, 1.0% and 1.5%, respectively, are reported.

Table 3.12 – Comparison of the sensitivity to experimental noise for different sample

		2nd series		3rd series		4th series	
Es		210.0 GPa		70.0 GPa		210.0 GPa	
h$_s$		4.000 mm		4.000 mm		1.000 mm	
Ec/Es		0.19		0.57		0.19	
h$_s$/h$_c$		11.4		11.4		2.9	
Gaussian Noise		**E$_c$ [GPA]**	**G$_c$ [GPA]**	**E$_c$ [GPA]**	**G$_c$ [GPA]**	**E$_c$ [GPA]**	**G$_c$ [GPA]**
0.0%	$\bar{x}$	40.0	16.0	16.0	16.0	40.0	16.0
	$_x$%	0.0%	0.0%	0.0%	0.0%	0.0%	0.0%
0.5%	$\bar{x}$	39.6	16.7	39.5	16.4	40.3	16.3
	$_x$%	8.2%	8.4%	4.7%	4.5%	2.3%	2.7%
1.0%	$\bar{x}$	38.9	15.9	38.4	16.0	38.8	16.1
	$_x$%	16.7%	16.7%	8.0%	6.1%	6.5%	3.6%
1.5%	$\bar{x}$	40.5	15.5	41.3	15.9	39.6	16.1
	$_x$%	18.9%	22.3%	9.4%	9.7%	8.0%	5.9%

The results obtained by the simplex method coupled to the objective function φ_3 showed a high sensitivity of the technique to the optimization variables. This is due to the high impact that the shear modulus has on the second frequencies. This problem is very high in beam-like sample. To have a higher sensitivity to the Poisson's ratio a lower Young's modulus ratio (E_s/E_c) or lower thickness ratio (h_s/h_c) are more desirable. This can be confirmed by Table 3.12, where the mean and the standard deviation of the elastic moduli obtained on two series of twenty tests carried out on different layered samples are reported (in order to compare with the previous results the second series is also reported in the table). The third series of simulations has been carried out considering the same geometry described for the second series but using a lower Young's moduli ratio; while in the fourth series of simulations the same Young's moduli ratio and a lower thickness ratio of the second series have been taken into account.

3.5 Conclusions

The proposed identification procedure allows the elastic properties of isotropic materials to be easily determined. In particular, the Young modulus and Poisson ratio in a FE model of the specimen are updated until the corresponding

first four natural frequencies match the experimental ones as closely as possible. To this aim, different optimization methods and error functions have been compared in order to select the combination which provides the shortest solution times. The best performance has been obtained coupling the square root of the sum of the squares error function with the simplex method. Numerical simulations, carried out on a series of typical and atypical shaped plates models, have proven the effectiveness of the proposed approach. Moreover, the robustness of the identification process with respect to measurement noise has been also assessed. It has been observed that the sensitivity of the Young modulus to experimental errors in frequency measurement is negligible, no matter the shape of the plate. On the contrary, the sensitivity of the Poisson ratio to experimental errors is strongly influenced by the shape under investigation. Therefore, in order to avoid an incorrect estimation of the Poisson ratio in case of plates with a particularly complex shape, it is always recommended to previously verify the sensitivity. It is worth noting, that the usefulness of the proposed procedure can be fully exploited when the production of proper bulk specimens is not feasible or when the material sample to be tested cannot be damaged or processed to a conventional testing geometry (e.g. reduced machinability or high cost, etc.) and thus should be tested as is. Finally, numerical simulations have permitted to confirm the feasibility of using the dynamic technique to characterise the layered materials. The iterative method permits to find both the elastic moduli of the coating differently from the analytical methods by which only the Young modulus is carried out. The technique had shown a high sensitivity to the optimization variables and sample parameters like the thickness ratio and Young's moduli ratio. Unfortunately the technique presents some drawbacks. First of all, there is the computational time for the FEA, which may be reduced using cluster of computer or multi-processor computer.

3.6 Bibliography

Alfano, M., Pagnotta, L., 2007. A non destructive technique for the elastic characterization of thin isotropic plates. NDT&E International, 40 (2), 112-120.

Alfano, M., Pagnotta, L., Stigliano, G., 2007. Identifying elastic properties of isotropic materials by finite element analyses and vibration data. Key Engineering Materials, 346, 1327-1330.

Alfano, M., Pagnotta, L., Stigliano, G., 2006. International conference, ISMA 2006. Belgium. 2033-2040.

Antunes, J.M., Fernandes, J.V., Sakharova, N.A., Oliveira, M.C., Menezes, L.F., 2007. On the determination of the Young's modulus of thin films using indentation tests. International Journal of Solids and Structures, 44, 8313-8334.

ASTM Standard E1875-00e1. Standard test method for dynamic Young's modulus, shear modulus, and Poisson's ratio by sonic resonance, book of standards Volume 03.01.

ASTM Standard E132-04 Standard Test Method for Poisson's Ratio at Room Temperature.

ASTM Standard E111-04 Standard Test Method for Young's Modulus, Tangent Modulus, and Chord Modulus.

ASTM Standard C1161-02 Standard Test Method for Flexural Strength of Advanced Ceramics at Ambient Temperature.

ASTM Standard E143-01; Standard test method for shear modulus at room temperature; Annual book of ASTM standard; Vol.03.01; 2001.

ASTM Standard C1273-95; Standard test method for tensile strength of monolithic advanced ceramics at ambient temperature; Annual book of ASTM standard; Vol.15.01; 1995.

Araújo, L., Mota Soares, C.M., Herskovits, J., Pedersen, P., 2002. Development of a finite element model for the identification of mechanical and piezoelectric properties through gradient optimization and experimental vibration data. Composite Structures, 58 (3), 307-318.

Atri, R.R., Ravichandran, K.S., Jha, S.K., 1999. Elastic properties of in-situ processed Ti-TiB composites measured by impulse excitation of vibration. Material Science and Engineering A, 271, 150-159.

Ayorinde, E., 1995. Elastic constants of thick orthotropic composite plates. Journal of composite materials, 29, 1025-39.

Ayorinde, E., Gibson, R.F., 1993. Elastic constants of orthotropic composites materials using plates resonance frequencies, classical lamination theory and an optimized three mode Rayleigh formulation. Composites Engineering, 3, 395-407.

Beghini, M., Benamati, G., Bertini, L., Frendo, F., 2001. Measurement of coatings' elastic properties by mechanical methods: Part 2. Application to thermal barrier coatings Experimental Mechanics, 41 (4), 305-311.

Beghini, M., Bertini, L., Frendo, F., 2001. Measurement of coatings' elastic properties by mechanical methods: Part 1. Consideration on experimental errors. Experimental Mechanics, 41 (4), 293-304.

Bledzkia, A.K., Kesslera, A., Rikards, R., 1999. Determination of elastic constants of glass/epoxy unidirectional laminates by the vibration testing of plates Composites Science and Technology, 59 (13), 2015-2024.

Bruno, L., Furgiuele, F.M., Pagnotta, L., Poggialini, A., 2002. Determination of elastic constants of anisotropic plates by phase stepping speckle interferometry. Key Engineering Materials, 221 (2), 363-373.

Caillet, J., Carmona, J.C., Mazzoni, D., 2007. Estimation of plate elastic moduli through vibration testing. Applied Acoustics, 68, 334–349.

Chiu, C.C., Case, E.D., 1991. Elastic modulus determination of coating layers as applied to layered ceramic composites. Materials Science and Engineering A, 132, 39-47.

Chudoba, T., Schwarzer, N., Richter, F., 2002. Determination of elastic properties of thin films by indentation measurements with a spherical indenter. Surface and Coatings Technology, 127, 9-17.

Deobald, L.R., Gibson, R.F., 1988. Determination of elastic constants of orthotropic plates by modal analysis/Rayleigh-Ritz technique. Journal of Sound and Vibration, 124, 269-283.

D'Evelyn, M.P., Taniguchi, T., 1999. Elastic properties of translucent polycrystalline cubic boron nitride as characterized by the dynamic resonance methods. Diamond and Related Materials, 8, 1522-1526.

D'Evelyn, M.P., Zgonc, K., 1997. Elastic properties of polycrystalline cubic boron nitride and diamond by dynamic resonance measurements. Diamond and Related Materials, 6, 812-816.

De Wilde, W.P., Narmon, B., Sol, H., Roovers, M., 1984. Determination of the material constants of an anisotropic lamina by free vibration analysis. Proc. 2nd International Modal Analysis Conference. Orlando, Fl. 44-49.

De Wilde, W.P., Sol, H., Overmeire, M.V., 1986. Coupling of lagrange interpolation modal analysis and sensitivity analysis in the determination of anisotropic plate rigidities. Proc. 4th International Modal Analysis Conference. Los Angeles. 1058-1063.

Förster F., 1937. Ein neues messverfahren zur bestimmung des elastizitätsmoduls und der dämpfung (New method for determination of modulus of elasticity and damping). Zeitschrift fur Metallkunde. 29 (4), 109-115.

Fällström, K.E., Jonsson, M., 1991. A nondestructive method to determine material properties in anisotropic plates. Polymer Composites, 12 (5), 293-305.

Fällström, K.E., 1991. Determining material properties in anisotropic plates using Rayleigh's method. Polymer Composites, 8, 306-314.

Frederiksen, P.S., 1997. Numerical studies for the identification of orthotropic elastic constants of thick plate. European Journal of Mechanics A/Solids, 16 (1), 117-140.

Frederiksen, P.S., 1995. Single-layer plate theories applied to the flexural vibration of completely free thick laminates. Journal of Sound and Vibration, 186, 743-59.

Furgiuele, F.M., Muzzupappa, M., Pagnotta, L., 1997. A full-field procedure for evaluating the elastic properties of advanced ceramics. Experimental Mechanics, 37 (3), 285-290.

Grédiac, M., Paris, P.A., 1996a. Direct identification of elastic constants of anisotropic plates by modal analysis: theoretical and numerical aspects. Journal of Sound and Vibration, 195 (3), 401-415.

Grediac, M., Fourier, N., Paris, P.A., Surrel, Y., 1996b. Direct identification of elastic constants of anisotropic plates by modal analysis: experiment and results. Journal of Sound and Vibration, 210 (5), 645–659.

Hwang, S.F., Chang, C.S., 2000. Determination of elastic constants of materials by vibration testing. Composite Structures, 49, 183-190.

Ide, J.M., 1935. Some dynamic methods of determination of Young's modulus. Review of Scientific Instruments. 6 (10), 296-298.

Kim, H.J., Kweon, Y.G., 1999. Elastic modulus of plasma-sprayed coatings determined by indentation and bend tests. Thin Solid Films, 342 (1-2), 201-206.

Lai, T.C., Lau, T.C., 1993. Determination of elastic constants of a generally orthotropic plate by modal analysis. International Journal of Analytical and Experimental Modal Analysis, 8, 15-33.

Leisure, R.G., Willis, F.A., 1997. Resonant ultrasound spectroscopy. Journal Phys. Condens Matter, 9, 6001-6029.

Liu, G.R., Han, X., 2003. Computational inverse techniques in nondestructive evaluation. CRC Press LLC, Singapore.

Liu, S., Wang, Q.J., 2007. Determination of Young's modulus and Poisson's ratio for coatings. Surface and Coatings Technology, 201, 6470-6477.

Maletta, C., Pagnotta, L., 2004. On the determination of mechanical properties of composite laminates using genetic algorithms. International Journal of Mechanics and Materials in Design, 1 (2), 199-211.

Migliori, A., Darling, T.W., 1996. Resonant ultrasound spectroscopy for materials studies and non-destructive testing. Ultrasonics, 34 (2), 473-476.

Mencik, J., 1996. Mechanics of components with treated or coated surfaces. Kluwer Academic Publishers Group,

Mota Soares, C.M., Freitas, M.M.D., Araùjo, A.L., Pedersen, P., 1993. Identification of material properties of composite plate specimens. Composite Structures, 25 277-285.

Muthurajana, K.G., Sanakaranarayanasamyb, K., Nageswara Raoc, B., 2004. Evaluation of elastic constants of specially orthotropic plates through vibration testing. Journal of Sound and Vibration, 272, 413-424.

Oliver, W.C., Pharr, G.M., 1992. An improved technique for determining hardness and elastic modulus using load and displacement sensing indentation experiments. Journal of Materials Research, 7 (6), 1564-1583.

Pagnotta, L., 2007. Determining elastic constants of materials with interferometric techniques. Inverse Problems in Science and Engineering, 14 (8), 801 – 818.

Pagnotta, L., Stigliano, G., 2008. Elastic characterization of isotropic plates of any shape via dynamic tests: theoretical aspects and numerical simulations. Mechanics Research Communications, 35 (6), 351–360.

Pagnotta, L., Stigliano, G., 2006. A numerical-experimental approach for identification of material constants of composite laminates by displacement field measurement. WSEAS Transactions on Applied and Theoretical Mechanics, 1 (1), 39 – 46.

Pedersen, P., 1989. Optimization method applied to identification of materials parameters. In Eschenauer HA, Thierau G. editors, Discretization Methods and Structural Optimization-Procedures and Applications, Berlin, Springer-Verlag, 277-283.

Pedersen, P., Frederiksen, P.S., 1992. Identification of orthotropic material moduli by a combined experimental/numerical method. Measurement, 10, 113-118.

Pickett, G., 1945. Equations for computing elastic constants from flexural and torsional resonant frequencies of vibrating prisms and cylinders. Proceedings ASTM. 45, 846-865.

Qian, G.L., Hoa, S.V., Xiao, X., 1997. A vibration method for measuring mechanical properties of composite, theory and experiment. Composite Structures, 39, 31-38.

Radovic, M., Lara-Curzio, E., 2004. Mechanical properties of tape cast nickel-based anode materials for solid oxide fuel cells before and after reduction in hydrogen. Acta Materialia, 52, 5747-5756.

Radovic, M., Lara-Curzio, E., Riester, L., 2004. Comparison of different experimental techniques for determination of elastic properties of solids. Material Science and Engineering A, 368, 56-70.

Reddy, J.N., 1984. A Simple Higher-Order Theory for Laminated Composite Plates. Journal of Applied Mechanics, 51, 745-752.

Rikards, R., Chate, A., Gailis, G., 2001. Identification of elastic properties of laminates based on experimental design. International Journal of Solid and Structures, 38, 5097-5115.

Schmidt, R., Wicher, V., Tilgner, R., 2005. Young's modulus of moulding compounds measured with a resonance method. Polymer Testing, 24, 197-203.

Sol, H., 1986. Identification of anisotropic plate rigidities using free vibration data. PhD Thesis, University of Brussels.

Sol, H., Hua, H., De Visscher, J., Vantomme, J. and De Wilde, W.P., 1997. A mixed numerical/experimental technique for the nondestructive identification of the stiffness properties of fibre reinforced composite materials. NDT & E international, 30 (2), 85-91.

Spinner, S., Teft, W.E., 1961. A method for determining mechanical resonance frequencies and for calculating elastic moduli from these frequencies. Proceedings ASTM. 61, 1209-1221.

Timoshenko, S.P., Goodier, J.N., 1970. Theory of elasticity. McGraw-Hill Publishing Co., Tokyo.

Wang, W.T., Kam, T.Y., 2000. Material characterization of laminated composite plates via static testing. Composite Structures, 50 (4), 347-352.

Warburton, G.B., 1953. The vibration of rectangular plates. Proceedings of the Institution of Mechanical Engineers. 168, 371-384.

Wolfram S., 1999. The Mathematica Book, 4th ed. Wolfram Media. Cambridge University Press.

Yaoita, A., Adachi, T., Yamaji, A., 2005. Determination of elastic moduli for a spherical specimen by resonant ultrasound spectroscopy. NDE&T, 38 (7), 554-560.

4 EXPERIMENTAL VALIDATION OF THE DYNAMIC TECHNIQUE

4.1 Introduction

The dynamic characterization procedure has been successfully validated in a numerical way in the previous section. This chapter presents some experimental test-cases carried out on samples of different materials and shapes. The experimental-tests are intended to validate the proposed technique in an experimental way. The results have been compared with that obtained with other techniques (dynamic and static) carried out on the same samples. For layered materials there are problems in validation of the procedure due to inexistence of standardised methods for it, and so a comparison with values found in literature has been done.

4.2   Elastic constant identification of isotropic plate

In order to verify the effectiveness of the proposed procedure and to carry out a useful cross-check with the results provided by other methodologies, several test plates with different aspect ratios (*i.e. a/b*) (Alfano *et al.*, 2006a, 2006b, 2007; Deobald *et al.*, 1988; Hwang *et al.*, 2000; Bruno *et al.*, 2006) and different shapes (Bruno *et al.*, 2008) examined in literature have been considered. For plates of irregular shape a cheaper procedure for size and shape measurement of the samples is proposed, and, in the end, a comparison with values available in literature for the same material has been done.

4.2.1 Validation of the direct technique

In the present dissertation the direct procedure for determining the elastic properties of isotropic rectangular plates, described in the previous chapter, has been assessed using cold rolled aluminium alloy (6082-T6) thin plate samples. The length (*a*) and the width (*b*) of the plates, reported in Table 4.1, have been measured using a standard caliper while the thicknesses (*t*) have been determined by averaging a series of measurements carried out with a digital millesimal micrometer in various points of the sheet. Standard deviations for *a*, *b* and *t* measurements were never higher than 0.02%, 0.02% and 0.2%, respectively. The density of the material is calculated averaging the values of the ratio m/V, where m is the mass of the plate measured with a centesimal digital balance and V is the volume of the plate determined using the geometric data.

Table 4.1 – Dimensions, masses and acquired frequencies of the specimens

Length, $\bar{a}$ (mm)	Width, $\bar{b}$ (mm)	Aspect ratio, *a/b* nominal	actual*	Thickness, $\bar{t}$ (mm)	Mass, $\bar{m}$ (g)	Frequencies [Hz] I	II	III	IV
101.42	101.37	1.000	1.000 (0.0%)	0.936	25.85	298.7	437.1	555.4	775.4
151.50	101.18	1.500	1.497 (0.2%)	0.940	38.71	199.9	217.9	463.5	506.1
201.55	101.16	2.000	1.992 (0.4%)	0.939	51.57	121.2	149.9	330.3	339.9
250.52	101.39	2.500	2.471 (1.2%)	0.937	63.93	78.8	118.2	219.5	254.6

* the number in bracket represents the difference with respect to the nominal value

The resonant frequencies have been measured by the impulsive excitation technique (see Figure 4.1). The apparatus comprised a microphone with a passing band from 80 to 20000 Hz, and a sound card with a sampling frequency of 44.100 kHz (microphones and sound cards of this type are commercially available at low cost). A suitable dedicated software has been implemented in MATLAB^{TM} environment for analysing and processing the signal to identify the natural frequencies. A series of procedures have been developed by the MATLAB^{TM} function library. The first procedure carries out the function of spectrum analyzer, acquires the digitalised signals (8 or 16 bit) coming from the receiver and operates the transformation from the time domain to the frequency domain by a Fast Fourier Transform (FFT) algorithm. A second procedure allows the identification of the natural frequencies by searching, within the frequency spectrum, for the frequency values corresponding to a peak of amplitude greater than the threshold defined by the user. In order to obtain a resolution of less than 0.5 Hz, acquisition times greater than 3s have been assumed. To attenuate the effect of the background noise and highlight the peaks of the frequency spectrum of the signal, the average of several surveys impacting the plate at several points has been analysed. Tests carried out with the microphone placed at different distances from the surface (in a range between 5 and 20 millimetres), confirmed that the variation of frequencies due to acoustic stiffness is negligible.
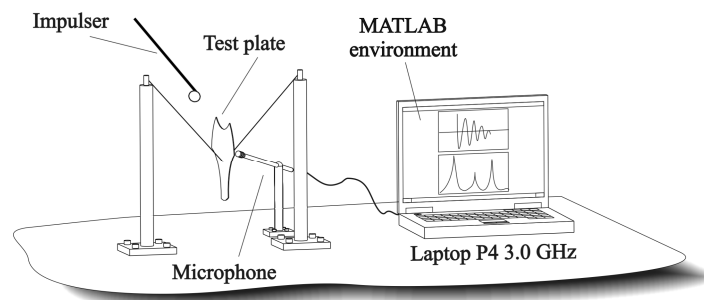

Figure 4.1 Equipment for resonant frequencies measurement

Using the measured natural frequencies and the test procedure described in the previous chapter it is possible to carry out the elastic characterization of the plate. For this purpose, one can choose a graphic or a numerical (with tables) approach. In the present dissertation the elastic properties have been calculated

using the second approach. In particular, suitable tables obtained by means of FEA calculations (following the procedure reported in Alfano and Pagnotta, 2007) have been used in MATLAB$^®$ that performs numerical interpolation. In Appendix C the algorithm, developed in MATLAB$^®$ environment is reported. A study has been done for each model to determine the mesh density at which values of the first 6 resonant frequencies converge (for mesh property see the next section). Damping has been neglected in the model because of its negligible influence on the natural frequencies and the normal modal analyses have been carried out by using Solution 103 and the Lanczos extraction method available in the FEA code (Sitton, 1997).

Table 4.2 - Values obtained for Young's modulus and Poisson's ratio

a/b	1.0		1.5		2.0		2.5	
ν	ν_{31}	0.338 (-)	ν_{42}	0.300 (-4.9%)	ν_{21}	0.321 (3.0%)	ν_{21}	0.336 (9.1%)
	ν_{32}	0.328 (-)	ν_{32}	0.372 (1.9%)	ν_{31}	0.297 (3.8%)	ν_{41}	0.305 (11.2%)
	ν_{43}	0.338 (-)	ν_{41}	0.333 (-0.8%)	ν_{42}	0.345 (2.5%)	ν_{32}	0.350 (7.7%)
	0.335±0.09%		0.335±0.42%		0.321±2.50%		0.330±1.88%	
E(GPa)	E_{32}	70.0 (-)	E_{32}	72.2 (0.2%)	E_{21}	69.0 (0.3%)	E_{21}	69.4 (1.0%)
	E_{31}	70.8 (-)	E_{42}	72.0 (0.1%)	E_{31}	69.2 (0.3%)	E_{41}	69.6 (1.0%)
	E_{43}	70.0 (-)	E_{41}	70.8 (-0.4%)	E_{42}	70.1 (0.2%)	E_{32}	70.1 (0.7%)
	70.3±0.22%		71.7±0.17%		69.4±0.83%		69.7±0.53%	

The number in bracket represents the difference with respect to the
elastic properties obtained using "nominal table sets"

However, in order to obtain the elastic properties, the sensitivity of   to the changes in frequency, factor ratio, represented from the slope of the curve considered, should be taken into account; in particular, it plays a very important role in choosing suitable frequency ratios $_{(h,k)}/_{(l,j)}$ to compute . Relatively flatter curves propagate the experimental errors on frequency measurements less and are recommended. The values of Poisson's ratio and Young's modulus obtained using the chosen frequency ratios are shown in Table 4.2 with the associated combined expanded uncertainty calculated with a confidence level of 95% (International Organization for Standardization, 1995). In particular $_{ij}$ represents Poisson's ratio calculated using the frequency ratio f_i/f_j, while E_{ij} is the average of the two values

calculated by means of Eq. 3.3 using ($_{ij}$, f_i) and ($_{ij}$, f_j), respectively. The elastic properties reported herein have been calculated using table sets developed ad hoc for each of the actual aspect ratio (namely, the "actual table sets"). The differences between these values and those obtained using the "nominal table sets" are reported in brackets.

As it can be seen, the reliability of the results is good, the overall uncertainties associated with the measurement of the elastic properties are low; furthermore, the differences due to the use of nominal table sets instead of the actual ones should not be neglected. A proper numerical calibration is recommended when the aspect ratio differs from the nominal value, especially for larger values of *a*/*b*.

The same plates have been also analysed by the mixed numerical-experimental technique, described in the previous chapter, and the results are reported in the next section.

4.2.2 Validation of the iterative technique

4.2.2.1 Description of the identification process

The first step of the identification process consist on the measurement of size, shape, mass and resonant frequencies of the plate (see Figure 4.2). This can be efficiently carried out by an expert technician in a suitable laboratory equipped with sophisticated and expensive instruments, but, such measurements can also be carried out, easily and without significant repercussions on the results, with ordinary and relatively inexpensive equipments. For example, the shape and the size of the plate, can be measured by a caliper, if the shape is regular, or by CMM (Coordinate Measuring Machine) if the shape is irregular but it can be measured also with a resolution of less than 0.02 mm by a common digital scanner connected to a personal computer. For this purpose, the contour of the plate is drawn by superimposing a series of splines on the image of the plate acquired by a scanner and the coordinates of the contour points exported in a format that can be directly read by a mesh generator program. Some commercial graphical software (for example, CorelDraw™, Gimp, PhotoShop™ and others) allow this to be done. Regarding the plate thickness measurement, instruments of high accuracy

such as digital micrometers with a resolution of 0.001 mm can be used (thickness measurement is always more critical than in-plane size measurement, since bending stiffnesses depend on the cube of the thickness). If the plate has uniform thickness, a spot measurement, in theory, would be enough but, in practice, it is always more reliable to determine the thickness by averaging several measurements carried out at different locations of the plate. Generally, the mass of the plate is not critical data for the calculation of the frequencies, so that a digital scale with a resolution of one-hundredth of a gram is sufficient.
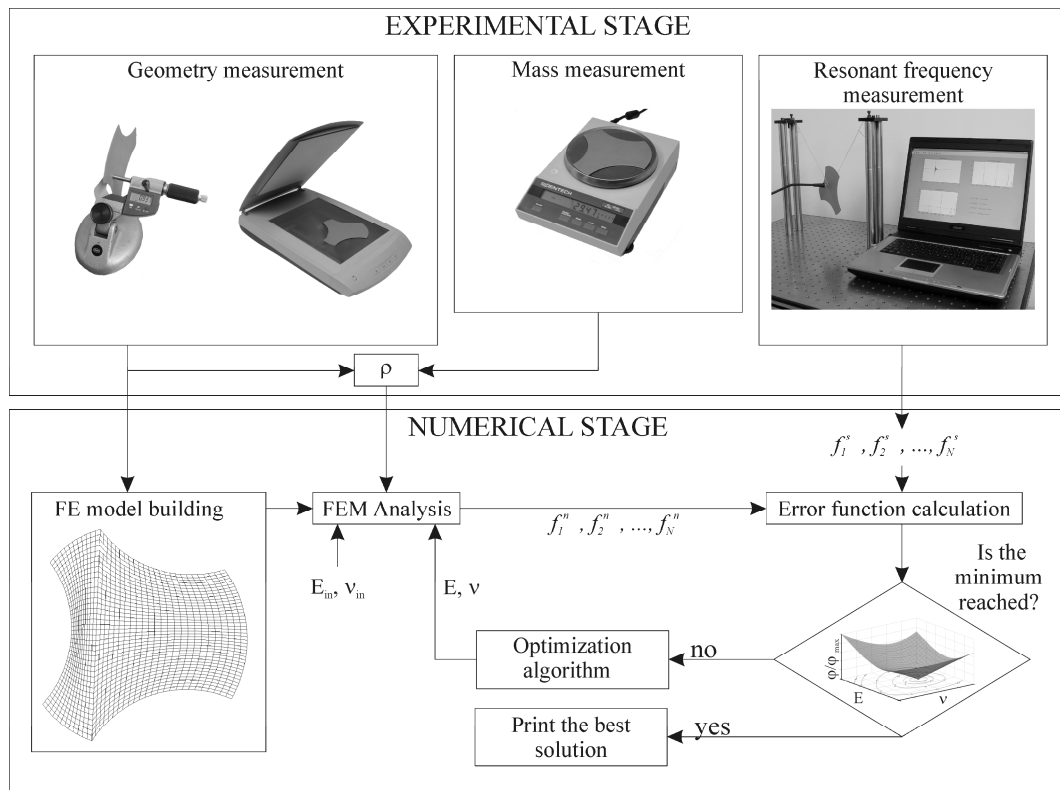

Figure 4.2 The identification process

Finally, for detecting the resonant frequencies, the simple and inexpensive impulsive excitation technique can be used. The experimental equipment is formed (see Figure 4.1) by a rigid frame, two elastic bands, a microphone to pick up the specimen response and a personal computer provided with a sound card. The plate is suspended in air with the two elastic bands fastened to the rigid frame. The exciting impulse is imparted repeatedly in various points by lightly hitting the plate with an impulser whose size and geometry depend on the size and the weight of the specimen and on the force required to induce vibrations. The dynamic response of the plate is detected by the microphone and sent in the form

of an electrical signal to the PC sound card. The signal is then analyzed and processed by dedicated software that identifies the values of the natural frequencies of vibration. Such software must operate as a spectrum analyzer, acquiring the digitalised signals coming from the receiver and operating the transformation from time domain to frequency domain by a Fast Fourier Transform (FFT) algorithm. Finally, the resonant frequencies must be identified. Such a procedure can be implemented in any environment (for example: LabView^{TM}, MATLAB^{TM}, etc.) using the proper library functions.

The second step of the identification process is the numerical stage (see Figure 4.2). In this phase the construction of the finite element model of the plate from the points acquired by digital scanner is carried out. The operation can be carried out with any of the commercial codes currently available for modelling and meshing a structural component (MSC/Patran^{TM}, Hypermesh^{TM} and others). The only requirement is the compatibility with the FEM solver used.

After that, the minimization process can start to identify the elastic moduli. This operation is carried out by a dedicated algorithm that can be implemented in any programming languages provided that this language can run the FEM solver and manipulate its input and output files. If a proper finite element code is not available, the resonant frequencies can be calculated by running a commercial FEM solver (for example: MSC/NASTRAN^{TM}, ANSYS^{TM}, ABAQUS^{TM}, etc.). The considered error function influences the choice of the optimization procedure and so is crucial in terms of solution time and accuracy. The robustness of the identification process with respect to noise measurement has been also assessed in the previous chapter. Taking into account the numerical results, the best error function in terms of solution time and accuracy is the following:

$$\varphi_3 = \sqrt{\sum_{i=1}^{N} \left(\frac{f_i^{\,n} - f_i^{\,e}}{f_i^{\,e}} \right)^2} \qquad\qquad (4.1)$$

4.2.2.2 Application and validation of the iterative technique

In order to show its effectiveness, the procedure has been applied first to four rectangular aluminium plates with different aspect ratio (these results have been compared with those obtained by applying the direct method), and to four differently shaped plates: a triangular aluminium plate, a thick circular steel plate

and two aluminium plates with irregular contours, one of which is drilled. The results obtained on the circular plate have been compared with that obtained by the ASTM standards method (ASTM E1876-01). In addition, the comparison with results found in literature on different materials are reported.

The aluminium plates have been all obtained from the same sheet. The thick circular plate machined from a steel bar (38NiCrMo4K) has a thickness of 6.027 mm. The plate dimensions have been chosen so that the resonant frequencies fall within the bandwidth of the microphone.

To create the FE model, the images of the plates have been acquired by an ordinary scanner (HP ScanJet 4400c) interfaced with a personal computer (Pentium 4 2.8 GHz). Using the software CorelDraw^{TM} the contours of each image have been outlined by superimposing a series of splines on them. The construction of the finite element models of the plates has been carried out starting from the coordinate data of the acquired contour points. Such points have been provided to MSC/PATRAN^{TM} software which has been used first to model and then to mesh the plate. The finite element models and the contours of the plates are illustrated in Table 4.3 and Table 4.4. In Table 4.5 the plate and FEM properties are reported.

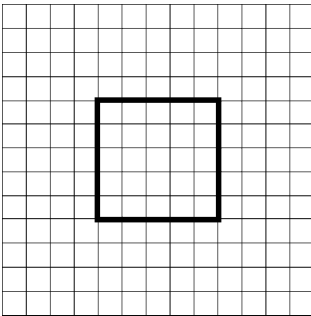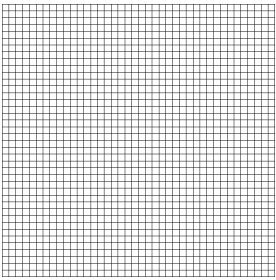**Table 4.3 - Contours and FEM of the plates**

Plate data	Finite element model
 ☐ = 20x20 mm	
 ☐ = 20x20 mm	
 ☐ = 20x20 mm	
 ☐ = 20x20 mm	
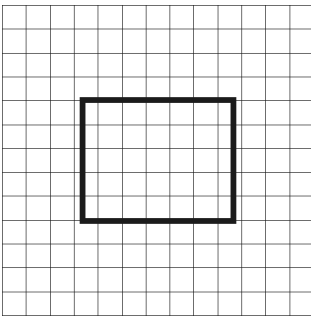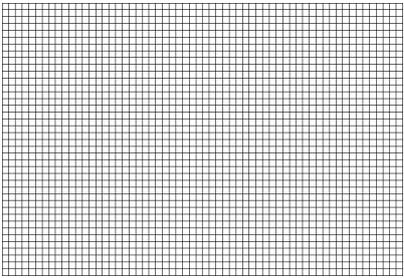
Table 4.4 - Contours and FEM of the plates

Plate data	Finite element models
  ☐ = 20x20 mm	
  ☐ = 20x20 mm	
  ☐ = 20x20 mm	
  ☐ = 20x20 mm	
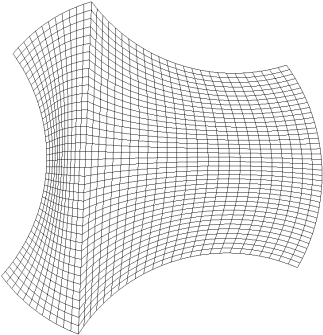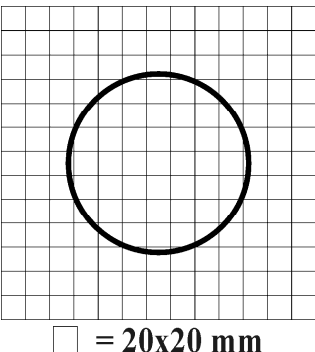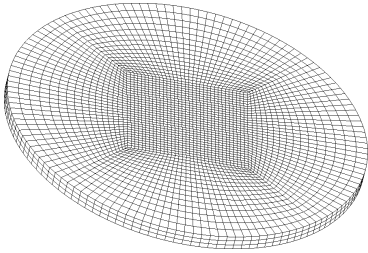
Table 4.5 - Dimensions, masses and mesh property of the specimens

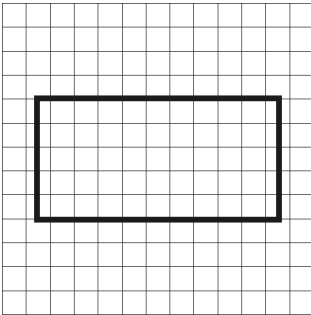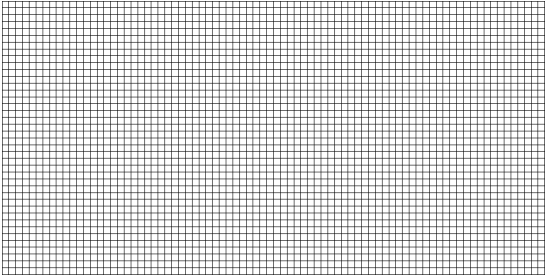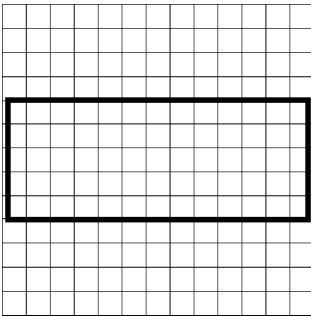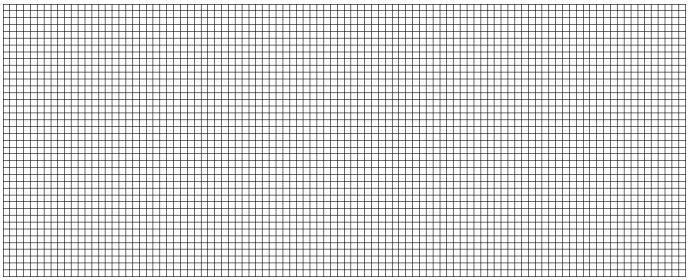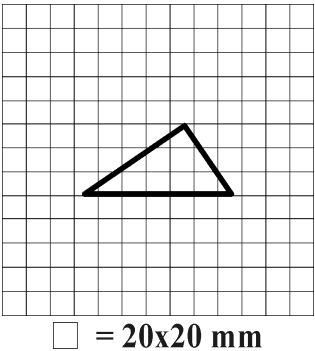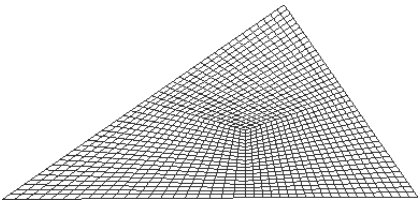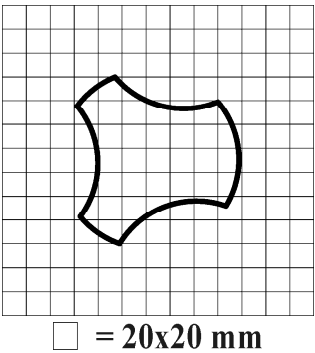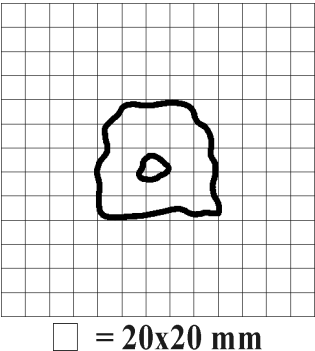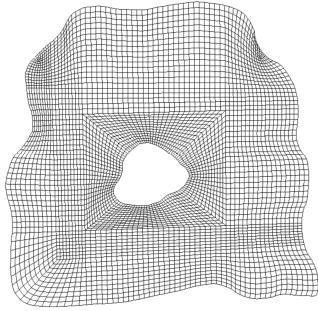| Shape	a/b*	Density [g/mm³]	Mass [g]	Thickness [mm]	Number of FE	FE Type
Rectangular	1.0	2.69·10⁻³	25.85	0.936	1600	Quad8
	1.5	2.69 10⁻³	38.71	0.940	2400	Quad8
	2.0	2.69 10⁻³	51.57	0.939	3200	Quad8
	2.5	2.69 10⁻³	63.93	0.937	4000	Quad8
Triangular	-	2.69 10⁻³	18.86	0.938	1200	Quad8
Irregular	-	2.69 10⁻³	29.31	0.937	1480	Quad8
Irregular and drilled	-	2.69 10⁻³	26.60	0.938	4460	Quad8
Circular	-	7.76 10⁻³	819.67	6.027	9602	Hex20

* nominal aspect ratio a/b;

The numerical procedure for the elastic identification has been implemented on a personal computer by using MATLAB^{TM}. The algorithm calls the finite element solver MSC/NASTRAN^{TM} for the dynamic analysis of the meshed model (see Figure 4.3). The simplex method (algorithm of Nelder and Mead) has been assumed as optimization method and has been called from the algorithm by the library function "fminsearch". The trial values for the elastic constants were included in the NASTRAN^{TM} input file which contains the topology of the FEM model for each iteration by using the MAT1 card which identifies the material properties. The modal analysis for predicting the resonant frequencies of the plates has been carried out using Solution 103, including the correction of transverse shear and rotary inertia effects, neglecting the damping and using the extraction method of Lanczos. In the post-processing stage, the desired first non-zero resonant frequencies have been saved (the first six modes for the free edge condition have zero frequency). Moreover, all the files generated from the FEM code were removed in order to release the memory of the computer. The error function described in equation (4.1) with N=4 has been assumed. The convergence test consists of controlling if, after a fixed number of successive iterations, the values of both elastic constants undergoing variation remain inside a prefixed tolerance. When, such a condition is verified the best solution is reached and the procedure is stopped.

Initial Solutions
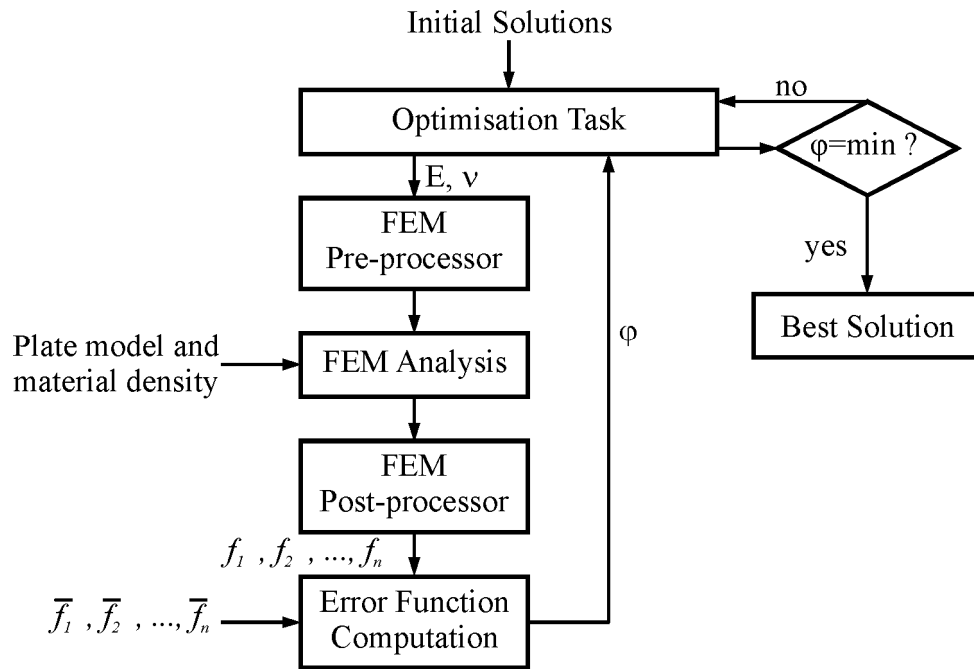
Figure 4.3 Optimization procedure

The results of the identification tests carried out on the aluminium specimens are reported in Table 4.6. The discrepancies among the identified values are due, certainly, to the many sources of error affecting the identification process. Classification of the sources of error and evaluation of the effects of each of these on the solutions is somewhat arduous.

Table 4.6 – Elastic moduli of the aluminium plates obtained by MNET

		Before annealing		After annealing	
Shape	**a/b***	ν	**E [GPa]**	ν	**E [GPa]**
	1.0	0.339	69.2	0.332	70.5
Rectangular	1.5	0.351	68.8	0.325	71.3
	2.0	0.369	69.1	0.329	69.9
	2.5	0.319	68.8	0.328	70.1
Triangular	-	0.337	70.3	0.326	71.3
Irregular	-	0.359	71.1	0.336	72.3
Irregular and drilled	-	0.342	70.6	0.344	70.0
Mean values	-	0.345	69.7	0.331	70.8
Standard deviation	-	4.7%	1.4%	2.0%	1.3%

* nominal aspect ratio a/b;

The errors mainly derive from the attempt to approximate the physical phenomenon by a mathematical model. In particular, in the identification process, the frequency calculation is carried out using an idealization of the real physical problem. As a result the real plate and the real test conditions can differ from the idealized models and this must be taken into account.

The plate vibration model, for example, is based on a theory that assumes small deformations and linear elastic behaviour of the material. In addition, damping is neglected and the plate is assumed to vibrate in vacuum with all edges free. In reality such conditions cannot be completely respected. When the impulsive excitation technique is used, a way to obtain a good approximation of the hypothesis of small deformations might consist in inducing low impact forces for causing small vibration amplitudes of the plate. The assumption of lack of damping is tolerable if materials exhibiting very low values of damping are examined. Metallic materials fall in such a category. In these cases, possible frequency shifts are, generally, negligible. Free boundary conditions can be accurately simulated locating support or suspension points along the nodal lines. If the latter are dubious or unknown for a mode of vibration, the location of the supports might be incorrect and affect the values of the related frequency. Generally, frequency values increase if there is additional stiffness. It must be stressed that, if the plate is suspended in air with wires, long wires reduce the stiffness but also increase the additional mass. Thus, if long but relatively light wires with respect to the mass of the plate are used, the influence of the suspension on the natural frequencies of the plate can be assumed to be negligible.

In addition, the finite element method gives approximated solutions with a level of accuracy depending on various factors: the mesh density, the type of theory used for the correction of transverse shear and rotary inertia effects, the type of eigenvalue extraction techniques employed, etc. Current commercial FEM codes provide a large number of possibilities for obtaining very reliable solutions with negligible errors in the calculation.

With regard to the plate model, it is assumed to be made of homogeneous and isotropic material and with geometry and nominal sizes which reproduce the real specimen with a high degree of accuracy. Dishomogeneities and anisotropies of the material affect the resonant frequencies and, if their presence is not recognized, they can lead to unreliable identified solutions. Moreover, the

dimensions of the model may not correspond perfectly to those of the real plate. Differences depend on the accuracy of the measurement system. For the sake of modelling simplicity, it is always preferable that the plate model is plane. Unfortunately, due to the fabrication process, real specimens can be inflected. Since even slight curvature could appreciably affect the values of the measured natural frequencies, they would always have to be avoided in the specimens.

The accuracy of measurements of the resonant frequencies is also affected by environmental noise and the resolution of the measurement system. In order to reduce the influence of the noise, the acoustic signal should not be acquired before the hammer strikes. In addition, the identification of the resonant frequencies would have to be carried out from an analysis of the frequency spectrum of the average of the plate responses, acquired in a series of tests performed at different impact points. Higher frequency spectrum resolutions could be obtained using long acquisition times of the signal and a zero-padding technique. However, the sensitivity analysis of the measurement errors, reported in previous section (and also in Pagnotta and Stigliano, 2008), where the effects of random noise on frequency measurements have been numerically simulated, have shown a very good stability of the solution even when the simulated noise was significant.

Among the causes disturbing the identification process, the effects of the cold rolling and cutting operations undergone by the specimens during the manufacturing processes are critical and difficult to control. Residual stresses and curvatures induced by these processes could cause the significant scattering (4.7%) observed in the Poisson ratio values reported in Table 4.6. To investigate the effects of cold working, the aluminium specimens have been first subjected to a typical annealing treatment (Davis, 1998) and then tested again. The results obtained before and after the treatment are compared in Table 4.6. As can be observed, the scattering in the Poisson ratio values is reduced significantly (1.3% as against 4.7%), after the thermal treatment, while no variation is observed on the value of the Young modulus. The reliability of such results is confirmed by the good agreement between their average values with the values obtained testing the same material by a static approach (Bruno *et al.*, 2008) reported in Table 4.7. In the same table the results of the investigation carried out on the circular steel plate are reported. In particular, a comparison with the results obtained testing the same

material according to the procedures recommended by the ASTM standard (E1876-01) is reported. Also in this case the agreement is very good.

Table 4.7. - Comparison with the results obtained by other techniques

	Method	ν	E [GPA]
Aluminium Irregular Plate	Present	0.336	72.3
	Static (Bruno *et al.*, 2008)	0.343	71.5
Steel Circular Plate	Present	0.281	205.5
	ASTM (*E1876-01*)	0.287	205.5

The effectiveness of the optimization methodology is well validated by the agreement (see Table 4.8) in the values of the measured frequencies after the thermal treatment and those calculated using the results of Table 4.6 and Table 4.7. It can be observed that the maximum percentage difference is less than 0,5%. This result confirms the effectiveness of the optimization algorithm.

Table 4.8 - Comparison of the calculated f_i^n and the measured f_i^e frequencies

Shape	a/b*		Mode (Hz)			
			I	II	III	IV
Rectangular	1.0	f_i^n	297.3	437.5	555.5	774.7
		f_i^e	298.7	437.1	555.4	775.4
		e_i (%)	0.5%	-0.1%	0.0%	0.1%
	1.5	f_i^n	199.3	219.0	463.3	505.6
		f_i^e	199.9	217.9	463.5	506.1
		e_i (%)	0.3%	-0.5%	0.0%	0.1%
	2.0	f_i^n	120.6	149.4	331.7	340.7
		f_i^e	121.2	149.9	330.3	339.9
		e_i (%)	0.5%	0.3%	-0.4%	-0.2%
	2.5	f_i^n	78.5	117.7	220.1	256.1
		f_i^e	78.8	118.2	219.5	254.6
		e_i (%)	0.4%	0.4%	-0.3%	-0.6%
Triangular	-	f_i^n	544.4	986.1	1422.9	1663.3
		f_i^e	545.0	986.7	1422.5	1662.4
		e_i (%)	0.1%	0.1%	0.0%	-0.1%
Irregular	-	f_i^n	249.9	323.6	383.4	610.9
		f_i^e	250.3	323.7	382.9	609.4
		e_i (%)	0.1%	0.0%	-0.1%	-0.2%
Irregular and drilled	-	f_i^n	286.0	373.4	472.9	737.2
		f_i^e	285.8	373.1	472.8	738.1
		e_i (%)	0.1%	0.1%	0.0%	-0.1%
Circular	-	f_i^n	1427.2	1427.2	2363.1	3274.4
		f_i^e	1426.6	1426.6	2363.4	3280.2
		e_i (%)	0.0%	0.0%	0.0%	-0.2%

* nominal aspect ratio a/b;

An additional validation has been done using experimental data found in literature. Material type, dimensions, masses and natural frequencies of the plates are reported in Table 4.9. Specimens S1-S2-S3 are aluminum, steel and CVD (Chemical Vapor Deposition) diamond square plates respectively. The natural frequencies of the plates have been measured using the impulse excitation technique.

Specimen S1 has been originally analyzed in Deobald and Gibson (1988) with a procedure suitable for orthotropic materials and, subsequently, in Alfano and Pagnotta (2006a) and Hwang and Chang (2000) using two different test methodologies. In particular, in Alfano and Pagnotta (2006a) the direct method showed in the previous section has been used; in Hwang and Chang (2000) an iterative procedure has been proposed in which up to ten resonant frequencies are given as input in order to obtain the elastic properties of both isotropic and orthotropic thin plates. In Alfano and Pagnotta (2006b, 2007) specimen S2-S3 have been analyzed. The specimen S3 has been also examined in Bruno *et al.* (2006) by means of full field measurements of the out-of-plane displacements, detected on the upper surface of the specimen in two biaxial bending tests.

Table 4.9 - Dimensions, masses and natural frequencies of the tested specimens

Sample[*]		Width a [mm]	Length b [mm]	Thickness h [mm]	Mass m [g]	f_1 [Hz]	f_2 [Hz]	f_3 [Hz]	f_4 [Hz]
S1	[1]	254.00	254.00	3.16	564.7	156.7	232.5	300.4	411.7
S2	[2]	101.10	101.10	0.945	73.74	315.0	458.0	563.0	813.0
S3		50.00	50.00	0.400	3.41	1608.0	2274.0	2412.0	3989.0

*S1: Al2024-T6; S2: Steel 38NiCrMo4K; S3: CVD-diamond;
[1]: Deobald and Gibson, 1988; [2]: Alfano and Pagnotta, 2006b, 2007

In order to implement the identification algorithm outlined in the previous section, 2-D finite element models have been developed. The number of elements chosen for the plate are: 40×40. Damping has been neglected in the model because of its negligible influence on the natural frequencies and the normal modal analyses have been carried out by using Solution 103 and the Lanczos extraction method available in the FEA code.

The results obtained are reported in Table 4.10: these are the mean values obtained using different starting guess points; the dispersion is negligible and convergence has been reached, on average, after about 60 runs of the FEA code.

Table 4.10 – Elastic moduli obtained with the present procedure and comparison with the results reported in literature

	Method	ν	E [GPA]
S1	Present	0.364	71
	Alfano and Pagnotta, 2006a [1]	0.363	71
	Deobald and Gibson, 1988 [2]	0.361	70
	Hwang and Chang, 2000 [2]	0.356	73
S2	Present	0.287	207
	Alfano and Pagnotta, 2007 [1]	0.289	209
S3	Present	0.083	691
	Alfano and Pagnotta, 2007 [1]	0.078	693
	Bruno et al., 2006	0.083	626

[1] average of the values obtained using different couples of frequencies according to the procedure proposed
[2] average of the Young moduli in the principal directions (*i.e.* E_1 and E_2)

The results obtained for S1 have been compared with those reported in Alfano and Pagnotta (2006a), Hwang and Chang (2000), Deobald and Gibson (1988). An excellent agreement among the results is observed (the relative errors are less than 2.8%). Also the results for steel are in good agreement with those obtained with other techniques. The results for CVD diamond present some difference with other technique, in particular for Poisson's ratio they are in agreement with that obtained in Bruno *et al.* (2006) while for Young's modulus are more close to the results of Alfano and Pagnotta (2007).

4.3 Elastic constant identification of layered material

In order to show the real applicability of the approach for layered materials, a real case has been studied. Steel plates (Fe-360) coated by plasma spray with ceria yttria co-stabilized zirconia (CYSZ) have been tested.

In order to improve the resistance against corrosion, wear and fatigue of mechanical components at high temperature, metallic as well as non metallic coatings are currently really widespread. In the last decades, thermal barrier coatings has been often the purpose of air plasma sprayed yttria stabilized zirconia (YSZ). It is used in stationary turbines of power plants and aircraft engines to improve thermal efficiency trough an increase of the inlet temperature. However, the drawback of YSZ is the tetragonal to martensitic transformation occurring at

high temperatures, which induces a disastrous volume expansion (from 3 to 5%) and the consequent fracture of the coating. In order to tackle this problem, new alternative materials have been proposed. In particular, it has been observed that the addition of ceria to tetragonal zirconia allows to obtain CYSZ which presents a higher phase stability than YSZ and is particularly promising for technical demanding applications.

Ceramic coatings deposition is mostly accomplished by Air Plasma Spray (APS) process. In a burner, a gas streaming through a high energy electric arc is changed into plasma with temperatures higher than 1000°C. These temperatures are sufficient for melting any materials, so the individual components, fed into the burner in the form of powder, are melted and driven by the plasma gas to impact with high velocity on the substrate. Thus, with APS the bonding between the substrate and the coating materials is achieved mechanically by high pressure. The rapid solidification of impacted molten droplets gives a highly heterogeneous microstructure consisting of irregular thin lamellae known as '*splats*'. This feature has a severe impact on the elastic response of the APS deposit and in particular on the Young modulus (Siebert et al., 1999; Kim and Kweon, 1999). As the basic properties of a coated system, for instance the adhesion strength or its thermo-mechanical behavior, mainly depend on the elastic modulus, it follows that APS CYSZ development demands an efficient, reliable and convenient methodology for its measurement.

Plasma spraying of the samples used for the experimental validation, has been carried out using a Sulzer Metco APS system, equipped with a F4-MB plasma torch (Sultzer Metco AG, Switzerland) mounted on an industrial robot. The feedstock is the commercial Metco 205NS (ZrO_2-25CeO_2-2.5Y_2O_3).

4.3.1 Application of the analytical formulation

Static test methods have proven to be powerful and effective for material characterization and, in addition, allow coatings to be tested in the same conditions as those encountered in real components. However, unlike dense ceramics, the final microstructure of plasma sprayed deposits is characterized by inter-lamellar pores and intra-lamellar cracks and this has a severe impact on the mechanical properties as they induce an anisotropic behaviour. In particular, inter-

lamellar cracks affect the in-plane elastic modulus, whereas the out of plane elastic modulus is affected by the intra-lamellar cracks (Kim and Kweon, 1999). As a consequence, it is necessary to consider the measurement direction when determining the elastic modulus of the deposit or comparing the results of different techniques. For instance, it has been demonstrated that the elastic modulus of the APS coatings determined by Nano-Indentation is different with respect to Bending Test (Kim and Kweon, 1999). Bending Test works at the macroscopic level and provides the in-plane elastic modulus from the tangent of the stress-strain curve of coated samples. Owing to splat boundary sliding and propagation of cracks, inelastic deformations occur during testing and, as a consequence, the results of Bending Tests are affected by this non linear stress-strain behaviour. Nano-Indentation probes the microstructure at the splat level, i.e. the microscopic scale, and, owing to the limited test volume, the resulting elastic modulus is nearly that of the splat itself. Therefore, it usually exhibits higher values with respect to the in-plane direction (usually up to 20 times higher) and this effect is more pronounced in ceramics than in metals coatings (Kroupa and J. Plesek, 2002). Even if Nano-Indentation and Bending Tests are currently used in order to obtain the elastic properties of plasma deposits, they are too tedious for a routine and cost-effective application in production. As an alternative, the use of dynamic test methods, in particular the resonant methods, has increased in the last decades. In Beghini et al. (2001a, 2001b) a comparison and a critical analysis, on the basis of the error propagation theory, of four-point bending tests and the resonance technique used for measuring the elastic properties of coatings have been presented.

From the experimental point of view, it is advisable to choose free ends condition, because it is easier to reproduce and affects less frequency measurements if compared, for instance, with clamped configurations. In order to simplify the identification procedure, the bond coat has been not applied. Nevertheless, the adhesion between coating and substrate was excellent. Other authors showed that the elastic modulus of the coating does not depend on coating thickness (Lauwagie, 2005). For each specimen a deposit thickness approximately equal to 350 µm has been chosen. So, the tests have been carried out on nominally identical coated samples whose dimensions are reported in Table 4.11. Thickness measurement is always critical for the quality of the results. Therefore, a digital

micrometer with a resolution of 0.001 mm has been used. For all the other length measurements a standard caliper with a resolution of 0.02 mm has been used.

The mass density of the steel substrates has been determined from the plate volume and mass. These last has been measured by a precision digital balance which is accurate to 0.01g. The mass density of the coating is that specified by the manufacturer (www.sulzermetco.com).

Table 4.11 - Geometrical and mass properties of coatings and substrates

Specimen		Density		Length L [mm]	Width B [mm]	Thickness	
		subs. ρ_s [g/cm^3]	coat. ρ_c [g/cm^3]			subs. h_s [mm]	coat. h_c [mm]
P1	$\bar{x}$	7.77	5.40	100.43	25.07	4.052	0.353
	$u(\bar{x})$	0.01	0.01	0.03	0.01	0.004	0.012
P2	$\bar{x}$	7.77	5.40	100.43	25.08	4.050	0.350
	$u(\bar{x})$	0.01	0.01	0.04	0.01	0.001	0.011
P3	$\bar{x}$	7.78	5.40	100.53	25.08	3.986	0.362
	$u(\bar{x})$	0.02	0.01	0.01	0.02	0.012	0.017
P4	$\bar{x}$	7.78	5.40	100.55	25.09	4.021	0.357
	$u(\bar{x})$	0.01	0.01	0.05	0.01	0.004	0.019
P5	$\bar{x}$	7.78	5.40	99.73	24.92	4.027	0.367
	$u(\bar{x})$	0.01	0.01	0.03	0.01	0.003	0.014

$\bar{x}$: mean value of n measurements;

$u(\bar{x})$: standard uncertainty (International Organization for Standardization);

The procedure adopted for elastic characterization requires specimens with all the edges free in order to accommodate the boundary conditions prescribed from ASTM standards. Therefore, each sample has been supported on direct contact supports. The supports have been made of soft material (*e.g.*, cotton pad, soft sponge) and had a minimal area in contact with the specimen. They have been placed in locations that allow the plate to oscillate without significant limitation in the desired mode (see Figure 4.4). Impact excitation has been imparted lightly hitting the beam in the horizontal plane and the resulting vibration has been picked up using a microphone placed near the surface of the sample under examination. The dynamic response detected by the microphone has been then analyzed and processed to identify the fundamental natural frequency. Each measurement was carried out by considering an acquisition time equal to 10s. Using a sampling frequency equal to 44100Hz, a resolution equal to $\Delta f = 1/\Delta t = 0.1$ Hz was achieved. No significant deviations have been observed among the values of repeated measurements. In order to mitigate the environmental noise and

to better illustrate the peaks of the frequency spectrum, the average signal obtained by impacting the plate three times has been analyzed.
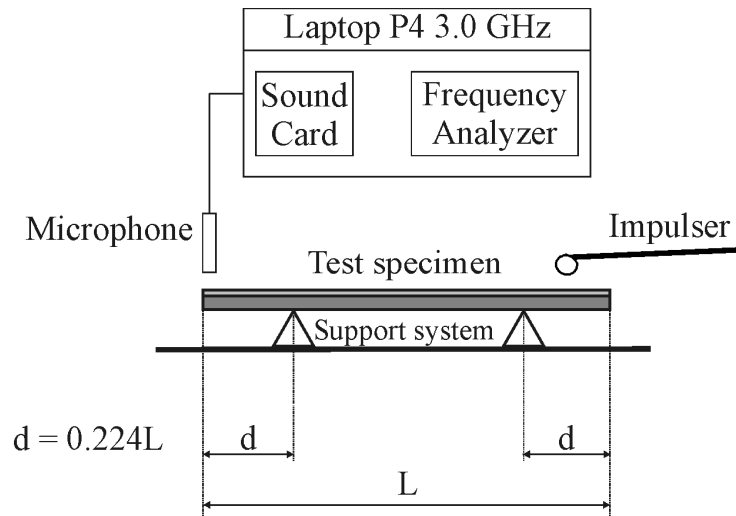
Figure 4.4 Schematization of the test set-up

The elastic properties of the substrates have been determined before plasma spraying. In particular Table 4.12 reports the fundamental natural frequency of each substrates before coating deposition (f_{1s}). This last, together with the geometrical dimension and the mass density of the material (see Table 4.11), allows to determine the Young's modulus, following the procedures and the recommendation of the ASTM standards for the elastic characterization of isotropic materials (E1876-01 Standard Test Method).

Table 4.12 - Fundamental natural frequency and Young's modulus of the samples

	f_{1s} [Hz]	E_s		
		$\bar{x}$ [GPa]	$u(\bar{x})$ [GPa]	$U(\bar{x})$ (95%)
P1	2110.1	205.04	0.70	1.81
P2	2108.3	204.93	0.26	0.73
P3	2104.5	212.13	1.90	4.87
P4	2107.1	208.92	0.70	1.71
P5	2148.9	209.95	0.51	1.24

$\bar{x}$: mean of the value calculated from n measurements;
$u(\bar{x})$: standard uncertainty (International Organization for Standardization);
U(x): combined standard uncertainty (coverage factor k=t_{95}, t is the t-student distribution)

The results present a reduced scatter and are in agreement with the common values reported for steel. The effect of the thermal spraying process on substrates

has been also investigated. In particular, the elastic modulus has been measured after a direct exposure to the plasma torch, using the same spraying parameters. No significant influence has been observed.

Table 4.13 presents the fundamental frequency of coated samples (f_{1sc}), which introduced in Eq. (3.10) and considering the geometrical and mass properties reported in Table 4.11, allows to obtain the elastic modulus of the coatings.

Table 4.13 - Fundamental natural frequency and Young's modulus of the coating

	f_{1sc} [Hz]	E_c		
		$\bar{x}$ [GPa]	$u(\bar{x})$ [GPa]	$U(\bar{x})$ (95%)
P1	2109.7	33.01	1.93	4.25
P2	2107.6	32.62	1.16	2.28
P3	2092.0	25.10	4.53	11.09
P4	2094.7	25.50	2.20	4.50
P5	2134.1	23.41	1.52	3.14

$\bar{x}$: mean of the value calculated from n measurements;
$u(\bar{x})$: standard uncertainty (International Organization for Standardization);
U(x): combined standard uncertainty (coverage factor k=t_{95}, t is the t-student distribution)

The Young's modulus of the coating, E_c, presents a relatively large scatter and this could be addressed mainly to the measurement error in determining the thickness, t_c, and in principle, also to specimen curvature that follows to the deposition process. To this aim, it is worth noting that thermal spraying process usually leads to samples affected by residual thermal stresses. Within the context of linear-elastic classical beam theory, the residual thermal stresses do not lead to any changes in the elastic response. Nevertheless, they may induce a curvature of the specimen thereby leading to a geometrical stiffening and to a variation in the fundamental natural frequency with respect to the corresponding undeformed configuration. It has been demonstrated in Lauwagie (2005) that the resonant frequencies of plate-shaped specimens are very sensitive to this out-of-plane deformation, while beam-shaped specimens are less sensitive to it. However, in the present study, the small differences among the thermal expansion between coating and substrate, as well as the higher stiffness which the latter presents compared to the coating, prevent large specimen curvature. Therefore it is possible to conclude that thermal stresses have a negligible influence on the

measurement of the fundamental frequency and, thus, on the obtained values of the elastic modulus.

The results obtained for the Young's modulus of the coating are in agreement with the values reported in Lauwagie (2005) for coatings of similar composition (E=24.1 ± 6.33 GPa, G = 12.6 ± 6.76 GPa, $\nu = 0.010 \pm 0.610$, 95%, d.o.f.=8). In this last case a yttria-stabilised zirconia (8YSZ) coating has been characterized by using nine samples simultaneously.

4.3.2 Application and validation of the iterative technique

As highlighted in the previous chapter, no equations are available in layered samples case that connect both the elastic moduli to frequencies and a MNET technique has to be used to find also the Poisson ratio of the coating materials. The procedure adopted as optimization process is the same of the one used for isotropic materials. Also in this case, first the elastic moduli of the substrate has been found and after the elastic characterization has been carried out on the coating layer. Even if two frequencies are enough, a number of four frequencies are preferred to decrease the effect of the experimental noise and to have a well-conditioned problem. For this purpose, the same procedure adopted for plates of irregular shape has been adopted (see Figure 4.1). The samples have been suspended in air with two elastic bands fastened to the rigid frame. The exciting impulse has been imparted repeatedly in various points by lightly hitting the sample with an impulser. The frequencies acquired before and after the coating deposition are reported in Table 4.14.

For the elastic identification procedure the same algorithm used for isotropic materials has been adopted. The error function described in equation (4.1) with N=4 has been assumed. A study has been done to determine the mesh density at which values of the first 6 resonant frequencies converge. The samples have been meshed using 50×15×4 Hex20 elements for the substrate layer and 50×15×2 Hex20 elements for the coating layer. The results of the identification tests carried out on the substrate layer and on the coating layer are reported in Table 4.15.

Table 4.14 - Natural frequencies of the samples, before (f_s) and after (f_{sc}) the coating process

Shape		Mode (Hz)			
		I	**II**	**III**	**IV**
P1	f_s	2110.1	4880.0	5780.1	10038.7
	f_{sc}	2109.7	4876.8	5785.4	10047.0
P2	f_s	2108.3	4876.5	5778.1	10039.5
	f_{sc}	2107.6	4878.8	5779.4	10042.0
P3	f_s	2104.5	4859.9	5766.6	10006.0
	f_{sc}	2092.0	4833.8	5724.4	9946.9
P4	f_s	2107.1	4860.8	5773.3	10007.0
	f_{sc}	2094.7	4832.7	5736.6	9949.9
P5	f_s	2148.9	4963.3	5887.0	10217.0
	f_{sc}	2134.1	4931.6	5840.9	10144.4

Table 4.15 - Values obtained for Young's modulus and Poisson's ratio

	Substrate			Coating		
	E_s [GPa]	G_s [GPa]	v_s	E_c [GPa]	G_c [GPa]	v_c
P1	204.40	79.99	0.278	41.17	16.37	0.257
P2	204.26	80.00	0.277	40.71	17.19	0.184
P3	211.08	82.28	0.283	33.87	14.16	0.196
P4	208.08	80.89	0.286	33.42	14.28	0.170
P5	209.02	81.73	0.279	28.40	13.05	0.088

From the results, reported in Table 4.15 it's possible to see the discrepancies among the identified values obtained by the analytical formlation and that obtained by the MNET for the coating layer (differences are more than 20%). This is mainly due to different models used in frequency computation. In MNET a discrete numerical model (FEM) has been used as approximation of the continuum while in the direct procedure an analytical formula has been used. Furthermore, it is to highlight that in the analytical formulation (see Eq. 3.10) the shear and rotary inertia effects have been neglected. For the substrate layer the ASTM standard method has been applied, and so little difference between the results have been obtained (less than 0.5%), in fact in ASTM standards method (E1876-01) the shear and rotary inertia effects have been take into account by a correction factor. Due to low sensitivity, a high dispersion has been obtained in Poisson's ratio value.

4.4   Conclusions

The feasibility of using an iterative procedure for determining the elastic properties of any-shaped thin (and moderately thick) isotropic plates which are also drilled has been experimentally and successfully assessed. The results have been compared with those obtained by different approaches and also with those reported in literature and the agreement is quite good. With such a procedure the identification of the Young modulus and Poisson ratio is carried out simultaneously, not destructively, in a single test. The measurement system is simple, inexpensive and fast. Furthermore it is contactless and could permit the characterization of materials at high temperature. The solution time typically depends on the selected trial values. This requires some minutes using a common PC, but this time can be consistently reduced if the finite element calculus is carried out directly inside the identification algorithm. Finally an experimental validation tests of the MNET showed that the procedure can also be applied for the identification of the elastic properties of each layer of layered materials. Unfortunately the procedure seems not suitable for orthotropic plates of any shape. Other problems can arise when the impulse excitation technique is applied on high damping materials, in this case to measure the natural frequencies the resonant technique is necessary and so that more expensive equipment are required.

4.5   Bibliography

Alfano, M., Pagnotta, L., 2006a. Determining the elastic constants of isotropic materials by modal vibration testing of rectangular thin plates. Journal of Sound and Vibration, 293 (1-2), 426-439.

Alfano, M., Pagnotta, L., 2006b. Measurement of the dynamic elastic properties of a thin coating. Review of Scientific Instruments, 77 (5), 056107-3.

Alfano, M., Pagnotta, L., Stigliano, G., 2006. International conference, ISMA 2006. Belgium. 2033-2040.

Alfano, M., Pagnotta, L., 2007. A non destructive technique for the elastic characterization of thin isotropic plates. NDT&E International, 40 (2), 112-120.

Alfano, M., Pagnotta, L., Stigliano, G., 2007. Identifying elastic properties of isotropic materials by finite element analyses and vibration data. Key Engineering Materials, 346, 1327-1330.

ASTM Standard E1876-01. Standard test method for dynamic Young's modulus, shear modulus, and Poisson's ratio by impulse excitation of vibration, Book of Standards Volume 03.01.

Beghini, M., Bertini, L., Frendo, F., 2001a. Measurement of coatings' elastic properties by mechanical methods: Part 1. Consideration on experimental errors. Experimental Mechanics, 41 (4), 293-304.

Beghini, M., Benamati, G., Bertini, L., Frendo, F., 2001b. Measurement of coatings' elastic properties by mechanical methods: Part 2. Application to thermal barrier coatings Experimental Mechanics, 41 (4), 305-311.

Bruno, L., Pagnotta, L., Poggialini, A., 2006. Elastic characterization of CVD diamond by static and dynamic measurement. Journal of the European Ceramic Society, 26 (12), 2419-2425.

Bruno, L., Felice, G., Pagnotta, L., Poggialini, A., Stigliano, G., 2008. Elastic characterization of plates of any shape via static testing. International Journal of Solids and Structures, 45 (3-4), 908–920.

Deobald, L.R., Gibson, R.F., 1988. Determination of elastic constants of orthotropic plates by modal analysis/Rayleigh-Ritz technique. Journal of Sound and Vibration, 124, 269-283.

Davis, J.R., 1998. Metals Handbook: Desk Edition. ASM International, Materials Park, Ohio, USA.

Hwang, S.F., Chang, C.S., 2000. Determination of elastic constants of materials by vibration testing. Composite Structures, 49, 183-190.

International Organization for Standardization, Guide to the Expression of Uncertainty in Measurement, Switzerland (1995), ISBN 92-67-10188-9.

Kim, H.J., Kweon, Y.G., 1999. Elastic modulus of plasma-sprayed coatings determined by indentation and bend tests. Thin Solid Films, 342 (1-2), 201-206.

Kroupa, F., Plesek, J., 2002. Nonlinear elastic behaviour in compression of thermally sprayed materials. Materials Science and Engineering: A, 328 (1-2), 1-7.

Lauwagie, T., 2005. PhD dissertation, Vibration-based methods for the identification of the elastic properties of layered materials, Katholieke Universiteit Leuven.

Pagnotta, L., Stigliano, G., 2008a. Elastic characterization of isotropic plates of any shape via dynamic tests: theoretical aspects and numerical simulations. Mechanics Research Communications, 35 (6), 351–360.

Pagnotta, L., Stigliano, G., 2008b. Elastic characterization of isotropic plates of any shape via dynamic tests:Practical aspects and experimental applications. Mechanics Research Communications, doi:10.1016/j.mechrescom.2008.09. 003

Siebert, B., Funke, C., Va en, R., Stöver, D., 1999. Changes in porosity and Young's Modulus due to sintering of plasma sprayed thermal barrier coatings. Journal of Materials Processing Technology, 92-93, 217-223.

Sitton Grant, 1997. MSC/NASTRAN Basic Dynamic Analysis User's Guide, The MacNeal-Schwendler Corporation, U.S.A.

Spinner, S., Tefft, W. E., 1961. A method for determining mechanical resonance frequencies and for calculating elastic moduli from these frequencies, in Proceedings of the American Society for Testing and Materials, ASTM , 61, 1221-1238.

Warburton, G.B, 1953. The vibration of rectangular plates, in Proceedings of the Institution of Mechanical Engineers, 168, 371-384.

5 NUMERICAL-EXPERIMENTAL METHODOLOGIES FOR THE MATERIALS CHARACTERIZATION BY STATIC TESTING

5.1 Introduction

As composite materials become more usually used, the need for a reliable method to nondestructively measure the material stiffness properties is becoming decisive for ensuring a reliable level of performance in both design and application. It is well known that traditional static (or quasi static) test procedures are expensive and time-consuming (Carlsson and Pipes, 1997). At least three separate tests are required to measure the four elastic constants describing the linear-elastic stress-strain relationship of thin unidirectional laminates. A simple test procedure consists in performing on three strain-gauged specimens a tensile

test, by orienting their principal axis at 0°, 45°, and 90° with respect to the loading direction. The analysis of the results obtained by testing the 0° and 90° specimens provides E_1, E_2, ν_{12}, and ν_{21}, while G_{12} is obtained by the 45° specimen. Unfortunately, the measurement of G_{12} is not so easy and accurate as for the other parameters. This limited applicability encouraged the development of several methods for the identification of the shear modulus (rail shear, picture-frame shear, off-axis tensile shear and Iosipescu shear tests are, just, some examples). Consequently the development of methodologies using a single specimen for measuring all the in-plane elastic constants could prove very advantageous. Orthotropic half-plane specimens have been proposed in Prabhakaran and Chermahini (1984), for whom an analytical solution for the strain and stress fields exists, consequently pointwise measurement with strain gauges can lead to the determination of the unknown parameters. When no analytical solution is available, inverse procedures based on updating the finite element models have been developed, either in the case of a reduced number of measurements (Wang and Kam, 2000) or in the case of whole-field data. This last case could occur when data (strain or displacement fields) are measured onto the surface of the specimen with an optical method. Several types of specimen and tests have been used as documented by the literature on the subject: open-hole uniaxial tensile tests (Molimard et al., 2005), in-plane loaded rectangular plate (Genovese et al., 2004), circular disk under diametrical compression (Wang et al., 2005; Hild and Roux, 2006), cruciform perforated specimens under biaxial tests (Lecompte et al., 2007), through-hole biaxially loaded plate (Cardénas-Garcia et al., 2005). However, the idea of determining the elastic constants of a material by the displacement fields undergone by a specimen has been well exploited in the past. Starting from the pioneers (Cornu, 1869; Timoshenko and Goodier, 1970), many authors, encouraged by the diffusion of the coherent light sources, developed a large number of static (Jones and Bijl, 1974; Archbold et al., 1978; Zhu, 1996; Ganesian, 1989; Grédiac and Vautrin, 1993; Gascon and Salazar, 1996; Furgiuele et al., 1997; Apalkov et al., 1999; Bruno et al., 2002a,b, 2006a,b; Bruno and Poggialini, 2005; Grédiac et al., 2006) or dynamic techniques (Fällström and Jonsson, 1991; Fällström et al., 1996; Grédiac et al., 1998; Gaul et al., 1999).

In the present thesis an inverse method, which combines finite element analysis and genetic algorithms (GAs) to identify the elastic properties of

isotropic or anisotropic materials by full-field measurement of the surface displacements of a plate of generic form under suitable flexural loads is presented. As for the dynamic technique, described in the previous chapters, an optimization process updates the elastic constants in a finite element model so that the outputs from the numerical analysis fit the experimental data. In this way, the unknown parameters can be identified simultaneously in a single test and without damaging the structure (Bruno et al., 2008). In this chapter theoretical aspects of the methodology and numerical simulations for testing the accuracy and sensitivity of the method are presented.

5.2 Problem formulation

The displacement field of a loaded body depends on the entity of the load, the coordinates of the loaded point considered, the constraints and the geometry of the body and, obviously, the elastic properties of the material. As for the dynamic behavior, if the analytical solution, that connect the displacement field to the elastic constants of the adopted loading configuration is attainable, the elastic moduli of the material could be determined, provided that the applied loads are previously measured or properly imposed. On the contrary if a reliable theoretical solution does not exist, a numerical solution becomes necessary and so a mixed numerical-experimental techniques has to be applied. Inverse procedures based on the updating of numerical models could be suitable for this purpose. When this approach is used for static characterization, the numerical displacement field of the specimen under test is correlated with the experimental observations performed on the real specimen. The unknown parameters (elastic constants) of the material in the numerical model are updated until the mechanical behaviour (displacements) matches the experimental observations as closely as possible. The values of the parameters used in the numerical model in the last computation are the results of the characterization procedure and they yield the elastic properties of the specimen. In principle, this approach enable the identification of all the elastic properties simultaneously from a single experiment and without damaging the structure. The elastic characterization becomes an optimization process and the elastic moduli are estimated by minimising an error function (φ), and so, as in dynamic field, the choice of it is very important. Note that it is not always easy to

minimize the error function (φ), especially in the case of orthotropic materials. Therefore the right choice of minimization procedure is fundamental. In any case, it is desirable to use a robust and reliable optimization procedure able to converge to the target values of elastic properties regardless of load type, initial guess values, boundary conditions etc.

5.2.1 Error function and minimization method

Genetic algorithms (GAs) are able to find the global optimum even for ill-conditioned functions. Therefore, they appear to be highly suitable for the characterization of anisotropic materials for which the error function is a highly non-smooth function and gradient-based optimization methods would not work well (Mitchell M., 1999). Based on probabilistic rules, GAs use the process of natural selection by imitating the concept of survival of the fittest. Due to the way the GA explores the region of interest, it avoids getting trapped at a particular local minimum and locates the global optimum. GAs, unlike the gradient-based method, do not require initial estimates, but instead work within a suitable set of bounds that can often be rather broad and can just affect the number of iterations to reach the solution. For these reasons in the recent years many researchers have used GAs for the elastic characterization of materials (Balasubramaniam, Rao, 1998; Cunha *et al.*, 1999; Liu *et al.*, 2002; Maletta, Pagnotta, 2004).

The first step of the GA is the creation of a population of individuals (initial population) randomly chosen from a set of potential solutions of the problem. Each individual, formed by two (isotropic material) or four (orthotropic material) elastic constants, is subjected to the evaluation of the fitness (based on a given error function). Then, a selection process permits those individuals of superior fitness to reproduce and create a new population, which combines the desirable characteristics of the old population. The reproduction is generally based on two operators: crossover and mutation. The new population then replaces the old one and the process restarts. New generations of solutions are created through the genetic manipulation, and this iterative process is repeated for a fixed number of generations or for a fixed number of analyses until there is no improvement in the best solution.
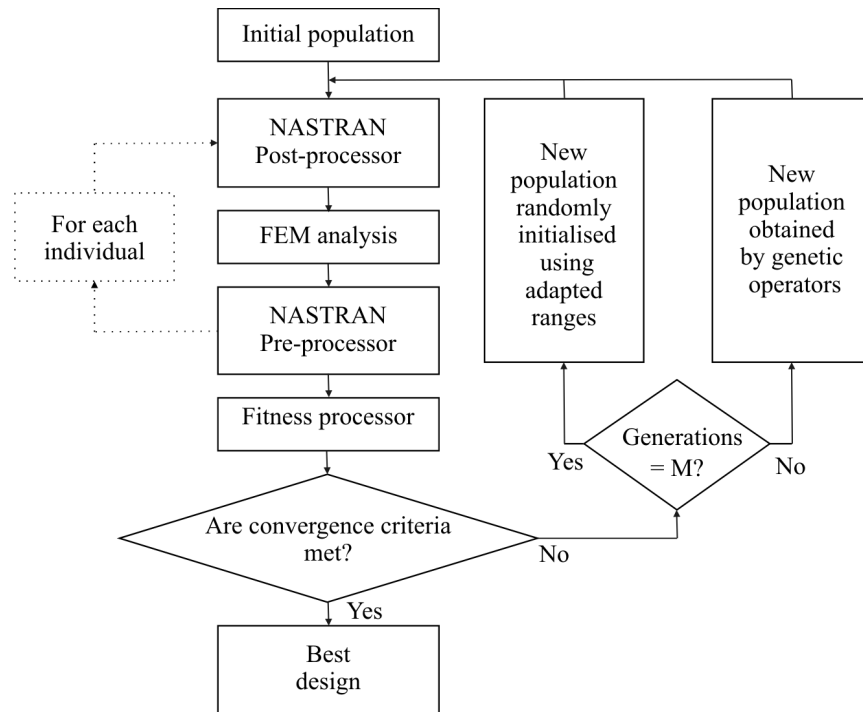
Figure 5.1 The identification process

The diagram of the GA used for the identification of the elastic constants is shown in Figure 5.1. It differs from that used in dynamic technique with regards to an adaptive range module (Oyama *et al.*, 2001.) that has been added to explore the search space more efficiently. The algorithm has been developed on a personal computer in MatLab environment. It applies the numerical code MSC/NASTRAN to carry out the static analysis. To take the proper set of elastic constants into account, for each design of the population, in the "NASTRAN pre-processor" stage, the MSC/NASTRAN input file ("*.bdf") is adjusted by modifying the MAT1, MAT8 or MAT9 bulk data entry, defining isotropic and two or three dimensional orthotropic stress-strain relationships, respectively. Then the real static analysis is carried out. In the post-processing stage, by using the displacement field extracted from the NASTRAN result file, for each design, the error function (φ) is evaluated. After that, both the fitness and the relative elastic constants are saved, all the FEM output files are removed to release the computer memory and the cycle restarts. The fitness processor begins to operate at the end of the processing of the population arranging the fitness values of the population in decreasing order and checking the convergence criteria. If the convergence criteria are not reached, the most suitable solutions are selected and then processed by means of the genetic operators to create the new population. The GA

has been provided with an adaptive range procedure by which the entire population is regenerated every M (with M>1) generations. Then, three additional steps have been incorporated into the structure of the algorithm. In the first step, every M generations, the top half (the fittest individuals) of the previous generation is collected as a group; for each elastic constant the average (μ_{group}) and standard deviation (σ_{group}) of this group is calculated, then a new average and standard deviation for each elastic constants are obtained updating the previous values according to the following equations:

$$\mu_{new} = \mu_{old} + \omega_\mu \ (\mu_{group} - \mu_{old})$$
$$\sigma_{new} = \sigma_{old} + \omega_\sigma \ (\sigma_{group} - \sigma_{old})$$

(5.1)

where ω_μ and ω_σ are relaxation factors that provide robustness during the range adaptation. In the second step, a new search range (l_{min}, l_{max}) for each elastic constant is calculated using average and standard deviation computed in the previous step by the following equations

$$l_{min} = \mu_{new} - \kappa \, \sigma_{new}$$
$$l_{max} = \mu_{new} + \kappa \, \sigma_{new}$$

(5.2)

where κ $(1 \ \kappa \ 10)$ is a measure of the overlapping between the group and the new generation. In the final step, all but two individuals in the population are generated randomly according to the new range. The new population is completed including the two fittest individuals of the old population. A proportional selection scheme has been adopted for the reproduction of the child generation and two procedures (arithmetical and replacing types) used to carry out the crossover operation. In order to speed up the evolution and to improve the convergence performance of the GA a mutation and elitism selection have also been introduced. Greater details on these operators can be found in Appendix B. The values of the parameters involved (population size, probability of mutation and crossover, etc.), selected on the basis of systematic trials, are reported in Table 5.1.

Table 5.1 – GA parameters

Population size	120	M	35
Crossover probability	80%	$\omega_\mu = \omega_\sigma$	0.5
Mutation probability	5%	κ	10

Among the wide variety of potential error functions, in the present static technique, the following fitness has been used:

$$\varphi = \sum_{i=1}^{N} \left| w_i^{\,n} - w_i^{\,e} \right| \tag{5.3}$$

which is calculated by summing the absolute value of the difference calculated between the numerical $w_i^{\,n}$ and the experimental $w_i^{\,e}$ out-of-plane displacements. The parameter N represents the total number of the data acquired experimentally. The functions φ_2 and φ_3 (relative error functions) showed in the dynamic section, instead, cannot be used because indeterminate expression could happen due to motionless points (point with zero displacement).

5.3 Optimization of loading and constraining configuration

In the last three decades coherent optics has provided several interferometric techniques which enable the full-field surface displacement of an object to be determined with an accuracy of a few tens of nanometers without any contact with the investigated surface (Cloud Gary, 1995.). The amount of data that optical interferometric whole-field methods provide is much greater than the number of the unknowns to be estimated. This fact makes the elastic characterization an over-posed inverse problem and its solution can be easily obtained when the problem is well-posed. For this reason, great care needs to be taken in choosing the geometry and the way of loading and constraining the specimen (Pagnotta, 2007). The resulting interferometric fringe pattern must contain sufficient information for determining all the unknown parameters quickly and unequivocally. Besides, to reduce the effects of noise that inevitably disturb the displacement field on the solution, it must also be sufficiently sensitive to the variation in each elastic parameter.

In the present dissertation, a method is proposed enabling the choice of an appropriate configuration which provides a fringe pattern satisfying the above requirements, without carrying out any experimental tests. The procedure could be of great help in carrying out the elastic characterization of both isotropic and anisotropic materials. To illustrate how the procedure works a simple example will be shown. Figure 5.2 shows a schematization of square isotropic plate that

has to be characterised. The locations of the three support points P_1, P_2 and P_3 are completely defined by the lengths l_1 and l_2 with respect to a rectangular coordinate system, 0xyz, with the origin located at the centre of the plate and the axes parallel to the edges of the plate.
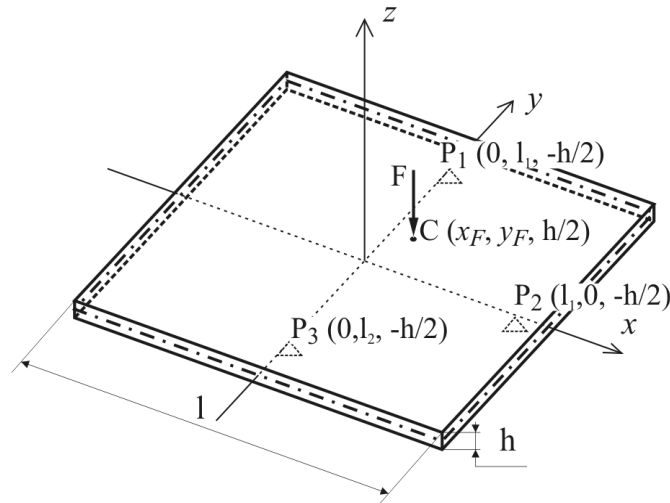

Figure 5.2 - Loading configuration used to identify
the best location for the load by the correlation index

The first step of the identification process is to generate a "suitable" superficial displacement field by which the Young modulus E and Poisson ratio of the material composing the plate can be conveniently determined by an iterative procedure such as that mentioned above. A simple way to deform the plate is by using a flexural load, for example, by a force F acting normally to its upper surface (see Figure 5.2). The main problem, in choice of constrain configuration, is to recognize if one displacement field is more suitable than another for elastic characterization. In other words, a method able to estimate how well-posed the problem is needed. The method has to find the best load position on the surface of the plate to obtain the optimal displacement field.

For example, assume that the field of the out-of-plane components of the displacements undergone by the upper surface of the plate is measured by an interferometric technique. For isotropic materials, the displacement (W) is a function of E and , i.e., $W=W(E,)$. An index of the suitability of the displacement field can be obtained by evaluating the degree of statistical correlation between the variation in the displacement field due to an increment of E, $\Delta W_E=[W(E+\Delta E,) - W(E,)]$ and the variation in the displacement field due to

an increment of , $\Delta W = [W(E, +\Delta) - W(E,)]$. Such an index is the correlation coefficient calculated as

$$r_{E\nu} = \frac{cov(\Delta W_E, \Delta W_\nu)}{s_{\Delta W_E} s_{\Delta W_\nu}}$$ (5.4)

where $cov(\Delta W_E, \Delta W_\nu)$ is the covariance between the two displacement fields ΔW_E and ΔW_ν, while $s_{\Delta W_E}$ and $s_{\Delta W_\nu}$ are the relative standard deviations. When $|r_{E\nu}| < 1$, the displacement field contains sufficient information for identifying both the elastic constants unequivocally. The lower is the value of the coefficient of correlation the better defined the problem.

Evidently, the value of $r_{E\nu}$ depends on the location of the force. The optimal location is the one which corresponds to the lowest correlation index. In Figure 5.3, the map of the absolute values of the correlation coefficient is reported for the case of a square plate supported as in Figure 5.2.

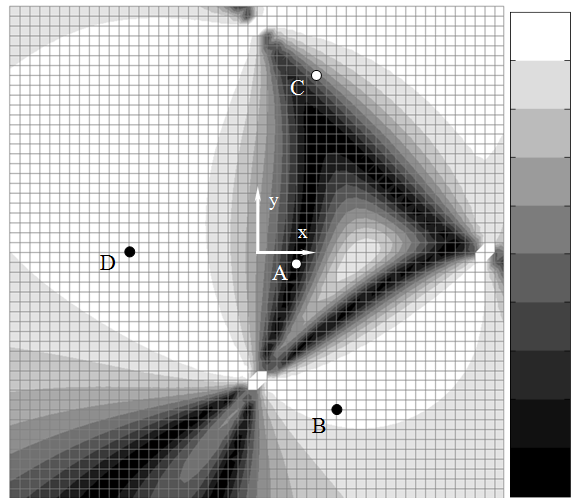*Figure 5.3 - Correlation index map of an isotropic material*

The correlation coefficient has been calculated for different locations of the force by an algorithm written in MatLab environment. The area around each location has been coloured with a grey level proportional to the corresponding value of the calculated correlation coefficient (ranging from black for $|r_{E\nu}| = 0$ to white for $|r_{E\nu}| = 1$).

113

The structural analyses for predicting the displacement fields have been carried out using the general-purpose finite element code MSC/NASTRAN. l_1 and l_2 are 23 mm and 13 mm, respectively. The dimension l and the thickness h of the plate are 50 mm and 1 mm, respectively, while the force applied is 1 N. A convergence study has been undertaken to determine the mesh density of the 2-D model of the plate by varying the mesh density in the plane directions. It was discretized into 2500 (50x50) quadratic four node QUAD elements. The analyses have been carried out on a steel plate (E=205 GPa, =0.3) by considering all the 2601 nodes of the mesh. ΔE and Δv were equal to 10 % of E and , respectively. However, a deeper analysis showed that the value of the correlation coefficient does not depend on the value of E and has a weak dependence on .

To better understand the map reported in Figure 5.3 two particular load conditions can be considered. In the first condition, the downward force is applied to the plate at point A of coordinates x_F=4 mm and y_F=-1 mm. The analysis of the displacement field gives $\left| r_{Ev} \right|$=0.001 for this configuration; the lowest value of the correlation index corresponds to this location. As discussed, in such circumstances, the inverse problem should be very well-posed and the information contained in the displacement field are more than sufficient to identify the two elastic constants. In the second loading condition the force is applied at point B of coordinates x_F=8 mm and y_F=-16 mm where the highest value of the correlation index (r_{Ev} =0.95) has been obtained. The value indicates that the information contained in the superficial displacement field is sufficient to identify the elastic constants unequivocally because r_{Ev} is less than one. However it is also a warning that the problem is not very well-posed.

The consideration above can be validated and better explained by Figure 5.4, where the error functions φ, defined as in equation (5.3), in the two load configurations are reported. The assumed reference values in this cases are E=205 GPa and =0.3. As expected, from Figure 5.4 a), where the contour plot of the first configuration is reported, it can be clearly seen that φ has only a very well defined minimum. Such a minimum is very easy to identify by any conventional or non conventional optimization procedures suitable for minimizing a two parameter function. They will converge very rapidly to the solution because the minimum is very well defined. From Figure 5.4 b), where the contour plot of the

second load configuration is reported, it can be observed that, also in this case, the objective function presents only one minimum. However, in contrast to the first case, it is not well defined and is difficult to identify from the neighbouring points. In such a situation, the elastic identification could be difficult. The convergence rate depends on the type of used minimization process.
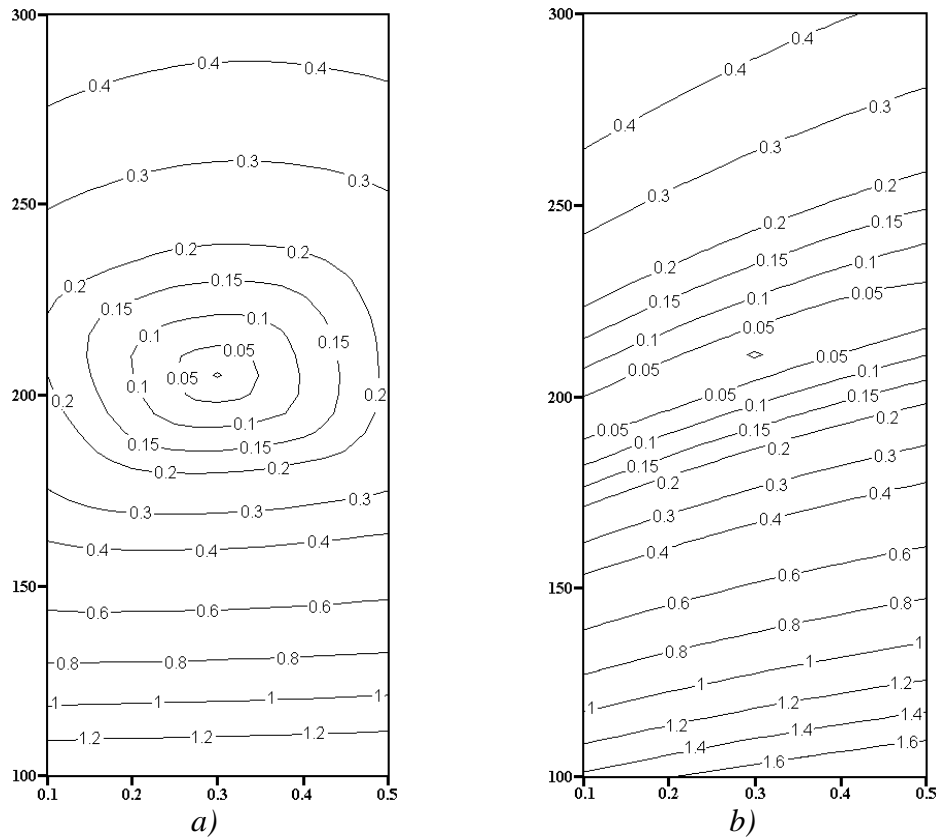

Figure 5.4 - Error function contour plot:

a) loading condition A; b) loading condition B

With regard to the sensitivity of the error function to a variation in   and E, it must be stressed that, when experimental errors affect the measure of the displacement field, a high sensitivity ensures accurate solutions. Obviously, the sensitivity depends on the geometry, constraining and loading conditions of the specimen and on the kind of measured component of the displacement. From Figure 5.4, it can be seen that, in the case under examination, the sensitivity of the error function to a variation in   is much lower than its sensitivity to a variation in E. As a consequence, the errors in the measured displacements propagate on   more than E.

In summary, when isotropic materials must be characterized, fast and accurate solutions are obtained if the force is applied inside the dark areas of the

correlation map reported in Figure 5.3. When, for some reasons, this condition cannot be satisfied, the solutions are reached more slowly and can be less accurate.

The procedure for the identification of the elastic constants by interferometric data can also be extended to orthotropic materials like composite laminates. If thin plates are considered, the number of elastic constants to be identified increases to four: E_1, E_2, ν_{12} and G_{12}. The error function can become a highly non-smooth multivariable function and if the inverse problem is not well-posed the time for its minimization is too long or, even worse, a solution is never reached. The use of a methodology based on the displacement correlation is of great help in such situations. For this purpose, the mean (r_{ave}) of the absolute values of the following correlation coefficients $r_{E_1 E_2}$, $r_{E_1 \nu_{12}}$, $r_{E_2 \nu_{12}}$, $r_{E_1 G_{12}}$, $r_{E_2 G_{12}}$, $r_{G_{12} \nu_{12}}$ is assumed as correlation index. The values of such coefficients are determined, one by one, in the same way as previously described in the case of isotropic materials.

The procedure has been applied to different unidirectional laminates with the principal axes parallel to the coordinate axes and constrained as illustrated in Figure 5.2. The properties of the material used to compute the correlation index are reported in Table 5.2. E_1 and E_2 are the longitudinal and transverse Young's moduli, respectively, ν_{12}, is the major Poisson's ratio and G_{12} the in-plane shear modulus. The subscripts 1 and 2 indicate the material directions, where 1 is the fiber direction and 2 is the direction transversal to the fiber direction. Fiber orientation is defined with respect to the x-axis. The generic unidirectional layer is assumed as homogeneous and transversally isotropic with respect to the fiber direction.

Table 5.2 –Material properties

Material	E_1 [GPa]	E_2 [GPa]	ν_{12}	G_{12} [GPa]
Aluminium	70.0	70.0	0.33	26.3
Carbon/Epoxy (C/E)	134.0	8.9	0.24	7.0
Glassy/Epoxy (G/E)	38.6	8.3	0.26	4.14
Pitch/Epoxy (P/E)	462.0	6.2	0.31	5.58

In contrast to what happened in the case of isotropic material, the shape of the map of the correlation index turned out to depend on the values of the elastic constants. A consequence of this is that the optimal position of the force depends

on the kind of material and, therefore, it is not possible to establish it a priori unless an approximate estimate of the elastic properties is available. A way to solve this problem is to analyse the map obtained averaging the correlation index maps of different materials. In Figure 5.5 the average of a number of maps (carbon steel, carbon/epoxy, glass/epoxy, pitch-epoxy, and aluminium) is reported. From the figure it can be seen that point C of coordinates x_F=6 mm and y_F=18 mm is the point with the minimal correlation index (r_{ave}=0.25). It has also been verified that a negligible standard deviation corresponds to this point. Therefore, the application of the force at this point is preferable to any other point. As will be shown in the following section, when the force is applied to a different location the inverse problem becomes too ill-posed and the time required for the identification unacceptable. In this case, to ensure fine solutions from the superficial displacement field, the used optimizer must find a global minimum even for ill-conditioned functions with numerous local minima.
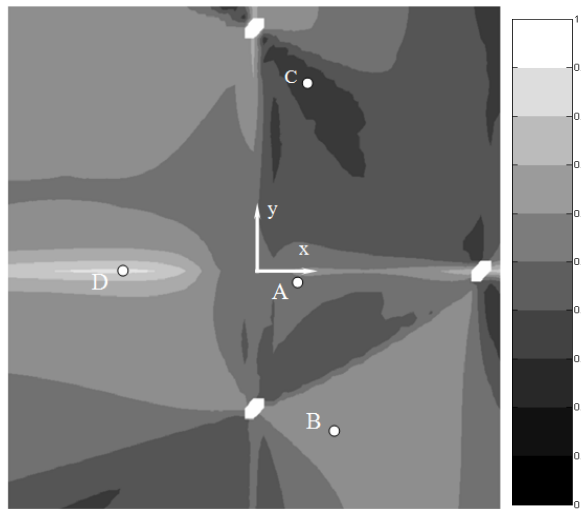

Figure 5.5 - Map of average correlation index for an orthotropic material

Unfortunately this configuration is suitable for solving the problem with two unknowns, but it is not very appropriate for solving the problem with four unknowns due to the practical experimental difficulty of applying the load at the location which corresponds to the lowest r_{ave}. In fact this point is close to the line that connect two support points and so that it is not easy to predict the direction of the third constrain point.

An alternative configuration which also solves the problems with four unknowns properly is reported in Figure 5.6. This configuration requires loading

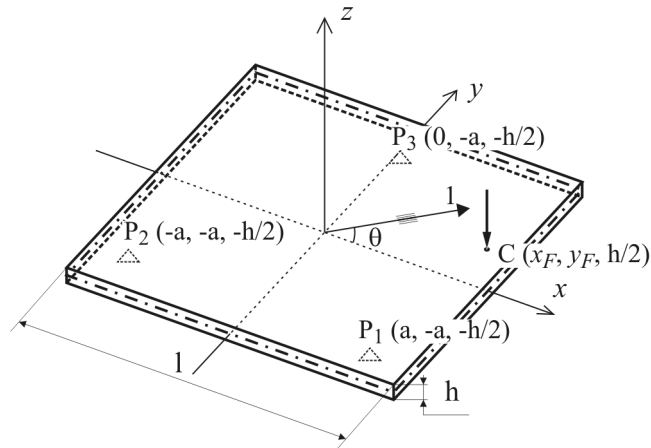and constraining conditions similar to those of the previous configuration, but which are easier to set up.

Figure 5.6 - Loading configuration used for orthotropic laminates

The square plate is simple supported on three points P_1, P_2 and P_3 lying on the corners of an isosceles triangle. By considering a rectangular coordinate system Oxyz with the origin at the centre of the plate and the axes parallel to the edges of the plate, the locations of the three support points are completely defined by means of the length a, that eventually could be related to the edge l of the plate ($a = 23 \times l/50$ mm, in this case). A concentrated force loads the plate transversally. The location of the force on the surface could be defined by the analysis of the correlation maps.

In Figure 5.7 the map relative to an aluminium plate is reported to show the behaviour of the isotropic materials with this constrain configuration.
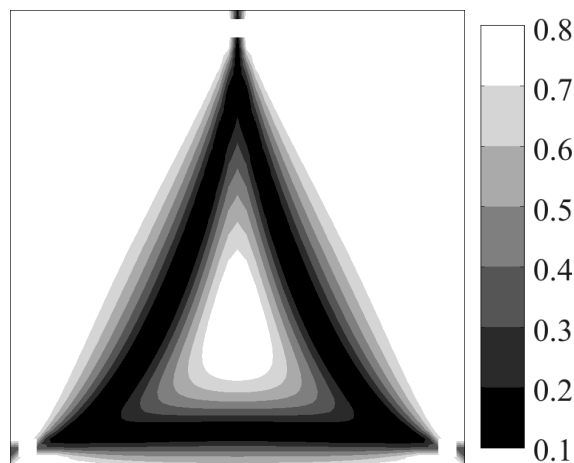

*Figure 5.7 - Aluminium correlation index map*

In addition, little difference has been observed among the maps of unidirectional thin laminates of different materials. In Table 5.3, for example, the maps of the correlation index of three different laminates with fibers parallel to the x-axis ($\theta = 0°$) are illustrated.

Table 5.3 – Correlation index maps of unidirectional laminates

[0°] Thin unidirectional laminates		
Carbon/Epoxy	Glass/Epoxy	Pitch/Epoxy
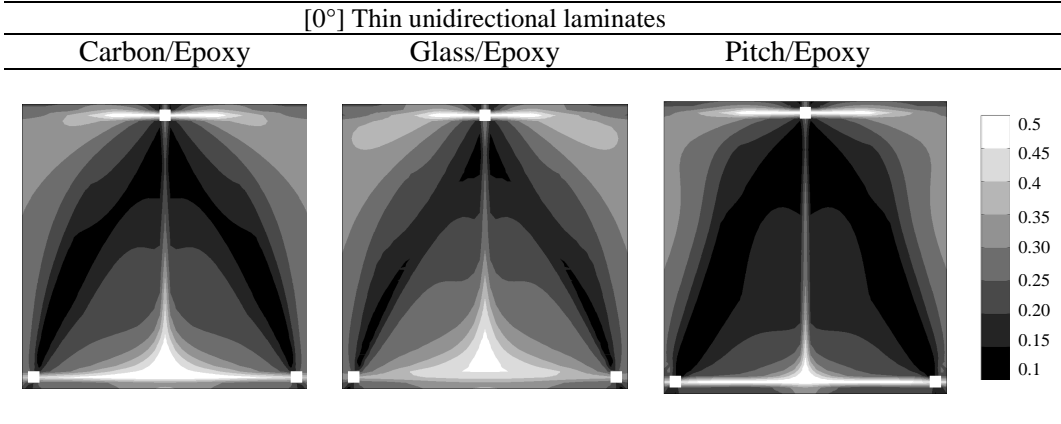
In all the cases, the distributions of the correlation index are characterized by low-level values and common areas can be distinguished, where the correlation index is minimal. Such areas can be more easily identified by observing the mean and the standard deviation of all the maps reported in Table 5.4.

**Table 5.4 – Mean and standard deviation of the correlation maps
of unidirectional laminates and isotropic plates**

[0°] Thin unidirectional laminates	
Mean	Standard deviation
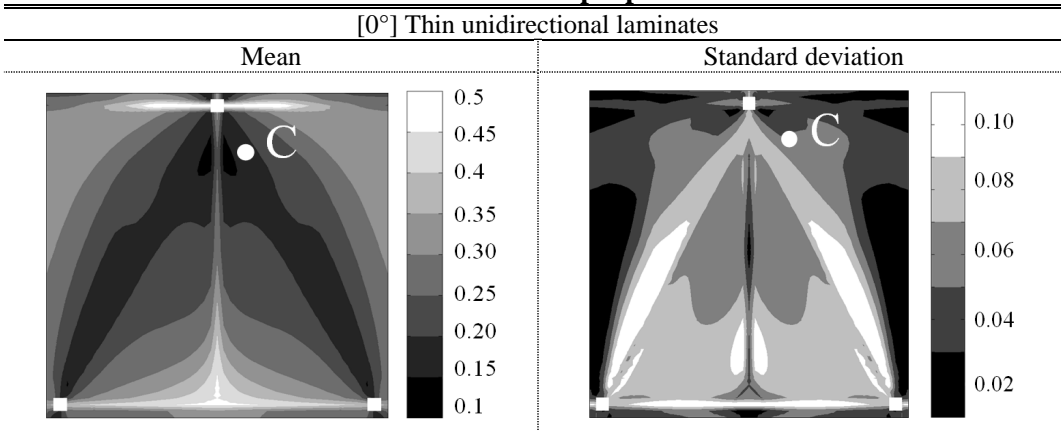
From such figures an area can be identified, around point C of coordinates $x_F = l/25$ mm and $y_F = 7 \times l/25$ mm, characterized by the lower values of the mean correlation index (r_{ave} 0.14) and with a negligible standard deviation (s_r 0.05). This area represents one of the best locations for the application of the force to profitably characterize both isotropic and unidirectional laminates.

119

Table 5.5 – Mean value and standard deviation of the correlation maps
of unidirectional laminates and isotropic plates

[90°] Thin unidirectional laminates	
Mean	Standard deviation
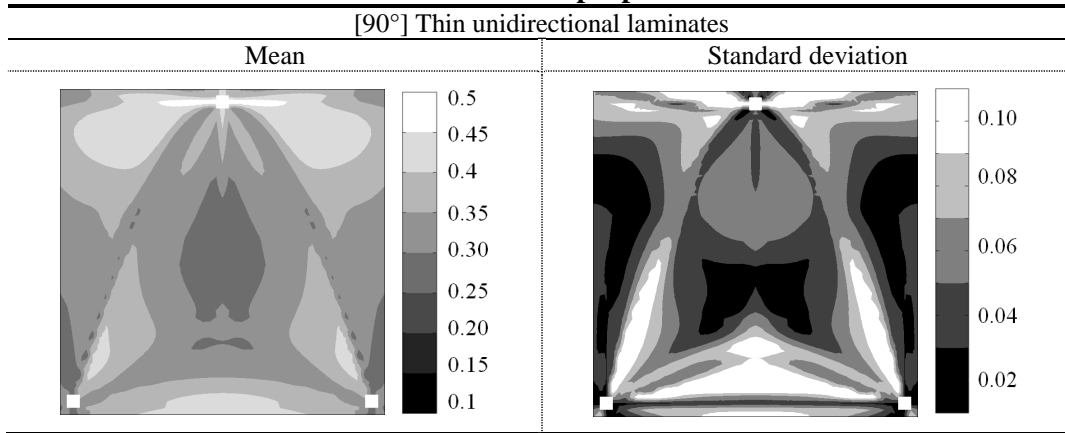
It is important to underline that when the fibers are oriented parallel to the *y*-axis ($\theta = 90°$) the values of the correlation index are generally higher than those obtained in laminates with the $0^°$ orientation (see in Table 5.5 the mean map). As a consequence this last orientation ($\theta = 0^°$) is certainly preferable for a faster and more accurate characterization.

Table 5.6 – Correlation maps of thin multidirectional laminates

	Carbon/Epoxy	Glass/Epoxy	Pitch/Epoxy
$[0^0, 90^0]_s$			
$[0^0, 60^0, -60°]_s$			
$[\pm 15^0]_s$			
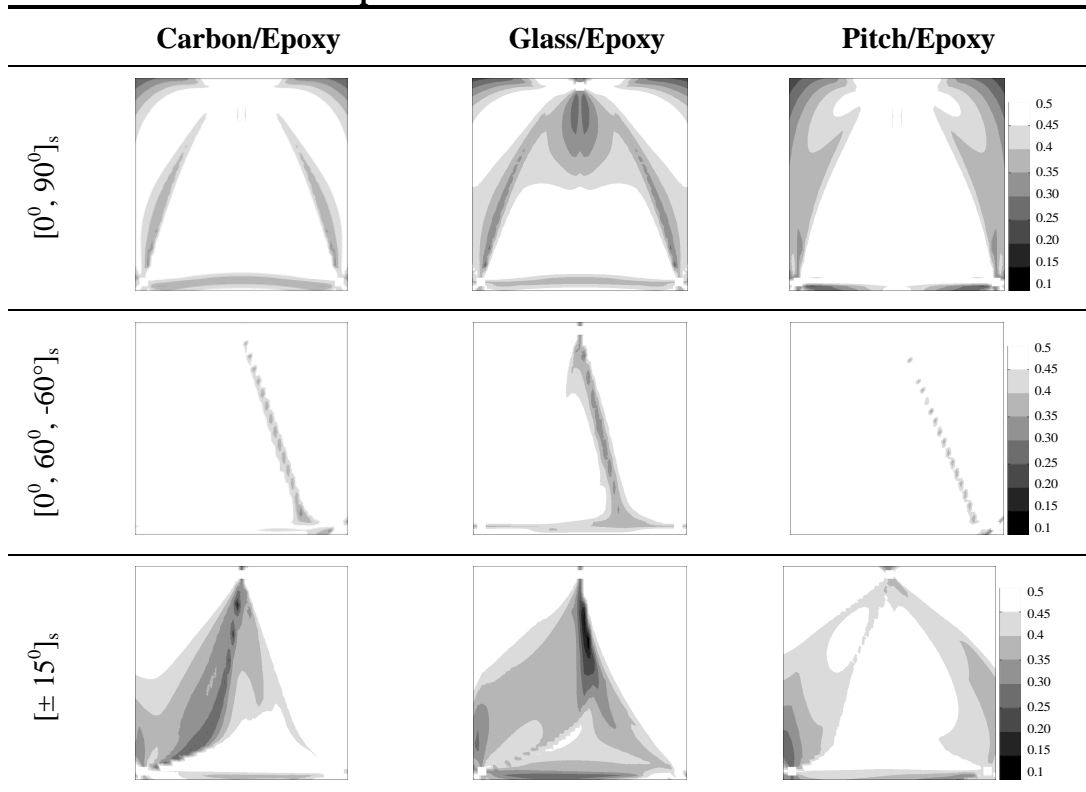
To investigate the limits of the proposed approach some multidirectional laminates have been also analysed. In Table 5.6, the correlation index maps

related to three of the simplest thin multidirectional laminates, a cross-ply laminate [0°, 90°]$_s$, an angle-ply laminate [±15°]$_s$ and a quasi-isotropic Pi/3 laminate [0°, 60°, -60°]$_s$, respectively, are shown. It can be observed that the correct point of application of the load depends on the type of laminate and point C is no longer suitable and so the technique has shown a poor applicability for multidirectional laminates characterization.

5.3.1 Plates of different shape

As in dynamic field, in the present dissertation, the feasibility of applying the present static technique to specimens with geometries different from those indicated above has been studied.

Table 5.7 reports the mean maps of the correlation coefficients for different shapes of the specimen obtained by considering a suitable number of either isotropic or orthotropic materials. In the first column of the table the shape of the specimen is schematically represented: the location of the support points are emphasized by the small squares, while the small circle represents the point of the application of the load, which is varied in the numerical simulation in order to evaluate the correlation maps. These maps are reported in the second column, for an isotropic material, and in the third column, for an orthotropic material. To highlight the good load location in correlation maps for orthotropic materials a different gray scale limits have been adopted ([0.0÷0.8] instead of [0.0÷0.5] used in the previous tables).

As it has been emphasised above, the darker is the area of the correlation maps, the lower is the degree of correlation and better is the choice for the point of application of the load. As it can be noticed by observing these maps and the maps reported in Table 5.4 for the orthotropic material, an acceptable level for the correlation index is obtained only for the square shaped plate, since for the other shapes the index never assumes values lower than 0.3. Finally it must be pointed out that in the first column, the portion of the specimen necessary to apply the procedure is delimited by a dashed closed line.

It is important to highlight that, even if for the orthotropic materials only the square plate showed a good correlation index value, for isotropic materials the

technique can be applied to plates with irregular shape and the point C ($x_F = l/25$ mm and $y_F = 7 \times l/25$ mm) seems to be the best load position in all the samples.

Table 5.7 – Maps of the correlation index

Geometry	Two constants	Four constants
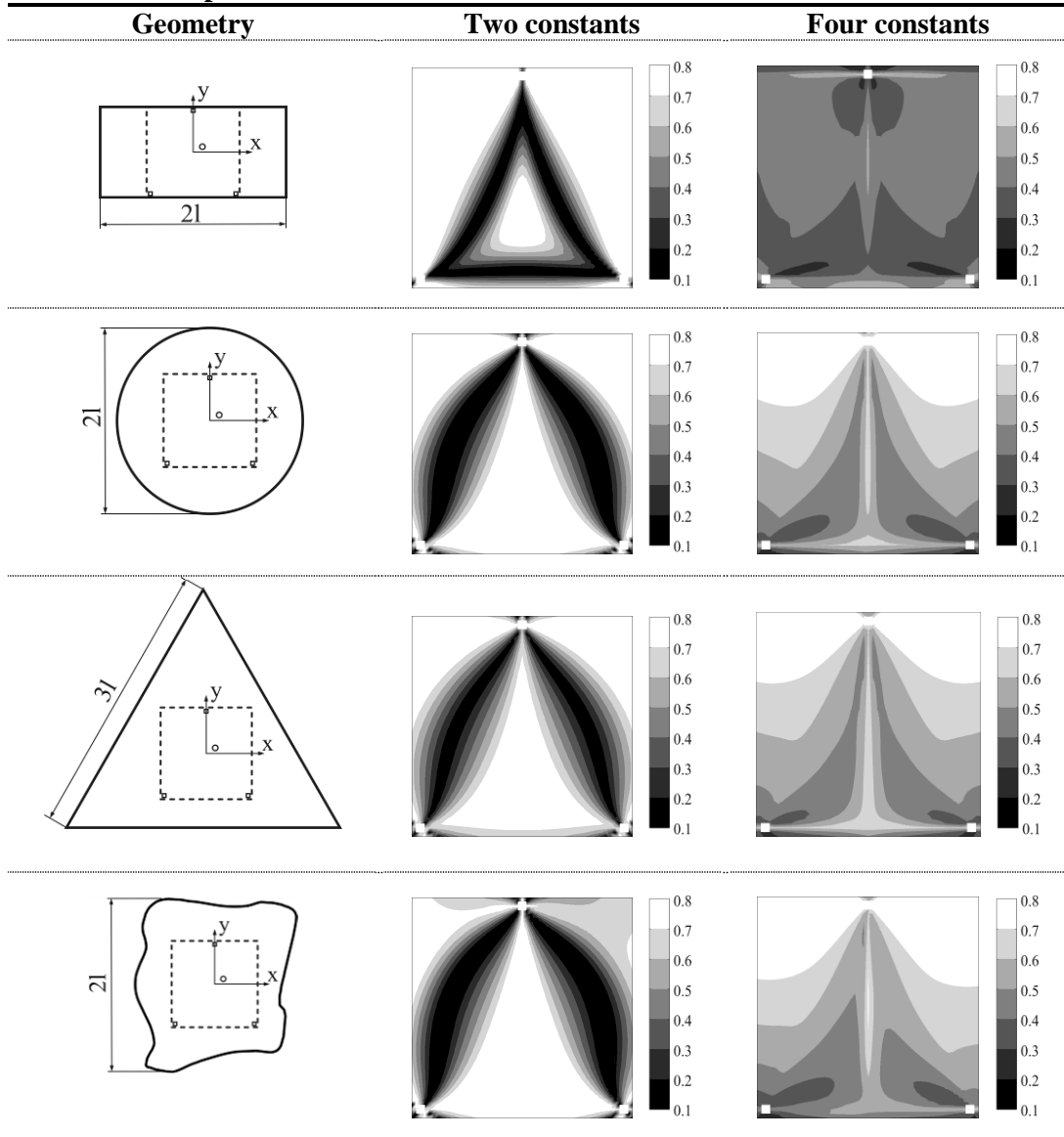
5.4 Numerical application and sensitivity analysis

The effectiveness and the robustness of the procedure with respect to the effects of measurement noise have been tested by means of several numerical simulations. First, the component of the displacement along the direction normal to the upper surface of the plate has been calculated at each node of the mesh and the resulting displacement field has been used in substitution of the experimental data. Then, the GA, using a part or the whole nodal displacement field, identified the elastic constants. A comparison between the results and the values of the

elastic properties used to simulate the experimental displacement field, allowed to refine the procedure and verify its accuracy.

Table 5.8 – Computer-simulated fringe patterns

Aluminium	Carbon/Epoxy	Glass/Epoxy	Pitch/Epoxy
-	[0°]	[0°]	[0°]
	C/E		
[90°]	[0°,90°]s	Pi/3	[±15°]s
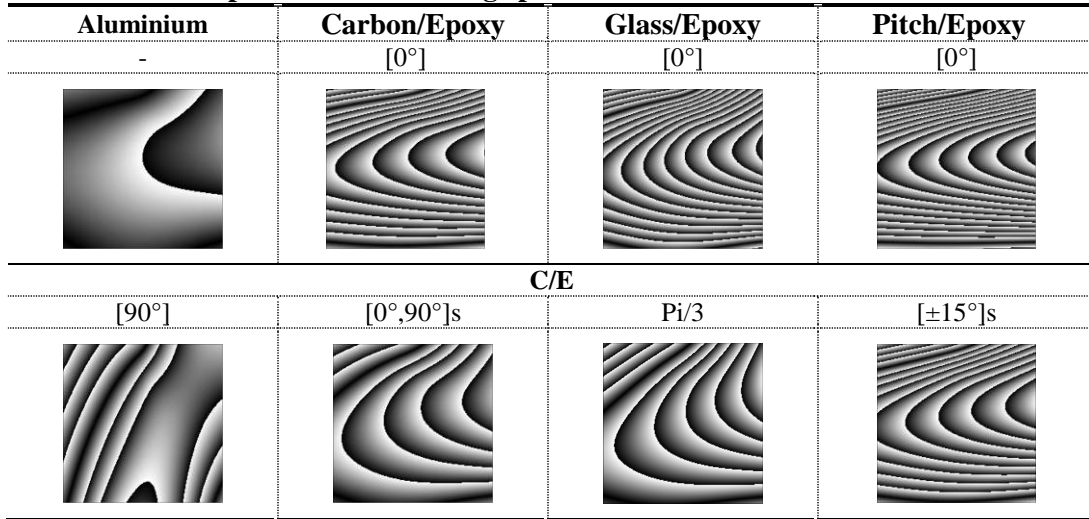
The contours of the computer-simulated displacement field (fringe patterns obtained, for example, by an interferometric technique with a sensitivity of 0.266 μm/fringe) due to a load force equal to 0.45 N are reported, for each square plate, in Table 5.8. The mean values of the number of executions of the FEM code to converge to the solution, with an error less than 0.1%, are reported for each case in Table 5.9. The bounds on parameters have been set at approximately ±100% from the true values. For each case three GA runs have been performed. Obviously, in case of aluminium plate, even if fine results can be obtained solving for four unknowns, the identification of only two elastic constants is recommended because requires shorter execution times.

Table 5.9 – Number of FEM runs for each material

Material	Fibers orientation	Number of parameter	FEA number executions
Aluminium	-	2	380
		4	4721
Glass/Epoxy	[0°]	4	4002
Pitch/Epoxy	[0°]	4	7861
Carbon/Epoxy	[0°]	4	4171
	[90°]	4	*
	Pi/3	4	*
	[0°,90°]s	4	*
	[±15°]s	4	*

* After 20000 runs convergence was not reached

The stability of the inverse procedure has been checked by using simulated measurements with Gaussian noise. In particular, a vector of random numbers has been generated from a Gaussian distribution with the mean $\overline{w}$ set to zero and standard deviation s_w equal to a percentage of the sensitivity of the interferometric technique. s_w can be defined as 0.266 p_{cnlv} where p_{cnlv} is the value to control the level of noise contamination. For example, $p_{cnlv} = 0.5$ means a 50% noise level; in terms of fringe order this noise level is equivalent to half fringe. The Gaussian noise has been directly added to the computer-generated fringe patterns.

Table 5.10 – Computer-simulated fringe patterns with noise

	Carbon/Epoxy [0°]	Glass/Epoxy [0°]	Pitch/Epoxy [0°]
Noise Free			
15% Noise			
30% Noise			
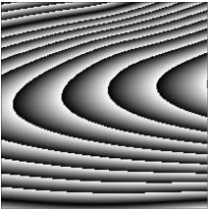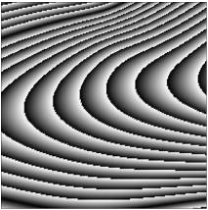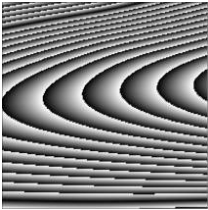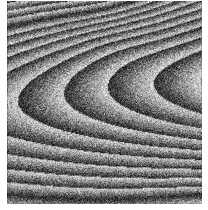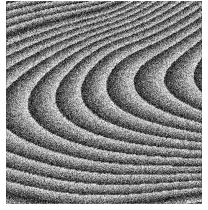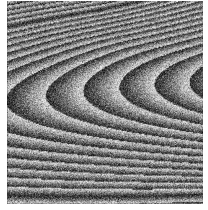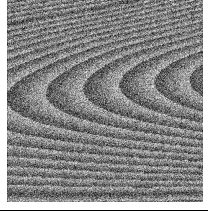
In Table 5.10, the fringe patterns affected by two levels of noise, 15% and 30%, respectively, are illustrated for the cases of carbon-epoxy plate, glass-epoxy plate and pitch-epoxy plate, respectively. For each case, three GA runs have been performed. The GA has been stopped if no improvements have been obtained after 35 generations.

The mean values of material properties obtained by the identification procedure are reported in Table 5.11. It has been found that the solutions are very stable and accurate not only for the noise-free case, but also for the other noise levels examined.

Table 5.11 – Results for the thin laminates based on computer-simulated responses

Material	Elastic Constant	Noise free		15% Noise		30% Noise	
		$\bar{x}$	$s_x\%$	$\bar{x}$	$s_x\%$	$\bar{x}$	$s_x\%$
[0°] Carbon/Epoxy	E_1 [GPa]	134	0.0	133.6	0.3	134.7	0.6
	E_2 [GPa]	8.9	0.0	8.9	0.0	8.9	0.0
	ν_{12}	0.24	0.0	0.24	0.2	0.24	1.0
	G_{12} [GPa]	7.0	0.0	7.0	0.0	7.0	0.1
[0°] Glass/Epoxy	E_1 [GPa]	38.6	0.0	38.6	0.2	38.6	0.2
	E_2 [GPa]	8.3	0.0	8.3	0.0	8.3	0.0
	ν_{12}	0.26	0.0	0.26	0.0	0.26	0.2
	G_{12} [GPa]	4.1	0.0	4.1	0.0	4.1	0.0
[0°] Pitch/Epoxy	E_1 [GPa]	462.0	0.0	463.2	1.1	462.1	2.3
	E_2 [GPa]	6.2	0.0	6.2	0.0	6.2	0.0
	ν_{12}	0.31	0.0	0.31	4.4	0.31	5.4
	G_{12} [GPa]	5.6	0.0	5.6	0.0	5.6	0.1

5.5 Conclusion

The feasibility of using an inverse procedure for determining the elastic constants of composite and isotropic materials from the full-field measurement of the surface displacements of any-shaped plates laminates under flexural loads has been tested. A correlation-based method has been proposed to find more suitable load and constrain configurations for any-shaped plates. It must be pointed out that the square plate allows to increase the convergence rate of the identification procedure, and obtaining a more stable behaviour in the presence of experimental noise. However, the correlation-based method is of great help in testing the flexibility of other specimen geometries for solving the elastic inverse problem. A real-coded adaptive range GA has been adopted to develop an optimization process by which the elastic constants are identified by updating their values in a numerical model until the calculated displacements fit on the experimental ones as accurately as possible. The procedure has proved to be suitable for the elastic identification of unidirectional laminates but less appropriate for multidirectional ones. The main advantage of the present identification method with respect to the traditional methodologies for the characterization of unidirectional laminates is that all elastic constants are determined from one static test by using a plate sample. Thus, the material is not destroyed by cutting samples in order to determine different elastic constants. The robustness of the procedure with respect to the effects of measurement noise has been investigated by adding Gauss noise to the simulated displacement field.

5.6 Bibliography

Apalkov, A.A., Odintsev, I.N., Pisarev, V.S., 1999. Implementation of compenzation speckle interferometry for high-precision determination of materials mechanical properties. Proceedings of SPIE. 3745, 169-179.

Archbold, E., Ennos, A.E., Virdee, M.S., 1978. The deformation of steel bars in a four-point bending machine, measured by holographic interferometry. VDI-Berichte, 313, 517-522.

Balasubramaniam, K., Rao, N.S., 1998. Inversion of Composite Material Elastic Constants from Ultrasonic Bulk Wave Phase Velocity Data Using Genetic Algorithms. Composites Part B - Engineering, 29, 171-180.

Bruno, L., Furgiuele, F.M., Pagnotta, L., Poggialini, A., 2002a. A full-field approach for the elastic characterization of anisotropic materials. Optics and Lasers in Engineering, 37 (4), 417-431.

Bruno, L., Furgiuele, F.M., Pagnotta, L., Poggialini, A., 2002b. Determination of elastic constants of anisotropic plates by phase stepping speckle interferometry. Key Engineering Materials, 221 (2), 363-373.

Bruno, L., Poggialini, A., 2005. Elastic characterization of anisotropic materials by speckle interferometry. Experimental Mechanics, 45 (3), 205-212.

Bruno, L., Felice, G., Pagnotta, L., Poggialini, A., 2006a. A mixed numerical-experimental methodology for determining the elastic constants of orthotropic materials. Speckle06. Nîmes, France. 6341, 0J-1-0J-6.

Bruno, L., Pagnotta, L., Poggialini, A., 2006b. Elastic characterization of CVD diamond by static and dynamic measurement. Journal of the European Ceramic Society, 26 (12), 2419-2425.

Bruno, L., Felice, G., Pagnotta, L., Poggialini, A., Stigliano, G., 2008. Elastic characterization of plates of any shape via static testing. International Journal of Solids and Structures, 45 (3-4), 908–920.

Cardénas-Garcia, J.F., Ekwaro-Osire, S., Berg, J.M., Wilson, W.H., 2005. Non-linear least-squares solution to the moiré hole method problem in orthotropic materials. part II: material elastic constants. Experimental Mechanics, 45 (4), 314-324.

Carlsson, L.A., Pipes, B.R., 1997. Experimental characterization of advanced composite materials. Technomic Publishing Company Inc., Lancaster Basel.

Cloud Gary, L., 1995. Optical Methods of Engineering Analysis. Cambridge: University Press.

Cornu, A., 1869. Méthode optique pour l'etude de la déformation de la surface extériere de solides elastique. Les Comptes Rendus de l'Académie des Science, Paris, 69, 333-337.

Cunha, J., Cogan, S., Berthod, C., 1999. Application of genetic algorithms for the identification of elastic constants of composite materials from dynamic tests. International Journal for Numerical Method in Engineering, 45, 891-900.

Fällström, K.E., Jonsson, M., 1991. A nondestructive method to determine material properties in anisotropic plates. Polymer Composites, 12 (5), 293-305.

Fällström, K.-E., Olofsson, K., Saldner, H.O., Schedin, S., 1996. Dynamic material parameters in an anisotropic plate estimated by phase-stepped holographic interferometry. Optics and Lasers in Engineering, 24 (5), 429-454.

Furgiuele, F.M., Muzzupappa, M., Pagnotta, L., 1997. A full-field procedure for evaluating the elastic properties of advanced ceramics. Experimental Mechanics, 37 (3), 285-290.

Ganesian, A.R., 1989. Measurement of Poisson's ratio using real-time digital speckle pattern interferometry. Optics and Lasers in Engineering, 11, 265-269.

Gascon, F., Salazar, F., 1996. A procedure for calculating through laser speckle interferometry the elastic constants of isotropic materials. Optics Communications, 123 (4), 734-742.

Gaul, L., Willner, K., Hurlebaus, S., 1999. Determination of material properties of plates from modal ESPI measurement. Paper presented at the 17th International Modal Analysis Conference. Orlando, FL. 1756-1763.

Genovese, K., Lamberti, L., Pappalettere, C., 2004. A new hybrid technique for in-plane characterization of orthotropic materials. Experimental Mechanics, 44 (6), 584-592.

Grédiac, M., Vautrin, A., 1993. Mechanical characterization of anisotropic plates: experiment and results. European Journal of Mechanics A/Solids, 12 (6), 819-838.

Grédiac, M., Fourier, N., Paris, P.A., Surrel, Y., 1998. Direct identification of elastic constants of anisotropic plates by modal analysis: Experiment and results. Journal of Sound and Vibration, 210 (5), 645-659.

Grédiac, M., Pierrot, F., Avril, S., Toussaint, E., 2006. The Virtual Field Method for Extracting Constitutive Parameters from Full-Field Measurements: a Review. Strain, 42, 233-253.

Hild, F., Roux, S., 2006. Digital image correlation: from displacement measurement to identification of elastic properties – a review. Strain, 42 (2), 69-80.

Jones, R., Bijl, D., 1974. A holographic inteferometric study of the end effects associated with the four-point bending technique for measuring poisso's ratio. Journal of Physics E: Scientific Instruments, 7 (5), 357-358.

Lecompte, D., A.Smits, Sol, H., Vantomme, J., Hemelrijck, D.V., 2007. Mixed numerical-experimental technique for orthotropic parameter identification using biaxial tensile tests on cruciform specimens. International Journal of Solids and Structures, 44 (5), 1643-1656.

Liu, G.R., Han, X., Lam, K.Y., 2002. A Combined Genetic Algorithm and Nonlinear Least Squares Method for Material Characterization Using Elastic Waves. Computer Methods in Applied Mechanics and Engineering, 191, 1909-1921.

Maletta, C, Pagnotta, L., 2004. On the determination of mechanical properties of composite laminates using genetic algorithms. International Journal of Mechanics and Materials in Design, 1 (2), 199-211.

Mitchell M., 1999. An Introduction to Genetic Algorithms, Apogeo Scientifica.

Molimard, J., Riche, R.L., Vautrin, A., Lee, J.R., 2005. Identification of the four orthotropic plate stiffnesses using a single open-hole tensile test. Experimental Mechanics, 45 (5), 404-411.

Oyama, A., Obayashi, S., Nakamura, T., 2001. Real-coded Adaptive Range Genetic Algorithm Applied to Ultransonic Wing Optimization. Applied Soft Computing, 1, 179-187.

Pagnotta, L., Stigliano, G., 2006. A numerical-experimental approach for identification of material constants of composite laminates by displacement field measurement. WSEAS Transactions on Applied and Theoretical Mechanics, 1 (1), 39 – 46.

Pagnotta, L., 2007. Determining elastic constants of materials with interferometric techniques. Inverse Problems in Science and Engineering, 14 (8), 801 – 818.

Pagnotta, L., Stigliano, G., 2007. Elastic characterization of isotropic plates of any shape via dynamic tests: theoretical aspects and numerical simulations. paper under review,

Prabhakaran, R., Chermahini, R.G., 1984. Application of the least-squares method to elastic and photoelastic calibration of orthotropic composites. Experimental Mechanics, 24 (1), 17-21.

Timoshenko, S.P., Goodier, J.N., 1970. Theory of elasticity. McGraw-Hill Publishing Co., Tokyo.

Wang, W.T., Kam, T.Y., 2000. Material characterization of laminated composite plates via static testing. Composite Structures, 50 (4), 347-352.

Wang, Z., Cardénas-Garcia, J.F., Han, B., 2005. Inverse method to determine elastic constants using a circolar disk and moiré interferometry. Experimental Mechanics, 45 (1), 27-34.

6 EXPERIMENTAL VALIDATION OF THE STATIC TECHNIQUE

6.1 Introduction

In order to validate the effectiveness of the proposed procedure and to carry out a cross-check with the results provided by the dynamic technique, some experimental tests have been executed on isotropic and orthotropic plates. In particular, two aluminium plates and a Graphite/PEEK plate of different shapes have been tested. The results have been compared with those obtained with other techniques. The tests have been carried out using the information obtained by the numerical simulations and the correlation-based method showed in previous chapter.

6.2   Identification process

The steps of the mixed numerical-experimental technique are the same of those showed for the dynamic technique. First of all, the operator has to carry out the experimental procedure, like the measurement of size, shape of the sample and displacement field (see Figure 6.1). As it has been shown in previous sections, the shape measurement can be efficiently carried out by a common digital scanner connected to a personal computer. After that, an image processor software can be used to export the picture into a mesh generator program. For detecting the experimental displacement of the loaded plate an optical technique can be used. In the present dissertation a speckle interferometric technique has been used.
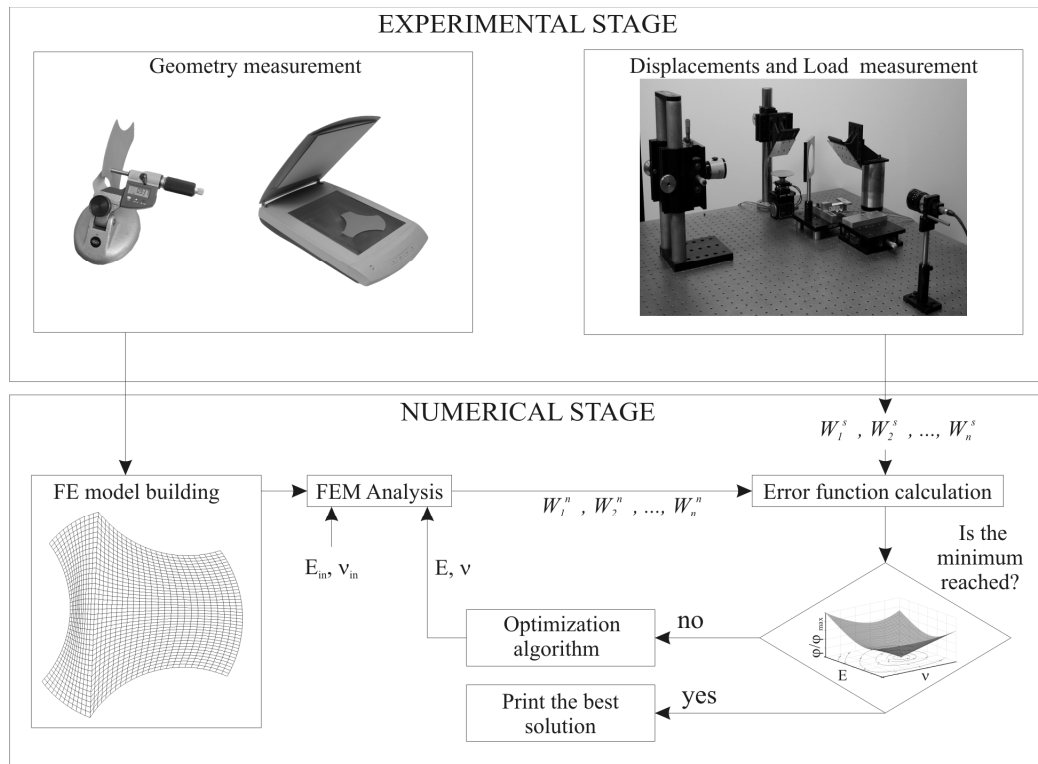
Figure 6.1 The identification process

After the experimental stage, the operator can identify the elastic moduli by the minimization process. This operation is carried out by a dedicated algorithm that can be implemented in any of the more common programming languages in which the FEM solver is managed by its input and output files. Previously the importance of the choice of the error function has been highlighted. It is crucial in terms of solution time and accuracy. In the

131

numerical study, it has been shown that in the static characterization the following error function can be used:

$$\varphi = \sum_{i=1}^{N} \left| w_i^{\,n} - w_i^{\,e} \right| \tag{6.1}$$

The numerical procedure for orthotropic materials is the same of that used for the isotropic materials; only a difference in computational time, due to larger number of unknown parameters to characterise, exists.

6.3   Experimental validation

In order to test the effectiveness and the repeatability of the procedure, this has been applied on two specimens of different shape and material. Figure 6.2 reports the dimensions and the shapes of the specimens: one square specimen has been cut from a unidirectional graphite reinforced PEEK panel, while the irregular shape specimen have been cut from a cold rolled sheet of aluminium alloy 6082-T6, which has been also used to validate the dynamic technique.

Figure 6.2 - The geometry and the acquired area (shaded) of the specimens
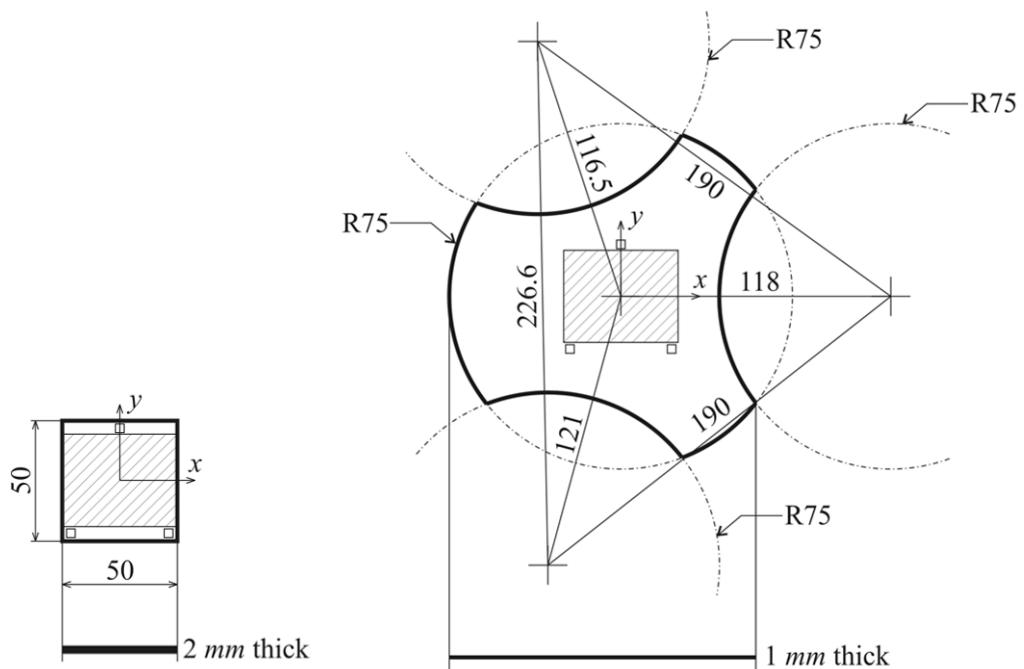
All the specimens have been painted, on the observed side, by a non depolarizing metallic spray paint. The edges of the square plate have been measured by a standard digital calliper with a resolution equal to 10 μm, while the irregular contours of the other specimen have been acquired by a common digital scanner.

With regards to the measurement of the thickness, an averaging over a number of measurements in different points has been carried out; these measurements have been performed by a digital micrometer with a resolution of a 1 μm.
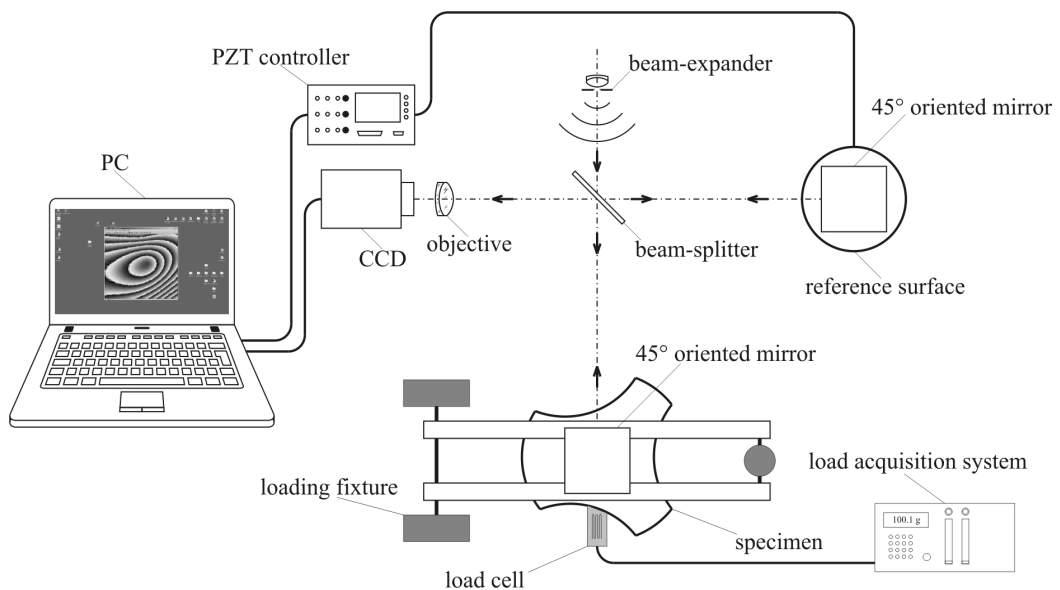
Figure 6.3 - Sketch of the experimental apparatus

The main components of the whole apparatus, which has been used for the experimentations, are shown in the sketch of Figure 6.3. The apparatus has been assembled on an optical bench supported by pneumatic vibration isolators. The light source is a *COHERENT 2W Nd-Yag Model Verdi* operating in single line mode at the wavelength λ=532 nm. The laser beam is filtered and expanded and the resulting spherical wavefront is divided by a beamsplitter into two equal intensity beams. The specimen and the reference surfaces are horizontal and are illuminated and observed by a 45° oriented mirror with the respect of the propagation direction of the beams. The scattered speckle wavefronts interfere at the image plane of the CCD of the TV camera. The camera is interfaced with a general purpose computer image processing system where the real time fringe

133

patterns are generated by the subtraction of digitalized images. Essentially, the optical setup constitutes a speckle interferometer, based on the Michelson design, for measuring the out-of-plane component of displacements. A picture of the optical layout is reported in Figure 6.4.
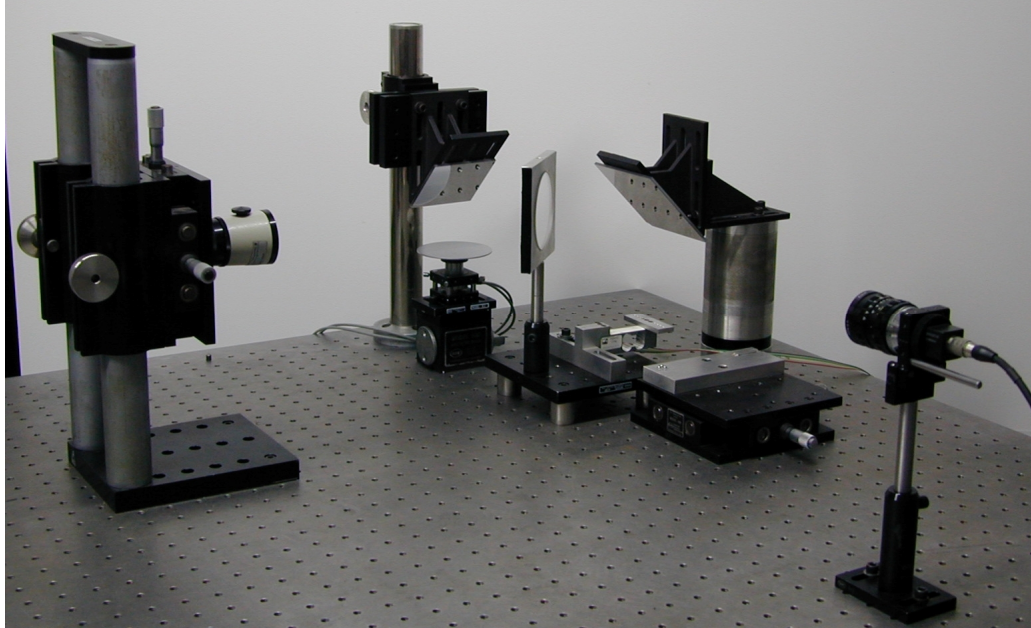
Figure 6.4 - Optical layout

The specimen is placed in the loading device, as shown in Figure 6.5a), and loaded according to the loading configuration reported in Figure 6.6. The length *a* has been assumed equal to 23 *mm* and the coordinates of the loading point are x_F=5 *mm* and y_F=3 *mm*.

a)

b)
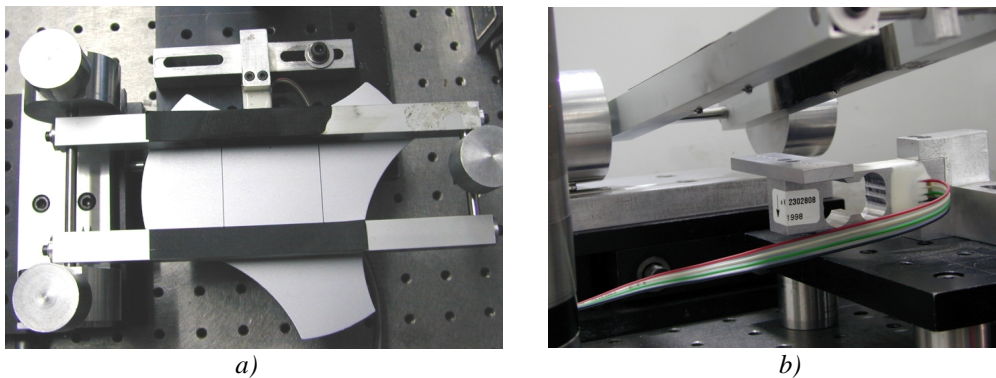
Figure 6.5 - The loading device: (a) the loading fixture and the aluminium plate;
(b) the spheres used for reproducing punctual constraints and load
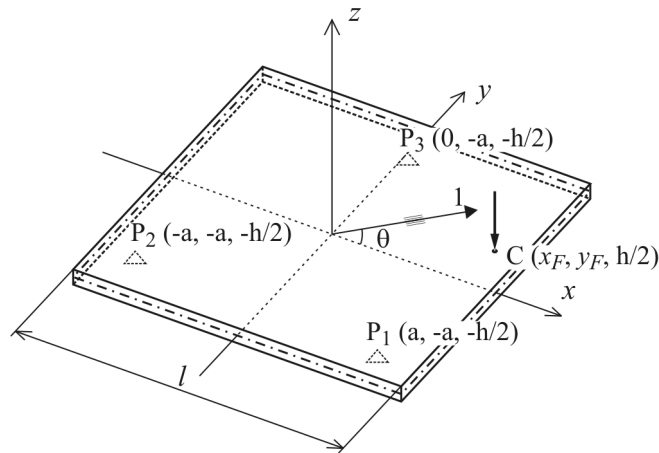
Figure 6.6 - The loading configuration used

As it the previous section shown, this load configuration is appropriate to characterise orthotropic square plates as well isotropic plates of any shape. This can be demonstrate by Figure 6.7 where the correlation map obtained for the irregular plate is reported. In Figure 6.7, point C represent the load position.
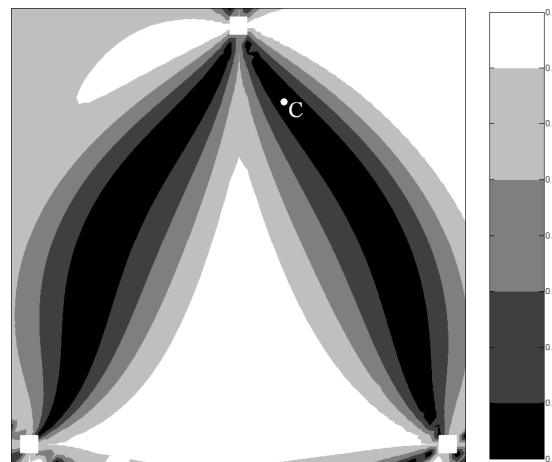
Figure 6.7 - Aluminium correlation map for
the irregular shape specimen

The force is applied by a small sphere of 2.3 *mm* diameter interposed between the lower surface of the specimen and a support plate mounted on a strain gauged load cell, by which the load is measured with a resolution of 10^{-3} *N*. Three small spheres of the same diameter support the specimen on the upper surface. These spheres are glued on two parallel rectangular aluminium bars which are rigidly connected to each other at their ends by two thin circular bars, as shown in Figure 6.5b). For a correct and repeatable location of the support

points, a suitable kinematic device has been properly designed and clamped at one end of the fixture. It allows to remove the fixture and subsequently to reposition it in the same location with interferometric accuracy.

The amplitude of the load is controlled by adding sample weights on a plate fixed at the other end of the fixture. A strain gauged load cell connected to an HBM amplifier has been used to measure the force applied to the plate (see Figure 6.5b). To test the repeatability of the experimental tests, different load levels have been employed, inside the range of values producing a pattern with a suitable number of fringes (from 0.3 N to 0.7 N and from 0.7 N to 1.15 N for the aluminium and composite plates, respectively).

Most of the surface of the specimen (50x44 mm^2) can be observed between the two rectangular bars of the fixture by the CCD camera. The out-of-plane displacements are measured with a sensitivity equal to $\lambda/2$, which can be increased if the phase variations due to the displacements are measured by applying a phase-shifting procedure. A four step algorithm has been applied by a proper Virtual Instrument (VI) implemented in *National Instruments LabView^{TM}* environment, in order to obtain the phase at each pixel of the visible part of the specimen. The technique requires that four speckle patterns must be captured by the CCD camera sequentially. Each frame is shifted by the same amount of phase with respect to the previous one. The phase shift between two successive frames is equal to $\pi/4$; in practice, this change in phase is obtained by translating the reference surface along the vertical axis of an amount equal to $\lambda/8$.

The light intensity at the k_{th} pixel varies according to the following relation:

$$i_k = i_m + i_a \cos(\delta + \Delta\varphi_k) \tag{6.2}$$

where i_m, i_a and δ are the mean intensity, the modulation and the phase, respectively, that is the parameters to be determined, while $\Delta\varphi_k$ is the known shift introduced by the phase-shifting procedure. The unknowns can be calculated locally at each pixel of the image by solving the system of linear equations obtained by writing as many equations as the number of steps (at least three). The phase is then calculated from the light intensity measured at

different steps. If a four equispaced $\pi/4$ step algorithm is adopted the phase is calculated according to the following relation:

$$\delta = \arctan \frac{I_4 - I_2}{I_1 - I_3} \tag{6.3}$$

where I_i is the light intensity of the i-th step.

The phase-shifting procedure is entirely performed by a personal computer interfaced by a standard RS232 serial port with the amplifier of a PZT actuator, able to move the reference surface with nanometric accuracy. In fact, by means of the implemented virtual instrument, it is possible to move the actuator and to acquire, by a CCD camera, the speckle intensity patterns scattered from the surface under test. By the virtual instrument is also possible to unwrap the phase maps by proper algorithms able to work in presence of severe noise.

A 2D finite element model is developed for each plate, paying attention that a node of the mesh falls in proximity, or eventually exactly at the location, of each support and loading point; the position of these points are traced on the painted side of the specimen before the beginning of the measurement sessions. Then, they are acquired together with the boundary of the plate and the obtained coordinates are used for defining the position of the nodes to be constrained and loaded. Quadratic four node elements (CQUAD4) have been used (2500 elements for the square plate and 7600 elements for the generic shape plate) and the effects of the transverse shear deformation has been considered in the analysis. The meshes are reported in Figure 6.8.

For characterising the material, the specimen must be introduced in the loading fixture by carefully controlling that the three points marked on the upper surface of the plate overlap as accurately as possible with the three support spheres of the loading fixture. If this fact is respected, the real loading and constraining condition coincides with the simulated one. Any definite area on the FEM model corresponds to an area observed by the camera and the measured displacement can be readily associated at each node of the mesh. The lack of alignment between the loading fixture and the plate could imply large errors in the solution.
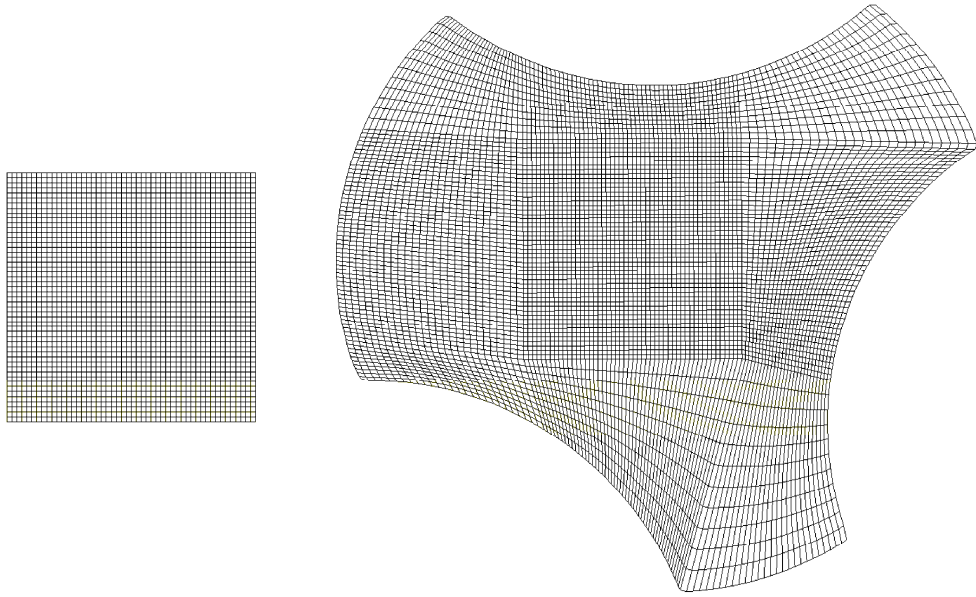
Figure 6.8 - The meshes created for the numerical analysis of the specimens

Typical phase maps are shown in Figure 6.9. In the optical arrangement, the sensitivity vector was normal to the surface of the specimen, with a module equal to half of the wavelength of the light source (532 *nm*); this means that between two adjacent fringes there is a difference in out-of-plane displacement equal to 266 *nm*. As it can be seen, fringes are very noisy due to the intrinsic noise of the speckle techniques.
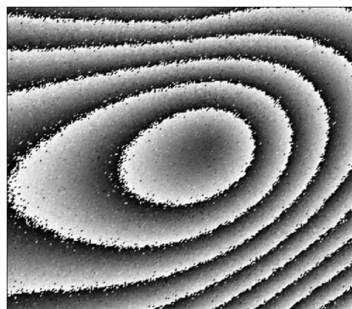
Aluminium irregular plate
Load 0.488 N
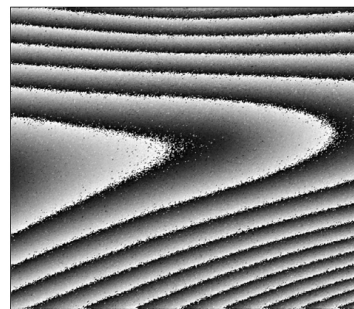
Graphite/PEEK plate
Load 0.733 N

Figure 6.9 - Experimental data for the two specimens

Many tests have been carried out on the plates for different load levels with the aim of verifying the repeatability and the accuracy of the procedure. At each time, the specimen has been removed from the fixture and then repositioned and, for each test, the procedure has been applied several times.

The unavoidable rigid body motion of the specimen due to the compliance of the fixture, consisting in a rigid translation along *z*-axis and two rigid

rotations about the *x*- and *y*-axis, affects drastically the fringe patterns, leading to an inability to properly identify the elastic constants. In order to calculate and hence compensate these unwanted effects the fitness of the genetic algorithm has been modified. Such a change is based on the fact that difference between the measured $W^e(x,y)$ and the numerically calculated $W^n(x,y)$ out-of-plane displacements of the plate, except for the measurement noise and the different elastic constants assumed in the numerical simulations, can be approximated in the space *Oxyz* by the plane $W(x,y)$ whose equation can be written as:

$$W(x, y) = p_1 x + p_2 y + p_3 \qquad (6.4)$$

where the coefficients *(p₁, p₂, p₃)* describe analytically the average plane calculated on the experimental data which represents, at the end of the optimization process, the overall rigid body motion. Then, the fitness could be defined as:

$$\varphi = \left(W^e - W^n \right) - W \qquad (6.5)$$

Therefore the coefficients p_i can be found by solving the following over-determined system of equations by applying the least mean square method:

$$\begin{bmatrix} 1 & x_1 & y_1 \\ 1 & x_2 & y_2 \\ \vdots & \vdots & \vdots \\ 1 & x_m & y_m \end{bmatrix} \begin{Bmatrix} p_1 \\ p_2 \\ p_3 \end{Bmatrix} = \begin{Bmatrix} w_1^n - w_1^e \\ w_2^n - w_2^e \\ \vdots \\ w_n^n - w_n^e \end{Bmatrix} \qquad (6.6)$$

where *(xᵢ, yᵢ)* are the coordinates of the *i*-th node. In a compact form, eq. (6.6) can be rewritten as:

$$[M]\{p\} = \{w\} \qquad (6.7)$$

where [*M*] and {*w*} are the coefficient matrix and the known vector of the over-determined equation system, respectively. By defining the matrix [*C*] as follows:

$$[C] = [M][M]^+ - [I] \qquad (6.8)$$

in which the superscript $^+$ indicates the pseudoinverse of $[M]$, and $[I]$ is the identity matrix. Finally the fitness is evaluated as:

$$\varphi = \left\| [C]\{w\} \right\| \tag{6.9}$$

Table 6.1 and Table 6.2 report the elastic moduli values of the examined specimens. Since aluminium is an isotropic material, the identification of only two elastic constants is enough. However, in order to investigate the capability of the genetic algorithm to identify the anisotropy of the material, the elastic constants have been also evaluated by the four constants algorithm. The results are accurate even if four elastic constants are determined.

Table 6.1 – Elastic moduli obtained on aluminium irregular plate

Load [N]	Four unknowns				Two unknowns	
	E_1 [GPa]	E_2 [GPa]	ν_{12}	G_{12} [GPa]	E [GPa]	ν
0.359	71.0	71.3	0.344	25.5	72.0	0.335
0.359	71.3	70.3	0.331	25.8	71.9	0.340
0.374	70.9	70.5	0.344	26.1	74.8	0.340
0.370	71.7	71.3	0.354	25.3	71.2	0.340
0.488	72.5	71.5	0.333	25.1	72.1	0.331
0.492	72.8	71.8	0.337	25.0	71.4	0.341
0.500	70.4	71.7	0.352	25.3	70.2	0.354
0.730	68.5	72.0	0.345	25.7	71.0	0.343
0.741	69.7	71.3	0.346	25.1	70.5	0.351
0.742	71.2	71.4	0.353	26.1	69.9	0.357
$\bar{x}$	71.0	71.3	0.344	25.5	71.5	0.343
s_x	1.8%	0.8%	2.4%	1.6%	1.9%	2.4%

Table 6.2 – Elastic moduli obtained on Graphite/PEEK square plate

Load [N]	E_1 [GPa]	E_2 [GPa]	ν_{12}	G_{12} [GPa]
0.722	136.7	10.9	0.255	6.4
0.722	138.1	10.9	0.262	6.3
0.733	136.7	10.9	0.317	6.3
0.734	136.5	10.9	0.269	6.2
0.734	141.9	10.8	0.267	6.2
1.096	137.7	10.9	0.274	6.2
1.097	132.5	10.9	0.264	6.2
1.097	132.5	10.9	0.264	6.2
1.099	140.8	10.9	0.256	6.3
1.465	142.6	10.9	0.283	6.3
$\bar{x}$	137.6	10.9	0.271	6.2
s_x	2.5%	0.3%	6.7%	1.1%

In Table 6.3 the mean value of the elastic constants obtained by the proposed technique are compared with those obtained on the same specimen by a dynamic test. The good agreement of the results obtained by the two different approaches confirms the validity of the procedure. Table 6.3 reports also the mean value obtained on the composite specimen, that is compared with those obtained by the ASTM standard (ASTM D3039M) on sample of the same materials; also for this material a high repeatability and a good agreement for E_1 with the results obtained by the ASTM standard can be observed. For the other elastic moduli a larger differences have been obtained. In particular difference of 22%, 23% and -11% have been achieved for E_2, ν_{12} and G_{12} respectively. Unfortunately, the ASTM standards gives a reference repeatability value of 2.7% for Young's modulus and no reference value for the other constant. Furthermore no reference value are given for the bias because no acceptable reference standard exists.

Table 6.3 – Mean value of the elastic moduli obtained with the present procedure and comparison with other technique

Sample	Method	E_1 [GPa]	E_2 [GPa]	ν_{12}	G_{12} [GPa]
Aluminium Irregular plate	Present (2 constants)	71.5	71.5	0.343	
	Present (4 constants)	71.0	71.3	0.344	25.5
	Dynamic test (iterative) [1]	72.3	72.3	0.336	
Graphite/PEEK Square plate	Present (4 constants)	137.6	10.9	0.271	6.2
	ASTM	134.0	8.9	0.240	7.0

[1]: Pagnotta and Stigliano, 2008.

Figure 6.9 reports the experimental data without any manipulation, while, Figure 6.10 reports the phase maps for the specimens: in the first row there are the phase maps relative to the aluminium specimens, in the second row those relative to the composite specimen. In particular Figure 6.10a) reports the phase maps which would be obtained if the out-of-plane displacement field matches exactly that obtained numerically. Figure 6.10b) shows the rigid body motion analytically described by eq.(6.4) and found by the application of the genetic algorithm when the fitness is calculated by eq.(6.9). Finally, Figure 6.10c) reports the experimental data obtained by subtracting the rigid body motion evaluated by the characterization procedure from the original data. It must be noticed the high similarity between the numerical data (Figure 6.10a)) and the experimental data without the rigid body motion (Figure 6.10c)).

141
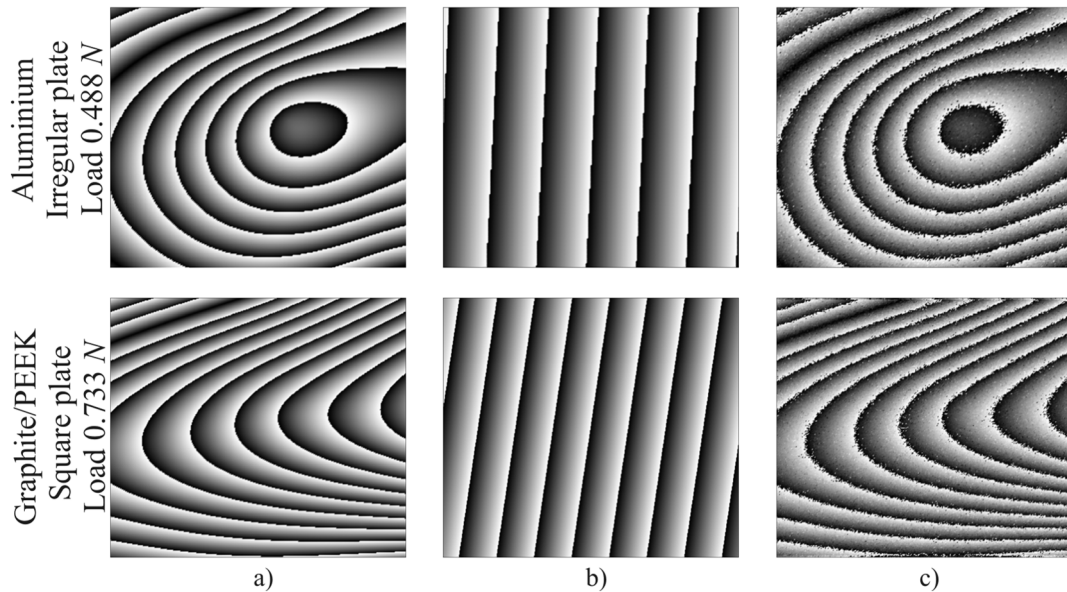
Figure 6.10 - Experimental and numerical data for the specimens: (a) phase maps obtained by numerical displacement fields; (b) rigid body motion evaluated by the genetic algorithm; (c) experimental data without rigid body motion

6.4   Conclusion

The feasibility of using the displacement field of a properly loaded plate in an iterative procedure for determining the elastic properties of isotropic and orthotropic materials has been experimentally and successfully assessed. The displacement fields have been measured with a speckle interferometer based on Michelson design. The results obtained have been compared with those reported with other techniques and the agreement is quite good. With such a procedure, the identification of the elastic moduli is carried out simultaneously, not destructively, in a single test. The main drawback of the present technique is the equipment cost; in fact it is more expensive than that used for dynamic characterization.

6.5   Bibliography

ASTM D3039M-00e2 Standard Test Method for Tensile Properties of Polymer Matrix Composite Materials.

Bruno, L., Felice, G., Pagnotta, L., Poggialini, A., Stigliano, G., 2008. Elastic characterization of plates of any shape via static testing. International Journal of Solids and Structures, 45 (3-4), 908–920.

Alfano, M., Pagnotta, L., Stigliano, G., 2006. International conference, ISMA 2006. Belgium. 2033–2040.

Pagnotta, L., Stigliano, G., 2008. Elastic characterization of isotropic plates of any shape via dynamic tests: theoretical aspects and numerical simulations. Mechanics Research Communications, 35 (6), 351–360.

Pagnotta, L., Stigliano, G., 2008. Elastic characterization of isotropic plates of any shape via dynamic tests:Practical aspects and experimental applications. Mechanics Research Communications, doi: 10.1016/j.mechrescom .2008.09.003

CONCLUSION

It was shown that traditional characterization procedures, based on static loading of standardized test specimens, are usually tedious and expensive to be applied. Moreover, these tests often yield unsatisfactory results. On the other hand, fast, accurate and inexpensive tests for determining all the elastic moduli by using a single experimental test are sought. In the present dissertation simple test procedures to determine the elastic properties of isotropic and composite samples have been developed. The aim of the present dissertation has been focalized on developing a rapid and inexpensive test to characterise all the elastic moduli using a single dynamic or static experimental test. The procedures proposed herein are often referred to Mixed Numerical Experimental Technique (MNET). They are based on an optimization procedure which minimizes the difference between numerical data (e.g. the natural frequencies of vibration or displacement field evaluated by a standard FEM code) and experimental data. Phase-shifting speckle interferometry has been employed to detect the out-of-plane displacement field of a portion of the observed surface of the specimen, while a Impulse Excitation Technique (IET) has been adopted to obtain the natural frequencies of the specimen.

The common thread in the two proposed characterization procedures is that the determination of material constants is regarded as an inverse problem. In particular, it has been shown that for isotropic materials the optimization problem can be solved using a standard algorithm (e.g. gradient-based methods). However, for an increasing number of unknown parameters (i.e. composite materials) a Genetic Algorithm (GA) was adopted. In addition, a comparative analysis of different error functions has been carried out using an *ad hoc* graphical method. Furthermore, the robustness of the identification procedure against experimental noise has been numerically assessed. In such a way, it was possible to select an error function which provided an increased convergence rate and a reasonable accuracy of the results. In particular, for dynamic and static characterization the

square root of the sum of the squares of the relative errors and the sum of the absolute values of the errors have been chosen respectively.

For dynamic characterization a number of natural frequencies equal to the number of unknown values have to be used but it is not enough if the frequencies are not well chosen. To solve this problem and to average the noise of experimental measurement a number equal to the double of the unknown values is advisable. Furthermore, the proposed method does not require modal shapes measurement, nor modal indices are required because frequencies are correlated simply by their number in a sequential order of magnitude. The dynamic method showed a high potentiality to determine the elastic properties of any-shaped (also drilled) isotropic plates. With such a procedure the identification of the elastic moduli is carried out simultaneously, not destructively, in a single test. The measurement system is simple, inexpensive and fast. Furthermore it is contactless and permits the characterization of materials at high temperature. Moreover, this method is applicable to orthotropic plates as well as laminated plates, but it presents some drawbacks. It has been shown that Poisson's ratio and the transverse shear modulus are not so sensitive, with regard to the eigenfrequencies, as the other parameters. Other problems can arise when the IET is applied on high damping materials: in this case a resonant method is necessary, and then more expensive equipment are required. However, the cost of the device necessary to carry out the dynamic characterization (pc provided with a sound card and a microphone) is very low compared to the cost of the device used in static technique (laser, optical component, optical bench and so on). Obviously these costs may be reduced, for instance, by using a low cost portable device working with laser diodes. Also for the proposed static technique, all the elastic constants are determined from one static test by using a plate sample; this is the main advantage with respect to the traditional methodologies used for the characterization of unidirectional laminates. It has been shown that great care is to be taken in choosing the geometry of the specimen and the way of loading and constraining it. For this purpose, a correlation-based method has been proposed to find more suitable load and constrain configurations for any-shaped plates. It has been found that the square plate increases the convergence rate of the identification procedure, and has more stable behaviour in the presence of experimental noise. Moreover, the correlation-based method is of great help in

testing the flexibility of other specimen geometries for solving the elastic inverse problem. It has been shown that the technique is able to identify the elastic constants of isotopic plate of any-shape without significant repercussion on the accuracy of the results. Moreover, the robustness of the procedure with respect to the effects of measurement noise has been investigated by adding Gauss noise to the input displacement field. However, the procedure proved to be suitable for the elastic identification of unidirectional laminates but less appropriate for multidirectional ones or for specimen geometry far from the square plate. As for the other static techniques, great care is needed for loading and constraining the specimens. In order to eliminate the rigid displacement present into the row data coming from speckle technique a numerical procedure has been carried out and successfully tested in numerical and experimental way. The major drawbacks for both the procedures proposed is, obviously, the computational costs of the optimization processes. However, these disadvantages might become less critical in the future with the advancement of computer technology. A possible future development could be the application of neural network. In fact, once the geometry of the specimen is defined, after a numerical training, it is possible to find the relation between the displacement (or the natural frequencies) of the sample and its elastic moduli.

APPENDIX A: MATLAB CODE TO ACQUIRE NATURAL FREQUENCIES

In order to acquire the natural frequencies of the sample a GUI (Graphical User Interfaces) has been developed in Matlab™ environment. The GUI allows to acquire by a microphone the audio signal coming from the impacted sample. After that, a fast Fourier transform (FFT) is carried out, thanks to the Matlab function "*fft()*". By the definition of the range search, the sill amplitude search (the green line in Figure A.1) and the high-pass filter value, the GUI finds automatically the peaks corresponding to the natural frequencies. Figure A.1 reports the front panel of the GUI, while below the Matlab code is reported.
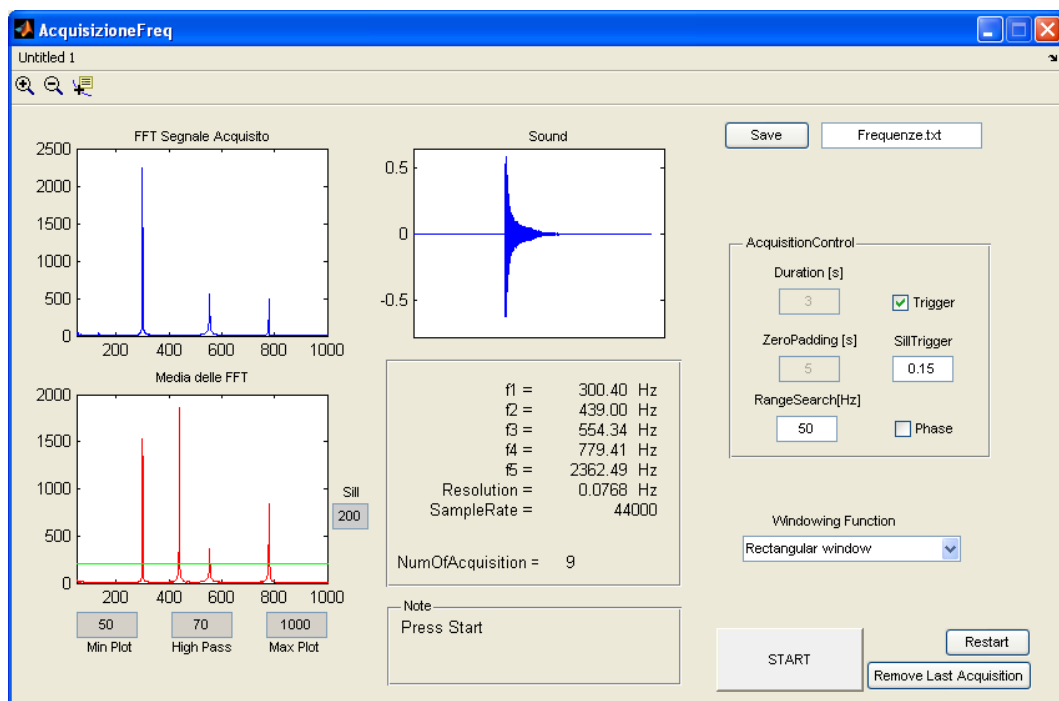

Figure A.1 – Front panel of the GUI.

function varargout = AcquisizioneFreq(varargin)
% Main program
gui_Singleton = 1;

```
gui_State = struct('gui_Name',        mfilename, ...
                'gui_Singleton',  gui_Singleton, ...
                'gui_OpeningFcn', @AcquisizioneFreq_OpeningFcn, ...
                'gui_OutputFcn',  @AcquisizioneFreq_OutputFcn, ...
                'gui_LayoutFcn',  [] , ...
                'gui_Callback',   []);
if nargin && ischar(varargin{1})
    gui_State.gui_Callback = str2func(varargin{1});
end
if nargout
    [varargout{1:nargout}] = gui_mainfcn(gui_State, varargin{:});
else
    gui_mainfcn(gui_State, varargin{:});
end
% End initialization code


function AcquisizioneFreq_OpeningFcn(hObject, eventdata, handles, varargin)
% This function has no output args, see OutputFcn.
handles.output = hObject;
handles.soglia=70;
set(handles.Sill, 'String', int2str(handles.soglia));
handles.filtroPassaAlto=70;  % high pass filter
set(handles.Sill, 'String', int2str(handles.filtroPassaAlto));
handles.min=50;
set(handles.MinPlot, 'String', int2str(handles.min));
handles.max=5000;
set(handles.MaxPlot, 'String', int2str(handles.max));
handles.duration=3;
set(handles.edit_Duration, 'String', int2str(handles.duration));
handles.IntervalloDiRicerca=50;
set(handles.edit_RangeSearch, 'String', int2str(handles.IntervalloDiRicerca));
handles.zeri_prec=5;
handles.zeri_suc=handles.zeri_prec; % zero paved
set(handles.edit_ZeroPadding, 'String', int2str(handles.zeri_suc));
set(handles.radiobutton1_Trigger,'Value',1);
handles.Trigger=get(handles.radiobutton1_Trigger,'Value');
handles.sogliaTrigger=0.15;
set(handles.axes10,'Visible','off');
handles.plottaFase=0;
set(handles.checkbox_Phase,'Value',0);
set(handles.text21_phase,'Visible','off');
handles.canc=0;
guidata(hObject, handles);


function varargout = AcquisizioneFreq_OutputFcn(hObject, eventdata, handles)
varargout{1} = handles.output;


function [fMAX]=trovaMassimiDalloSpettro(y,IntervalloDiRicerca,soglia,filtroPassaAlto)
dim_y=size(y,1);
salita=1; Max_relativo=y(2,:);Max_assoluto=y(2,:);
scritto=1;
indice=1;
for i=3:dim_y
    prova2=y(i,:);prova1=y(i-1,:);
    if y(i-1,2)>y(i,2) & y(i-1,2)>soglia & salita==1
        Max_relativo=y(i-1,:);
        salita=0; scritto=0;
    elseif y(i-1,2)<y(i,2)
        salita=1;
    end
    if salita==0 & Max_relativo(1,2)>Max_assoluto(1,2) & scritto==0
```

```
      Max_assoluto=Max_relativo;
   elseif Max_assoluto(1,1)+IntervalloDiRicerca<y(i,1) & scritto==0
      if Max_assoluto(1,1)>filtroPassaAlto
       fMAX(indice)=Max_assoluto(1,1);
        indice=indice+1;
      end
      scritto=1;
      Max_assoluto(1,2)=0;
   end
   if scritto==0 & i==dim_y
      if Max_assoluto(1,1)>filtroPassaAlto
       fMAX(indice)=Max_assoluto(1,1);
        indice=indice+1;
      end
      scritto=1;
      Max_assoluto(1,2)=0;
   end
end

function pushbutton1_START_Callback(hObject, eventdata, handles)
guidata(hObject,handles)
set(handles.edit_Duration,'Enable','off');
set(handles.edit_ZeroPadding,'Enable','off');
set(handles.text_note,'String','Waiting For Trigger')
handles.SampleRate=44000;
clc
RisultatoIn_dB=0;
%============= end input ==================
AI = analoginput('winsound');
chan = addchannel(AI,1); % Add channels -- Add one channel to AI.
set(AI,'SampleRate',handles.SampleRate);
handles.ActualRate = get(AI,'SampleRate');
set(AI,'SamplesPerTrigger',handles.duration*handles.ActualRate)
handles.blocksize = get(AI,'SamplesPerTrigger');
handles.Fs = handles.ActualRate;
% The trigger executes when a signal with a negative slope passing through
... 0.2.volts is detected on channel 1. set(ai,'TriggerChannel',ch)
if handles.Trigger
   set(AI,'TriggerType','Software');set(AI,'TriggerCondition','Falling');
   set(AI,'TriggerConditionValue',handles.sogliaTrigger);set(AI,'TriggerChannel',chan);
   set(AI,'Timeout',10);start(AI)
else
   set(AI,'TriggerType','Manual');start(AI);trigger(AI)
end
data = getdata(AI);
set(handles.text_note,'String','Acquisizione')
data_zeri_prec=zeros(44100*handles.zeri_prec,1)+1e-17;
data_zeri_suc=zeros(44100*handles.zeri_suc,1)+1e-17;
handles.data=[data_zeri_prec;data;data_zeri_suc];
handles.blocksize=handles.blocksize+44100*handles.zeri_prec+44100*handles.zeri_suc;
 set(handles.text_note,'String','Acquisizione Terminata')
%========== FFT average ===
try
   set(handles.numProveTxt, 'String', int2str(handles.numProve+1));
catch
   set(handles.numProveTxt, 'String','1');
end
handles.numProve=str2num(get(handles.numProveTxt, 'String'));
delete(AI)
clear AI
handles.canc=1;
```

```
guidata(hObject,handles)
 Calcola_FFT(hObject,handles)
```

function Calcola_FFT(hObject,handles)
```
%=========== avaluate FFT ===============
popup_sel_index = get(handles.popupmenu_Windowing, 'Value');
dimensioneData=size(handles.data,1);
switch popup_sel_index
    case 1
       w=1;
    case 2
      w = hann(dimensioneData);
    case 3
      w = blackman(dimensioneData);
    case 4
      w = hamming(dimensioneData);
    case 5
      w = flattopwin(dimensioneData);
end
handles.data_wind=handles.data.*w;
xfft = abs(fft(handles.data_wind));
% Avoid taking the log of 0.
index = find(xfft == 0);
xfft(index) = 1e-17;
mag = (xfft);
size(mag);
handles.mag = mag(1:floor(handles.blocksize/2));
f = (0:length(handles.mag)-1)*handles.Fs/handles.blocksize;
handles.f = f(:);
handles.y=[handles.f,handles.mag];
try handles.mag_n=handles.mag+handles.mag_n;
catch  handles.mag_n=handles.mag; end
guidata(hObject,handles)
calcolaMax(hObject,handles)
```

function calcolaMax(hObject,handles)
```
handles.y_ave=[handles.y(:,1),handles.mag_n/handles.numProve];
handles.media=handles.mag_n/handles.numProve;
try
[handles.fMax]=trovaMassimiDalloSpettro(handles.y_ave,handles.IntervalloDiRicerca,handles.so
glia,handles.filtroPassaAlto);
    fMax = handles.fMax;
catch
   set(handles.text_note,'String','Colpire+Forte')
end
    try f1=fMax(1,1);catch f1=1;end;
    try f2=fMax(2);catch f2=1;end;
    try f3=fMax(3);catch f3=1;end;
    try f4=fMax(4);catch f4=1;end;
    try f5=fMax(5);catch f5=1;end;
    try f6=fMax(6);catch f6=1;end;
     handles.f4Freq=[f1 f2 f3 f4 f5 f6]';
     guidata(hObject,handles)
     plotta(hObject,handles)
```

function plotta(hObject,handles)
```
handles.rangePlott=[handles.min handles.max];
axes(handles.axes3); %Acquired signal Plot
   cla;
   plot(handles.data_wind);
    set(handles.axes3,'XTick',[]);
```

```matlab
axes(handles.axes5); %FFT plot
   cla;
   plot(handles.f,handles.mag);
   xlim(handles.axes5,handles.rangePlott);
 risoluzione=handles.f(2,1);
 f1=handles.f4Freq(1); f2=handles.f4Freq(2); f3=handles.f4Freq(3);
 f4=handles.f4Freq(4);f5=handles.f4Freq(5);
 set(handles.edit_Freq,'String',{[num2str(f1,'%8.2f'),'                Hz'],[num2str(f2,'%8.2f'),'
Hz'],[num2str(f3,'%8.2f'),'  Hz'],...
 [num2str(f4,'%8.2f'),'        Hz'],[num2str(f5,'%8.2f'),'        Hz'],[num2str(risoluzione,'%8.4f'),'
Hz'],num2str(handles.ActualRate)})
if handles.plottaFase
   axes(handles.axes10);
   cla;
   fase=angle(fft(handles.data_wind));
   plot(handles.f,fase(1:size(handles.f)));
   xlim(handles.axes10,handles.rangePlott);
else
   axes(handles.axes6);
   cla;
   plot(handles.f,handles.media,'-r');
   hold on;
   MatSoglia=zeros(size(handles.f))+handles.soglia;
   plot(handles.f,MatSoglia,'-g');
   hold off
   xlim(handles.axes6,handles.rangePlott);

end


function edit1_CreateFcn(hObject, eventdata, handles)
if ispc && isequal(get(hObject,'BackgroundColor'), get(0,'defaultUicontrolBackgroundColor'))
   set(hObject,'BackgroundColor','white');
end


function Remove_Callback(hObject, eventdata, handles)
if handles.canc
handles.mag_n=handles.mag_n-handles.mag;
set(handles.numProveTxt, 'String', int2str(handles.numProve-1));
handles.numProve=handles.numProve-1;
handles.canc=0;
set(handles.text_note,'String','Acquisizione Rimossa')
guidata(hObject,handles)
calcolaMax(hObject,handles)
axes(handles.axes5);
cla;
end


function HighPass_Callback(hObject, eventdata, handles)
handles.filtroPassaAlto=str2num(get(handles.HighPass, 'String'));
guidata(hObject,handles);
calcolaMax(hObject,handles);


function HighPass_CreateFcn(hObject, eventdata, handles)
if ispc && isequal(get(hObject,'BackgroundColor'), get(0,'defaultUicontrolBackgroundColor'))
   set(hObject,'BackgroundColor','white');
end


function Sill_Callback(hObject, eventdata, handles)
handles.soglia=str2num(get(handles.Sill, 'String'));50;
guidata(hObject,handles);
calcolaMax(hObject,handles);
```

151

```
function Sill_CreateFcn(hObject, eventdata, handles)
if ispc && isequal(get(hObject,'BackgroundColor'), get(0,'defaultUicontrolBackgroundColor'))
    set(hObject,'BackgroundColor','white');
end

function edit_Duration_Callback(hObject, eventdata, handles)
handles.duration=str2num(get(handles.edit_Duration, 'String'));
guidata(hObject,handles);

function edit_Duration_CreateFcn(hObject, eventdata, handles)
if ispc && isequal(get(hObject,'BackgroundColor'), get(0,'defaultUicontrolBackgroundColor'))
    set(hObject,'BackgroundColor','white');
end

function MinPlot_Callback(hObject, eventdata, handles)
handles.min=str2num(get(handles.MinPlot, 'String'));
guidata(hObject,handles);
plotta(hObject,handles);

function MinPlot_CreateFcn(hObject, eventdata, handles)
if ispc && isequal(get(hObject,'BackgroundColor'), get(0,'defaultUicontrolBackgroundColor'))
    set(hObject,'BackgroundColor','white');
end

function MaxPlot_Callback(hObject, eventdata, handles)
handles.max=str2num(get(handles.MaxPlot, 'String'));
guidata(hObject,handles);
plotta(hObject,handles);

function MaxPlot_CreateFcn(hObject, eventdata, handles)
if ispc && isequal(get(hObject,'BackgroundColor'), get(0,'defaultUicontrolBackgroundColor'))
    set(hObject,'BackgroundColor','white');
end

function edit_ZeroPadding_Callback(hObject, eventdata, handles)
handles.zeri_prec=str2num(get(handles.edit_ZeroPadding, 'String'));
handles.zeri_suc=handles.zeri_prec;
guidata(hObject,handles);

function edit_ZeroPadding_CreateFcn(hObject, eventdata, handles)
if ispc && isequal(get(hObject,'BackgroundColor'), get(0,'defaultUicontrolBackgroundColor'))
    set(hObject,'BackgroundColor','white');
end

function edit_RangeSearch_Callback(hObject, eventdata, handles)
handles.IntervalloDiRicerca=str2num(get(handles.edit_RangeSearch, 'String'));
guidata(hObject,handles);
calcolaMax(hObject,handles);

function edit_RangeSearch_CreateFcn(hObject, eventdata, handles)
if ispc && isequal(get(hObject,'BackgroundColor'), get(0,'defaultUicontrolBackgroundColor'))
    set(hObject,'BackgroundColor','white');
end

function edit_SillTrigger_Callback(hObject, eventdata, handles)
handles.sogliaTrigger=str2num(get(handles.edit_SillTrigger, 'String'));
guidata(hObject,handles);

function edit_SillTrigger_CreateFcn(hObject, eventdata, handles)
if ispc && isequal(get(hObject,'BackgroundColor'), get(0,'defaultUicontrolBackgroundColor'))
```

```matlab
    set(hObject,'BackgroundColor','white');
end


function radiobutton1_Trigger_Callback(hObject, eventdata, handles)
handles.Trigger=get(handles.radiobutton1_Trigger, 'Value');
if handles.Trigger
    set(handles.edit_SillTrigger,'Visible','on');
    set(handles.text_SillTrigger,'Visible','on');
else
    set(handles.edit_SillTrigger,'Visible','off');
    set(handles.text_SillTrigger,'Visible','off');
end
guidata(hObject,handles);


function edit_Freq_CreateFcn(hObject, eventdata, handles)
if ispc && isequal(get(hObject,'BackgroundColor'), get(0,'defaultUicontrolBackgroundColor'))
    set(hObject,'BackgroundColor','white');
end


function checkbox_Phase_Callback(hObject, eventdata, handles)
handles.plottaFase=get(handles.checkbox_Phase, 'Value');
if handles.plottaFase
    set(handles.axes10,'Visible','on');
    set(handles.text21_phase,'Visible','on');
    set(handles.axes6,'Visible','off');
    axes(handles.axes6);
    cla;
else
    axes(handles.axes10);
    cla;
    set(handles.axes10,'Visible','off');
    set(handles.text21_phase,'Visible','off');
     set(handles.axes6,'Visible','on');
end
plotta(hObject,handles)
guidata(hObject,handles);


function pushbutton_Restart_Callback(hObject, eventdata, handles)
set(handles.edit_Duration,'Enable','on');
set(handles.edit_ZeroPadding,'Enable','on');
set(handles.popupmenu_Windowing,'Enable','on');
set(handles.numProveTxt, 'String', '0');
handles.numProve=0;
handles.mag_n={}; handles.mag={}; handles.y_ave={}; handles.y={};
handles.fMax={};handles.f4Freq={};handles.media={};handles.data={};
handles.data_wind={};handles.f={};handles.y={};
axes(handles.axes3);cla;
axes(handles.axes5);cla;
axes(handles.axes6);cla;
guidata(hObject,handles);


function popupmenu_Windowing_Callback(hObject, eventdata, handles)
if handles.canc
Calcola_FFT(hObject,handles)
end


function popupmenu_Windowing_CreateFcn(hObject, eventdata, handles)
if ispc && isequal(get(hObject,'BackgroundColor'), get(0,'defaultUicontrolBackgroundColor'))
    set(hObject,'BackgroundColor','white');
end
```

```
function edit11_nameFile_CreateFcn(hObject, eventdata, handles)
if ispc && isequal(get(hObject,'BackgroundColor'), get(0,'defaultUicontrolBackgroundColor'))
    set(hObject,'BackgroundColor','white');
end


function pushbutton_Save_Callback(hObject, eventdata, handles)
fid=fopen(get(handles.edit11_nameFile,'String'), 'wt');
fprintf(fid,'%6.4f%',handles.f4Freq(1));
try fprintf(fid,'\n'); fprintf(fid,'%6.4f%',handles.f4Freq(2)); end
try fprintf(fid,'\n'); fprintf(fid,'%6.4f%',handles.f4Freq(3)); end
try fprintf(fid,'\n'); fprintf(fid,'%6.4f%',handles.f4Freq(4)); end
try fprintf(fid,'\n'); fprintf(fid,'%6.4f%',handles.f4Freq(5)); end
try fprintf(fid,'\n'); fprintf(fid,'%6.4f%',handles.f4Freq(6)); end
fprintf(fid,'\n');
try fprintf(fid,'\n'); fprintf(fid,'%s%6.4f%','Resolution = ',handles.f(2,1)); end
fprintf(fid,'\n'); fprintf(fid,'%s%s','Time = ',datestr(clock));
set(handles.text_note,'String',['Saved in ',get(handles.edit11_nameFile,'String')]);
% fprintf(fid,'\n');
% fprintf(fid,'\n'); fprintf(fid,'%s','freq [Hz]   Ampl');
% try
%    for dim=1:size(handles.f)
%        fprintf(fid,'\n'); fprintf(fid,'%s',mat2str(handles.f(dim)));
%        fprintf(fid,'%s%s','    ',mat2str(handles.media(dim)));
%    end
% end
fclose(fid);
set(handles.edit12,'String',mat2str(handles.f4Freq(1)));
guidata(hObject,handles);


function figure1_CloseRequestFcn(hObject, eventdata, handles)
delete(hObject);


function edit12_CreateFcn(hObject, eventdata, handles)
if ispc && isequal(get(hObject,'BackgroundColor'), get(0,'defaultUicontrolBackgroundColor'))
    set(hObject,'BackgroundColor','white');
end
```

APPENDIX B: GENETIC ALGORITHM CODE

Often, due to the number of unknown parameters or to the presence of local optimums, the minimization problem is not easy to carry out by the standard optimization algorithms and so a Genetic Algorithm (GA) may be used. GA is a stochastic method for solving optimization problems that is based on natural selection. It repeatedly modifies a population of individual solutions. At each step, the genetic algorithm selects individuals, in a random way, from the current population to be parents and uses them to produce the children for the next generation. The new populations "evolves" toward an optimal solution by the evolution functions (crossover and mutation). A proportional selection scheme has been adopted for the reproduction of the child generation and two procedures have been used to carry out the crossover operation. In the first procedure the crossover used is arithmetical. Two parents, randomly chosen (pondered by fitness) are crossed and two new individual children are generated. Two children vectors c_1 and c_2 are obtained by a linear combination of two parent vectors p_1 and p_2 as follows:

$$c_1 = \alpha p_1 + (1 - \alpha) p_2$$
$$c_2 = (1 - \alpha) p_1 + \alpha p_2$$

(B.1)

where α is a random number in the range [0,1]. In the second procedure, the cross-over is done by randomly choosing one or more positions on the solution vector and replacing the corresponding components of p_1 in p_2 and vice versa. For the choice of the parents the Roulette Wheel (or fitness proportional) method has been adopted. This method chooses parents by simulating a roulette wheel, in

which the area of the section of the wheel, corresponding to an individual, is proportional to the individual's expectation and so is inversely proportional to the individual's fitness. In order to speed up the evolution a mutation has also been introduced: when the offspring are produced, some of the elastic constant sets are mutated by adding a quantity $r \cdot \Delta_i$, where r is a random number in the range [-1,1] and Δ_i is an initially fixed quantity, to one or more components. The choice of the mutated components is again random. To ensure that fit individuals are not lost due to change, elitism selection has been also applied, so the best individuals of the current generation are replicated in the next generation. As mentioned the GA has been provided with an adaptive range procedure by which the entire population is regenerated every M generations, in this case the algorithm is called ARGA (Adaptive Range Genetic Algorithm) ARGA permits to improve the convergence performance of the GA. This property can be comprehended observing Figures B.1 a) and b) where the distributions of Poisson's ratio in the optimization process for the AG and ARGA are reported. In the ARGA case the search range is more close to the solution and so it avoids unnecessary FEA. The points located out of range are due to the mutation function.

a)   b)
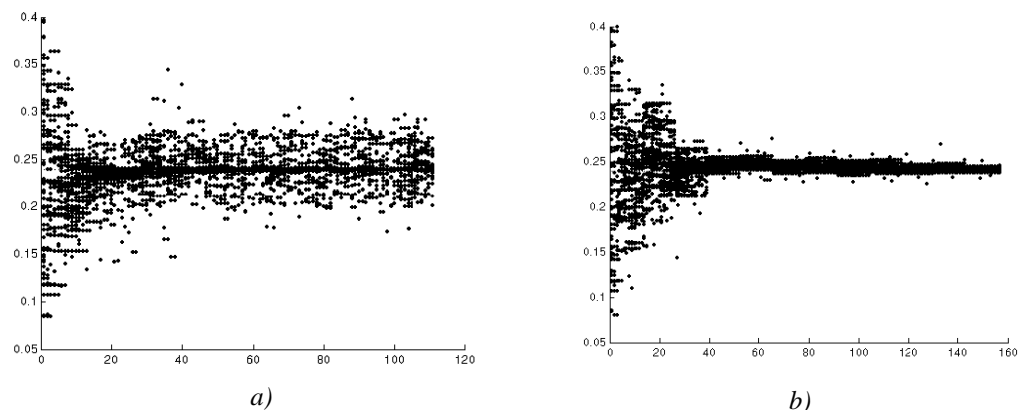
Figure B.1 - Distribution of the unknown parameters value in: a) GA b) ARGA

The ARGA has been developed in Matlab™ environment. In the following the algorithm code is reported. It uses the general-purpose numerical code MSC-Nastran™ to carry out the finite element analysis (FEA). Table B.1 reports an example of Nastran™ input file used in the FEA. Note that the "referenced material records" is written into *"material.bdf"* that is an ASCII file modified in automatic way by the Matlab code.

Table B.1 – Extract of the Nastran™ input file "*Laminato_simmetrico.bdf*".

Section	Function	Nastran™ code
Executive Control	Analysis definition	SOL 101 CEND

Case Control	Subcase definition	SET 2 = 154 THRU 2447,2448
		SEALL = ALL
		SUPER = ALL
		TITLE = MSC.Nastran job created on 30-Jan-06 at 16:07:40
		ECHO = NONE
		SUBCASE 1
		  SUBTITLE=Default
		  SPC = 2
		  LOAD = 2
		  DISPLACEMENT(SORT1,REAL)=2

	Analysis parameters definition	BEGIN BULK PARAM POST 0 PARAM PRTMAXIM YES

Bulk Data	Element properties definition	PCOMP 1 0. 0. SYM
		       1 .25 0. YES 1 .25 0. YES
		       1 .25 0. YES 1 .25 0. YES

	Elements definition	CQUAD4 1 1 1 2 53 52 CQUAD4 2 1 2 3 54 53 **...** CQUAD4 2500 1 2549 2550 2601 2600
	Referenced material records	**INCLUDE 'material.bdf'**
	Nodes of the model	GRID 1 -25. -25. 0. GRID 2 -24. -25. 0. **...** GRID 2601 25. 25. 0.
	Loads and constraints	SPCADD 2 1 3 LOAD 2 1. 1. 1 SPC1 1 23 105 151 SPC1 3 13 2474 FORCE 1 1459 0 1.114 0. 0. -1.

```
function [gen, individuo_finale, pop_finale] = ARGA(esatti, dimPop, iterazioni, num_elit,
num_cross, num_mut, M);
% main function
maxCanali=4; %NumberOfNastranChannelUsed
t=cputime;
%%%%  Card For Numerical Simulation  %%%% %%%% %%%% %%%% %%%%
% esatti1=esatti;
% lambda=0.0005;
% fattore_moltipl=1/sqrt(3);
% media=0;
% fattore_divisore=1;
% DeltaErrore=(fattore_moltipl*(lambda/4)/fattore_divisore);
% errore=media+DeltaErrore*rand(1, 2601);
% esatti=esatti+esatti.*errore;
% errore=0+sqrt(0.05)*randn(1, 2601);
% mean((esatti-esatti1)/esatti1*100)
%%%% %%%% %%%% %%%% %%%% %%%% %%%% %%%% %%%% %%%% %%%%
```

157

```
%SearchRange
E1_min=60;
E1_max= 90;
E2_min= 60;
E2_max= 90;
ni_min=0.200;
ni_max=0.400;
G_min=2;
G_max=50;
analisi=0; % #FEA
%FirstGenerationCreation
[Pop, analisi] = prima_generazione_new(dimPop, esatti, E1_min, E1_max, E2_min, E2_max,
ni_min, ni_max, G_min, G_max, analisi, maxCanali);
Pop=sortrows(Pop, 5);
best_pop=Pop(1:num_elit, :);
migliore=best_pop(1, :)
gen=1;
Storia(gen, 1)=gen;
Storia(gen, 2)=migliore(1, 5);
Storia(gen, 3)=mean(Pop(:, 5));
Storia(gen, 4)=migliore(1, 6);
Storia(gen, 5)=migliore(1, 7);
Storia(gen, 6)=migliore(1, 8);
Storia(gen, 7)=migliore(1, 9);
Storia(gen, 8)=analisi;
temp=int2str(gen);
filename=['C:\MATLAB6p5\work\soluzioni\generazione_', temp]; %SaveFirstGen
save(filename, 'Pop', 'migliore', 'Storia');
while(gen<iterazioni+1)
  if (gen>40 & Storia(gen, 2)==Storia(gen-35, 2)) %StopCondition
    break
  else
  if rem(gen, M)
    analisi=0;
    %SuccessiveGenerationCration
  [new_pop, analisi] = new_generazione(best_pop, Pop, num_mut, num_cross, E1_min, E1_max,
E2_min, E2_max,   ni_min, ni_max, G_min, G_max, esatti, analisi, maxCanali);
    Pop=new_pop;
    best_pop=Pop(1:num_elit, :);
    migliore=best_pop(1, :)
    gen=gen+1;
    Storia(gen, 1)=gen;
    Storia(gen, 2)=migliore(1, 5);
    Storia(gen, 3)=mean(Pop(:, 5));
    Storia(gen, 4)=migliore(1, 6);
    Storia(gen, 5)=migliore(1, 7);
    Storia(gen, 6)=migliore(1, 8);
    Storia(gen, 7)=migliore(1, 9);
    Storia(gen, 8)=analisi;
    temp=int2str(gen);
    filename=['C:\MATLAB6p5\work\soluzioni\generazione_', temp];
    save(filename, 'Pop', 'migliore', 'Storia');
    %PlotOfTheResults
    close
    subplot(2, 2, 1);plot(Storia(:, 1), Storia(:, 2), 'r-', Storia(:, 1), Storia(:, 3), 'b-');
    subplot(2, 2, [2, 4]); plot(Storia(:, 1), Storia(:, 4), 'r-', Storia(:, 1), Storia(:, 5), 'b-', Storia(:, 1),
Storia(:, 6), 'k-', Storia(:, 1), Storia(:, 7), 'g-');
    legend('E1', 'E2', 'ni', 'G')
    subplot(2, 2, 3);text(.01, .9, [' %E1= ', num2str(100*Storia(gen, 4), 3), '      %E2= ',
num2str(100*Storia(gen, 5), 3)])
```

```
  text(.01, .8, [' %Ni= ', num2str(100*Storia(gen, 6), 3), '   %G= ', num2str(100*Storia(gen, 7),
3)])
  text(.01, .7, ['FitPop= ', num2str(Storia(gen, 3), 3), ' FitMigl= ', num2str(Storia(gen, 2), 3)])
  text(.01, .5, '-----------Limiti-----------        ----min max popolazione--------')
  text(.01, .4, [' E1 Max/min=   ', num2str(E1_min, 3), ' <-> ', num2str(E1_max, 3), ' min=',
num2str(round(min(Pop(:, 1))*1000)/1000), ' max=', num2str(round(max(Pop(:, 1))*1000)/1000)])
  text(.01, .3, [' E2 Max/min=   ', num2str(E2_min, 3), ' <-> ', num2str(E2_max, 3), ' min=',
num2str(round(min(Pop(:, 2))*1000)/1000), ' max=', num2str(round(max(Pop(:, 2))*1000)/1000)])
  text(.01, .2, [' Ni12 Max/min= ', num2str(ni_min, 3), ' <-> ', num2str(ni_max, 3), ' min=',
num2str(round(min(Pop(:, 3))*1000)/1000), ' max=', num2str(round(max(Pop(:, 3))*1000)/1000)])
  text(.01, .1, [' G12 Max/min= ', num2str(G_min, 3), ' <-> ', num2str(G_max, 3), ' min=',
num2str(round(min(Pop(:, 4))*1000)/1000), ' max=',num2str(round(max(Pop(:, 4))*1000)/1000)]);
 else
  %ARGA Implementation
  if gen==M
   %VarianceAndAverageValuesComputationOfTheFirstGeneration
   [mE1p, sE1p] = primaMedia(Pop, 1);
   [mE2p, sE2p] = primaMedia(Pop, 2);
   [mNip, sNip] = primaMedia(Pop, 3);
   [mGp, sGp] = primaMedia(Pop, 4);
  else
   %VarianceAndAverageValuesComputationOfTheSuccessiveGeneration
   [mE1new, sE1new] = Media_new(Pop, 1, mE1p, sE1p);
   [mE2new, sE2new] = Media_new(Pop, 2, mE2p, sE2p);
   [mNinew, sNinew] = Media_new(Pop, 3, mNip, sNip);
   [mGnew, sGnew] = Media_new(Pop, 4, mGp, sGp);
   mE1p=mE1new;
   mE2p=mE2new;
   mNip=mNinew;
   mGp=mGnew;
   sE1p=sE1new;
   sE2p=sE2new;
   sNip=sNinew;
   sGp=sGnew;
  end
  k=10; %GainOfTheARGA
  if gen>60, k=9; end
  if gen>100, k=7;end
  if gen>160, k=4;end
  if gen>180, k=2;end
  if sE1p<.25, sE1p=0.25;end
  if sE2p<.25, sE2p=0.25;end
  if sNip<.008, sNip=0.008;end
  if sGp<.25, sGp=0.25;end
  %%%% New Range Definition %%%% %%%% %%%% %%%%
  E1_min=mE1p-k*sE1p;
  E1_max=mE1p+k*sE1p;
               E2_min=mE2p-k*sE2p;
               E2_max=mE2p+k*sE2p;
               ni_min=mNip-k*sNip;
               ni_max=mNip+k*sNip;
               G_min=mGp-k*sGp;
               G_max=mGp+k*sGp;
  temp=int2str(gen);
  %%%% %%%% %%%% %%%% %%%% %%%% %%%% %%%% %%%%
  filename=['C:\MATLAB6p5\work\soluzioni\media_', temp];
  save(filename, 'E1_min', 'E1_max', 'E2_min', 'E2_max', 'ni_min', 'ni_max', 'G_min', 'G_max',
'sE1p', 'sE2p', 'sNip', 'sGp', 'mE1p', 'mE2p', 'mNip', 'mGp');
  Migliori2=Pop(1, :);
  analisi=0;
  %NewGenerationCreation
```

```
  [new_pop, analisi] = prima_generazione_new(dimPop-1, esatti, E1_min, E1_max, E2_min,
E2_max, ni_min, ni_max, G_min, G_max, analisi, maxCanali);
  Pop=[Migliori2;new_pop];
  Pop=sortrows(Pop, 5);
  best_pop=Pop(1:num_elit, :);
  migliore=best_pop(1, :)
  gen=gen+1;
  Storia(gen, 1)=gen;
  Storia(gen, 2)=migliore(1, 5);
  Storia(gen, 3)=mean(Pop(:, 5));
  Storia(gen, 4)=migliore(1, 6);
  Storia(gen, 5)=migliore(1, 7);
  Storia(gen, 6)=migliore(1, 8);
  Storia(gen, 7)=migliore(1, 9);
  Storia(gen, 8)=analisi;
  temp=int2str(gen);
  filename=['C:\MATLAB6p5\work\soluzioni\generazione_', temp];
  save(filename, 'Pop', 'migliore', 'Storia');
  %PlotOfTheResults
  close
  subplot(2, 2, 1);plot(Storia(:, 1), Storia(:, 2), 'r-', Storia(:, 1), Storia(:, 3), 'b-');
  subplot(2, 2, [2, 4]); plot(Storia(:, 1), Storia(:, 4), 'r-', Storia(:, 1), Storia(:, 5), 'b-', Storia(:, 1),
Storia(:, 6), 'k-', Storia(:, 1), Storia(:, 7), 'g-');
  legend('E1', 'E2', 'ni', 'G')
  subplot(2, 2, 3);text(.01, .9, [' %E1= ', num2str(100*Storia(gen, 4), 3), '    %E2= ',
num2str(100*Storia(gen, 5), 3)])
  text(.01, .8, [' %Ni= ', num2str(100*Storia(gen, 6), 3), '   %G= ', num2str(100*Storia(gen, 7),
3)])
  text(.01, .7, ['FitPop= ', num2str(Storia(gen, 3), 3), ' FitMigl= ', num2str(Storia(gen, 2), 3)])
  text(.01, .5, '-----------Limiti-----------       ----min max popolazione--------')
  text(.01, .4, [' E1 Max/min=  ', num2str(E1_min, 3), ' <-> ', num2str(E1_max, 3), '  min=',
num2str(round(min(Pop(:, 1))*1000)/1000), ' max=', num2str(round(max(Pop(:, 1))*1000)/1000)])
  text(.01, .3, [' E2 Max/min=  ', num2str(E2_min, 3), ' <-> ', num2str(E2_max, 3), '  min=',
num2str(round(min(Pop(:, 2))*1000)/1000), ' max=', num2str(round(max(Pop(:, 2))*1000)/1000)])
  text(.01, .2, [' Ni12 Max/min= ', num2str(ni_min, 3), ' <-> ', num2str(ni_max, 3), '  min=',
num2str(round(min(Pop(:, 3))*1000)/1000), ' max=', num2str(round(max(Pop(:, 3))*1000)/1000)])
  text(.01, .1, [' G12 Max/min= ', num2str(G_min, 3), ' <-> ', num2str(G_max, 3), '  min=',
num2str(round(min(Pop(:, 4))*1000)/1000),' max=', num2str(round(max(Pop(:, 4))*1000)/1000)]);
 end
 end
end
individuo_finale=migliore;
pop_finale=Pop;
x=cputime;
tempoEsecuzione=x-t


function [Pop, analisi] = prima_generazione(dimPop, esatti, E1_min, E1_max, E2_min,
E2_max, ni_min, ni_max, G_min, G_max, analisi, canaliMax)
t=cputime;
n_analisi=dimPop;
analisi_inviata=1;
indice=1;
Pop=zeros(dimPop, 12);
vettore_analisi=zeros(8, canaliMax);
%implementation of multi-channel analysis
while indice<dimPop+1
 vettore_analisi(1, :)=vettore_analisi(1, :)*2;
 if analisi_inviata==1
  E1= E1_min +(E1_max-E1_min) * rand(1);
  E2= E2_min +(E2_max-E2_min) * rand(1);
  ni=ni_min +(ni_max-ni_min) * rand(1);
```

```
  G=G_min +(G_max-G_min) * rand(1);
  E1=E1*1000;E1=round(E1)/1000;
  E2=E2*1000;E2=round(E2)/1000;
  ni=round(ni*1000)/1000;
  G=G*1000;G=round(G)/1000;
 end
 for i=1:canaliMax
  if vettore_analisi(1, i)==0 & n_analisi
    call_nastran(E1, E2, ni, G, i); %CallSolverAndStartFEA
    vettore_analisi(:, i)=[1;E1;E2;ni;G;0;0;0];
    analisi_inviata=1;
    n_analisi=n_analisi-1;
    analisi=analisi+1;
    break
  end
 end
 pause(1)
 %FEAResultsReading
 for i=1:canaliMax
  fileName=['dir C:\SUPPORT\ANALISI', int2str(i), '\SIMULAZIONE\*.ASG >null'];
  if vettore_analisi(1, i)>8 & dos(fileName)==1
    Pop(indice, :)=crea_individuo(vettore_analisi(:, i), i, esatti);
    indice=indice+1;
    vettore_analisi(1, i)=0;
  end
 end
end
end
x=cputime;
tempoEsecuzione=x-t


function [fileName] = call_nastran(E1, E2, ni, G, canale)
%StartTheFEAOnChannel "canale"
fileName=['C:\SUPPORT\ANALISI', int2str(canale), '\materiale', int2str(canale), '.bdf'];
matcard(fileName, E1, E2, ni, G); %WriteTheConstantValueIntoMAT8Card
fileName2=['erase /q /a:a ', 'C:\SUPPORT\ANALISI', int2str(canale), '\SIMULAZIONE\', '*.*'];
dos(fileName2);
fileName3=['C:\SUPPORT\ANALISI', int2str(canale), '\nastran.bat >null'];
dos(fileName3); %CallNastran


function[] = matcard(filename, E1, E2, ni, G)
 %WriteTheConstantValueIntoMAT8Card
E1=E1*1000;E1=round(E1);
E2=E2*1000;E2=round(E2);
ni=round(ni*1000)/1000;
G=G*1000;G=round(G);
fid = fopen(filename, 'wt');
fprintf(fid, '%s%4.f%s%4.f%s%4.3g%s%s%4.f%s', 'MAT8, 1, ', E1, '., ', E2, '., ', ni, ', ', G, '.');
fclose(fid);


function [individuo] = crea_individuo(vettore_analisi, canale, esatti)
%read the results of the FEA in "canale" folder and evaluate the fitness
fileName=['C:\SUPPORT\ANALISI',  int2str(canale),  '\SIMULAZIONE\Laminato_simmetrico',
int2str(canale), '.f06'];
[spostamenti, r] = spost_piastra(fileName, 2295);
load('matPinv_conf2_areaSperimentale_44x50.mat');
% load the cooridnate points for rigid displacements elimination procedure
X=matCoord*matPInversa-eye(2295, 2295); %2295 are the point acquired
val=sum((X*(spostamenti-esatti)').^2)*10^9; % fitness evaluation
E1p=vettore_analisi(2);
E2p=vettore_analisi(3);
nip=vettore_analisi(4);
```

161

```
Gp=vettore_analisi(5);
load('costanti')
perc_E1=(E1p-E1)/E1;
perc_E2=(E2p-E2)/E2;
perc_ni=(nip-ni)/ni;
perc_G=(Gp-G)/G;
individuo=[E1p E2p nip Gp val perc_E1 perc_E2 perc_ni perc_G vettore_analisi(6)
vettore_analisi(7) vettore_analisi(8)];
```

function[spostamenti, r] = spost_piastra(file_name, nodi)
% read displacements from the output Nastran file (.f06 file)*
```
fid=fopen(file_name, 'r');
stop=1;
resto=rem(nodi, 50);
iterazioni=fix(nodi/50)+1;
  while (feof(fid)==0&stop)
  tline=fgetl(fid);
  [a, b] = size(tline);
   if (b==82)
     for(j=1:iterazioni)
      for(i=1:3)
       tline=fgetl(fid);
      end
       for i=1:50
        if j==iterazioni&i==resto
          r=parse2(tline);
          tline=fgetl(fid);
          t=[r(5,1) r(5,2) r(5,3) r(5,4) r(5,5) r(5,6) r(5,7) r(5,8) r(5,9) r(5,10) r(5,11) r(5,12) r(5,13)];
          dispi(i, j)=str2double(t);
          break
        else
          r=parse2(tline);
          tline=fgetl(fid);
          t=[r(5,1) r(5,2) r(5,3) r(5,4) r(5,5) r(5,6) r(5,7) r(5,8) r(5,9) r(5,10) r(5,11) r(5,12) r(5,13)];
          dispi(i, j)=str2double(t);
        end
       end
       for(i=1:4)
       tline=fgetl(fid);
       end
    end
    break
   end
  end
  fclose('all');
```

function [x] = parse2(inStr)
%StringToVector function
```
sz=size(inStr); strLen=sz(2); x=blanks(strLen); wordCount=0; last=0; a=0;
for i=1:strLen,
 if inStr(i) == ' '
 last=i; a=0;
 else
  if a ==0
   wordCount = wordCount + 1;
   x(wordCount, i-last)=inStr(i);
   a=1;
  else
   x(wordCount, i-last)=inStr(i);
  end
 end
```

```
end

function [nuova, analisi] = new_generazione(best_matr, Pop_matr, num_mut, num_cross,
E1_min, E1_max, E2_min, E2_max, ni_min, ni_max, G_min, G_max, esatti, analisi,
CanaliMax);
% create a new generation
dim_figli=(size(Pop_matr, 1)-size(best_matr, 1))
dim_mutati=num_mut;
dim_accoppiati=num_cross;
[crossover_matr, analisi] = crossover(dim_accoppiati, Pop_matr, esatti, analisi, CanaliMax,
E1_min, E1_max, E2_min, E2_max, ni_min, ni_max, G_min, G_max, best_matr);
mutazione_=1
[mutati_matr, analisi] = mutazione(dim_mutati, Pop_matr, esatti, E1_min, E1_max, E2_min,
E2_max, ni_min, ni_max, G_min, G_max, analisi, CanaliMax);
nuova=[best_matr;crossover_matr;mutati_matr];
nuova=sortrows(nuova, 5);

function [acc_comb_matr, analisi] = crossover(dim_accoppiati, Pop_matr, esatti, analisi,
maxCanali, E1_min, E1_max, E2_min, E2_max, ni_min, ni_max, G_min, G_max,
best_matr)
%crossover function
indici_processati=[0 0];
esistenti=best_matr;
indice=1;
analisi_inviata=1;
vettore_analisi=zeros(8, maxCanali); %vettore_analisi(1, k)==0 --> the channel is free
%arithmetical crossover
accoppiati_matr=zeros(round((dim_accoppiati/2)), 12);
n_analisi=round(size(accoppiati_matr, 1)/2);
termina=0;
DeltaAccoppia=160;
while indice<round(dim_accoppiati/2)+1 | sum(vettore_analisi(1, :))>0
  vettore_analisi(1, :)=vettore_analisi(1, :)*2;
  if analisi_inviata==1 & n_analisi
    analisi_inviata=0;
    prescelti=selezione_indici(Pop_matr, indici_processati);
    indici_processati=[indici_processati;prescelti];
    r=rand(1);
  end
 if r<=1%0.6
   % start FEA
   for j=1:maxCanali/2
     i=j*2-1;
     if vettore_analisi(1, i)==0 & n_analisi
       [vettore_analisi(2, i) vettore_analisi(2, i+1) vettore_analisi(3, i) vettore_analisi(3, i+1)
vettore_analisi(4, i) vettore_analisi(4, i+1) vettore_analisi(5, i) vettore_analisi(5, i+1)] =
accoppia(Pop_matr(prescelti(1, 1), :), Pop_matr(prescelti(1, 2), :), i, i+1, E1_min, E1_max,
E2_min, E2_max, ni_min, ni_max, G_min, G_max, DeltaAccoppia);
       vettore_analisi(1, [i i+1])=1;
       vettore_analisi(6, [i i+1])=1;
       vettore_analisi(7, [i i+1])=prescelti(1, 1);
       vettore_analisi(8, [i i+1])=prescelti(1, 2);
       analisi_inviata=1;
       n_analisi=n_analisi-1;
       analisi=analisi+2;
       break
     end
   end
 else
   accoppiati_matr(indice, :)=Pop_matr(prescelti(1, 1), :);
   indice=indice+1;
```

```
    accoppiati_matr(indice, :)=Pop_matr(prescelti(1, 2), :);
    indice=indice+1;
    analisi_inviata=1;
    n_analisi=n_analisi-1;r=0;
    indici_prescelti=prescelti;
  end
 pause(1)
 %read results
 for j=1:maxCanali/2
   i=j*2-1;
   fileName1=['dir C:\SUPPORT\ANALISI', int2str(i), '\SIMULAZIONE\*.ASG >null'];
   fileName2=['dir C:\SUPPORT\ANALISI', int2str(i+1), '\SIMULAZIONE\*.ASG >null'];
   if vettore_analisi(1, i)>7 & dos(fileName1)==1 & dos(fileName2)==1
     figlio1=crea_individuo(vettore_analisi(:, i), i, esatti);
     figlio2=crea_individuo(vettore_analisi(:, i+1), i+1, esatti);
     famiglia=[figlio1;figlio2;Pop_matr(vettore_analisi(7, i), :);Pop_matr(vettore_analisi(8, i), :)];
     accoppiati_matr(indice, :)=famiglia(1, :);
     esistenti=[best_matr;accoppiati_matr];
     indice=indice+1;
     accoppiati_matr(indice, :)=famiglia(2, :);
     indice=indice+1;
     esistenti=[best_matr;accoppiati_matr];
     vettore_analisi(1, [i i+1])=0;
   end
         end
end
indici_processati1=indici_processati;
%
%replacing crossover
indici_processati=[0 0];
indice=1;termina=0;
analisi_inviata=1;
vettore_analisi=zeros(8, maxCanali); %vettore_analisi(1, k)==0 --> the channel is free
combinati_matr=zeros(round((dim_accoppiati/2)), 12);
n_analisi=round(size(accoppiati_matr, 1)/2);
while indice<round(dim_accoppiati/2)+1 | sum(vettore_analisi(1, :))>0
  vettore_analisi(1, :)=vettore_analisi(1, :)*2;
  if analisi_inviata==1 & n_analisi
    analisi_inviata=0;
    prescelti=selezione_indici(Pop_matr, indici_processati);
    indici_processati=[indici_processati;prescelti];
    r=rand(1);
  end
  if r<=1
    %start FEA
    for j=1:maxCanali/2
      i=j*2-1;
      if vettore_analisi(1, i)==0 & n_analisi
        [vettore_analisi(2, i) vettore_analisi(2, i+1) vettore_analisi(3, i) vettore_analisi(3, i+1)
vettore_analisi(4, i) vettore_analisi(4, i+1) vettore_analisi(5, i) vettore_analisi(5, i+1)] =
combina(Pop_matr(prescelti(1, 1), :), Pop_matr(prescelti(1, 2), :), i, i+1);
        vettore_analisi(1, [i i+1])=1;
        vettore_analisi(6, [i i+1])=2;
        vettore_analisi(7, [i i+1])=prescelti(1, 1);
        vettore_analisi(8, [i i+1])=prescelti(1, 2);
        analisi_inviata=1;
        n_analisi=n_analisi-1;
        analisi=analisi+2;
        break
      end
    end
```

```
  else
    combinati_matr(indice, :)=Pop_matr(prescelti(1, 1), :);
    indice=indice+1;
    combinati_matr(indice, :)=Pop_matr(prescelti(1, 2), :);
    indice=indice+1;
    analisi_inviata=1;
    n_analisi=n_analisi-1;r=0;
  end
 pause(1)
%read
 for j=1:maxCanali/2
  i=j*2-1;
  fileName1=['dir C:\SUPPORT\ANALISI', int2str(i), '\SIMULAZIONE\*.ASG >null'];
  fileName2=['dir C:\SUPPORT\ANALISI', int2str(i+1), '\SIMULAZIONE\*.ASG >null'];
  if vettore_analisi(1, i)>7 & dos(fileName1)==1 & dos(fileName2)==1
    figlio1=crea_individuo(vettore_analisi(:, i), i, esatti);
    figlio2=crea_individuo(vettore_analisi(:, i+1), i+1, esatti);
    famiglia=[figlio1;figlio2;Pop_matr(vettore_analisi(7,i),:);Pop_matr(vettore_analisi(8,i+1),:)];
    combinati_matr(indice,:)=famiglia(1,:);
    esistenti=[best_matr;combinati_matr;accoppiati_matr];
    indice=indice+1;
    combinati_matr(indice,:)=famiglia(2,:);
    indice=indice+1;
    esistenti=[best_matr;accoppiati_matr;combinati_matr];
    vettore_analisi(1, [i i+1])=0;
   end
  end
end
acc_comb_matr=[accoppiati_matr;combinati_matr];
```

function [E1_figl1, E1_figl2, E2_figl1, E2_figl2, ni_figl1, ni_figl2, G_figl1, G_figl2] = accoppia(padre, madre, canale1, canale2, E1_min, E1_max, E2_min, E2_max, ni_min, ni_max, G_min, G_max, DeltaAccoppia)

```
%arithmetical crossover
a=rand(1); b=rand(1); r=(b-0.5)/DeltaAccoppia;
E1_figl1=(padre(1, 1)*a+madre(1, 1)*(1-a)-r*(padre(1, 1)+madre(1, 1))/2);
E1_figl2=(padre(1, 1)*(1-a)+madre(1, 1)*a-r*(padre(1, 1)+madre(1, 1))/2);
c=rand(1); d=rand(1); r1=(d-0.5)/DeltaAccoppia;
ni_figl1=(padre(1, 3)*c+madre(1, 3)*(1-c)-r1*(padre(1, 3)+madre(1, 3))/2);
ni_figl2=(padre(1, 3)*(1-c)+madre(1, 3)*c-r1*(padre(1, 3)+madre(1, 3))/2);
e=rand(1); f=rand(1); r2=(f-0.5)/DeltaAccoppia;
E2_figl1=(padre(1, 2)*e+madre(1, 2)*(1-e)-r2*(padre(1, 2)+madre(1, 2))/2);
E2_figl2=(padre(1, 2)*(1-e)+madre(1, 2)*e-r2*(padre(1, 2)+madre(1, 2))/2);
g=rand(1); h=rand(1); r3=(h-0.5)/DeltaAccoppia;
G_figl1=(padre(1, 4)*g+madre(1, 4)*(1-g)-r3*(padre(1, 4)+madre(1, 4))/2);
G_figl2=(padre(1, 4)*(1-g)+madre(1, 4)*g-r3*(padre(1, 4)+madre(1, 4))/2);
% range evaluation first child
if E1_figl1<E1_min, E1_figl1=E1_min; end
if E1_figl1>E1_max, E1_figl1=E1_max; end
if E2_figl1<E2_min, E2_figl1=E2_min; end
if E2_figl1>E2_max, E2_figl1=E2_max; end
if ni_figl1<ni_min, ni_figl1=ni_min; end
if ni_figl1>ni_max, ni_figl1=ni_max; end
if G_figl1<G_min, G_figl1=G_min; end
if G_figl1>G_max, G_figl1=G_max; end
% range evaluation second child
if E1_figl2<E1_min, E1_figl2=E1_min; end
if E1_figl2>E1_max, E1_figl2=E1_max; end
if E2_figl2<E2_min, E2_figl2=E2_min; end
if E2_figl2>E2_max, E2_figl2=E2_max; end
if ni_figl2<ni_min, ni_figl2=ni_min; end
```

```
if ni_figl2>ni_max, ni_figl2=ni_max; end
if G_figl2<G_min, G_figl2=G_min; end
if G_figl2>G_max, G_figl2=G_max; end
```
% preparation of the Nastran input file and start the FEA
```
E1_figl1=E1_figl1*1000;E1_figl1=round(E1_figl1)/1000;
E2_figl1=E2_figl1*1000;E2_figl1=round(E2_figl1)/1000;
ni_figl1=round(ni_figl1*1000)/1000;
G_figl1=G_figl1*1000;G_figl1=round(G_figl1)/1000;
E1_figl2=E1_figl2*1000;E1_figl2=round(E1_figl2)/1000;
E2_figl2=E2_figl2*1000;E2_figl2=round(E2_figl2)/1000;
ni_figl2=round(ni_figl2*1000)/1000;
G_figl2=G_figl2*1000;G_figl2=round(G_figl2)/1000;
fileName=['C:\SUPPORT\ANALISI', int2str(canale1), '\materiale', int2str(canale1), '.bdf'];
matcard(fileName, E1_figl1, E2_figl1, ni_figl1, G_figl1);
fileName2=['erase /q /a:a ', 'C:\SUPPORT\ANALISI', int2str(canale1), '\SIMULAZIONE\', '*.*'];
dos(fileName2);
fileName3=['C:\SUPPORT\ANALISI', int2str(canale1), '\nastran.bat >null'];
dos(fileName3); pause(3)
fileName=['C:\SUPPORT\ANALISI', int2str(canale2), '\materiale', int2str(canale2), '.bdf'];
matcard(fileName, E1_figl2, E2_figl2, ni_figl2, G_figl2);
fileName2=['erase /q /a:a ', 'C:\SUPPORT\ANALISI', int2str(canale2), '\SIMULAZIONE\', '*.*'];
dos(fileName2);
fileName3=['C:\SUPPORT\ANALISI', int2str(canale2), '\nastran.bat >null'];
dos(fileName3);


function [E1_figl1, E1_figl2, E2_figl1, E2_figl2, ni_figl1, ni_figl2, G_figl1, G_figl2] =
combina(padre, madre, canale1, canale2)
```
%replacing crossover funtion
```
figlio1_temp=padre;
figlio2_temp=madre;
r=rand(1);
if r<=0.66
  cost= round(1+ 3*rand(1));
  figlio1_temp(1, cost)=madre(1, cost);
  figlio2_temp(1, cost)=padre(1, cost);
 else
  cost1=round(1+ 3*rand(1));
  cost2=round(1+ 3*rand(1));
  while cost1==cost2
    cost2=round(1+ 3*rand(1));
  end
  figlio1_temp(1, cost1)=madre(1, cost1);
  figlio1_temp(1, cost2)=madre(1, cost2);
  figlio2_temp(1, cost1)=padre(1, cost1);
  figlio2_temp(1, cost2)=padre(1, cost2);
end
E1_figl1=figlio1_temp(1, 1); E1_figl2=figlio2_temp(1, 1);
E2_figl1=figlio1_temp(1, 2); E2_figl2=figlio2_temp(1, 2);
ni_figl1=figlio1_temp(1, 3); ni_figl2=figlio2_temp(1, 3);
G_figl1=figlio1_temp(1, 4); G_figl2=figlio2_temp(1, 4);
E1_figl1=E1_figl1*1000;E1_figl1=round(E1_figl1)/1000;
E2_figl1=E2_figl1*1000;E2_figl1=round(E2_figl1)/1000;
ni_figl1=round(ni_figl1*1000)/1000;
G_figl1=G_figl1*1000;G_figl1=round(G_figl1)/1000;
E1_figl2=E1_figl2*1000;E1_figl2=round(E1_figl2)/1000;
E2_figl2=E2_figl2*1000;E2_figl2=round(E2_figl2)/1000;
ni_figl2=round(ni_figl2*1000)/1000;
G_figl2=G_figl2*1000;G_figl2=round(G_figl2)/1000;
```
% preparation of the Nastran input file and start the FEA
```
fileName=['C:\SUPPORT\ANALISI', int2str(canale1), '\materiale', int2str(canale1), '.bdf'];
matcard_2(fileName, E1_figl1, E2_figl1, ni_figl1, G_figl1);
```

166

```
fileName2=['erase /q /a:a ', 'C:\SUPPORT\ANALISI', int2str(canale1), '\SIMULAZIONE\', '*.*'];
dos(fileName2);
fileName3=['C:\SUPPORT\ANALISI', int2str(canale1), '\nastran.bat >null'];
dos(fileName3);
pause(2)
fileName=['C:\SUPPORT\ANALISI', int2str(canale2), '\materiale', int2str(canale2), '.bdf'];
matcard_2(fileName, E1_figl2, E2_figl2, ni_figl2, G_figl2);
fileName2=['erase /q /a:a ', 'C:\SUPPORT\ANALISI', int2str(canale2), '\SIMULAZIONE\', '*.*'];
dos(fileName2);
fileName3=['C:\SUPPORT\ANALISI', int2str(canale2), '\nastran.bat >null'];
dos(fileName3);


function[mutati_matr, analisi] =mutazione(dim_mutati, Pop_matr, esatti, E1_min, E1_max,
E2_min, E2_max, ni_min, ni_max, G_min, G_max, analisi, maxCanali)
%mutation function
indice=1;
analisi_inviata=1;
vettore_analisi=zeros(8, maxCanali); %vettore_analisi(1, k)==0 --> the channel is free
mutati_matr=zeros(dim_mutati, 12);
n_analisi=round(dim_mutati);
t=0;
while indice<dim_mutati+1
  vettore_analisi(1, :)=vettore_analisi(1, :)*2;
  if analisi_inviata==1 & n_analisi
   analisi_inviata=0;
  c=1+(size(Pop_matr, 1)-1)*rand(1);
  indice_c=round(c);
  fitness=Pop_matr(indice_c, 5)*10;
  if fitness<0.1
    m=.1
    var_ni=Pop_matr(indice_c, 3)*.15;
    var_E1=Pop_matr(indice_c, 1)*.015;
    var_E2=Pop_matr(indice_c, 2)*.015;
    var_G=Pop_matr(indice_c, 4)*.015;
   elseif fitness<5
    m=5
    var_ni=Pop_matr(indice_c, 3)*.3;
    var_E1=Pop_matr(indice_c, 1)*.06;
    var_E2=Pop_matr(indice_c, 2)*.06;
    var_G=Pop_matr(indice_c, 4)*.06;
   elseif fitness<10
    m=10
    var_ni=Pop_matr(indice_c, 3)*.5;
    var_E1=Pop_matr(indice_c, 1)*.14;
    var_E2=Pop_matr(indice_c, 2)*.14;
    var_G=Pop_matr(indice_c, 4)*.14;
   else
    var_ni=Pop_matr(indice_c, 3)*.6;
    var_E1=Pop_matr(indice_c, 1)*.3;
    var_E2=Pop_matr(indice_c, 2)*.3;
    var_G=Pop_matr(indice_c, 4)*.3;
   end
  r=rand(1);
  end
  if r<=0.9
    for i=1:maxCanali
     if vettore_analisi(1, i)==0 & n_analisi
      [vettore_analisi(2, i) vettore_analisi(3, i) vettore_analisi(4, i) vettore_analisi(5, i)] =
muta(Pop_matr(indice_c, :), E1_min, E1_max, E2_min, E2_max, ni_min, ni_max, G_min,
G_max, var_E1, var_E2, var_ni, var_G, i);
       vettore_analisi(1, i)=1;
```

167

```
      vettore_analisi(6, i)=3;
      vettore_analisi(7, i)=indice_c;
      vettore_analisi(8, i)=0;
      analisi_inviata=1;
      n_analisi=n_analisi-1;
      analisi=analisi+1;
      break
     end
    end
  else
   mutati_matr(indice, :)=Pop_matr(indice_c, :);
   indice=indice+1;
   analisi_inviata=1;
   n_analisi=n_analisi-1;r=0;
  end
 pause(1)
 %read FEA results
 for i=1:maxCanali
   fileName=['dir C:\SUPPORT\ANALISI', int2str(i), '\SIMULAZIONE\*.ASG >null'];
   if vettore_analisi(1, i)>6 & dos(fileName)==1
     figlio1=crea_individuo(vettore_analisi(:, i), i, esatti);
     figlio2=Pop_matr(indice_c, :);
     famiglia=[figlio1;figlio2];
     famiglia=sortrows(famiglia, 5);
     ran=rand(1);
     if ran>.5
       mutati_matr(indice, :)=famiglia(1, :);
     else
       mutati_matr(indice, :)=figlio1;
     end
     indice=indice+1;
     vettore_analisi(1, i)=0;
   end
 end
end
sum(vettore_analisi(1, :))


function [E1, E2, ni, G] = muta(individuo, E1_min, E1_max, E2_min, E2_max, ni_min,
ni_max, G_min, G_max, var_E1, var_E2, var_ni, var_G, canale);
%mutation subfunction
E1=individuo(1, 1);E2=individuo(1, 2);ni=individuo(1, 3);G=individuo(1, 4);
r=rand(1);soglia=.5; vettore_estratti=[1 1 1 1];
n_geni_da_mutare=1+round(3*rand(1));
for i=1:n_geni_da_mutare
 x=1/sum(vettore_estratti);
 a=vettore_estratti(1, 1)*x; b=a+vettore_estratti(1, 2)*x;
 c=b+vettore_estratti(1, 3)*x; d=c+vettore_estratti(1, 4)*x; y=rand(1);
 if y<=a
  dE1=(-1+2*rand(1))*var_E1
  E1=individuo(1, 1)+dE1;
 if E1<E1_min & r>soglia
   E1=E1_min; end
 if E1>E1_max & r>soglia
   E1=E1_max; end
  vettore_estratti(1, 1)=0;
 elseif a<y & y<=b
  dE2=(-1+2*rand(1))*var_E2
  E2=individuo(1, 2)+dE2;
 if E2<E2_min & r>soglia
   E2=E2_min; end
 if E2>E2_max & r>soglia
```

168

```
   E2=E2_max; end
  vettore_estratti(1, 2)=0;
 elseif b<y & y<=c
  dni=(-1+2*rand(1))*var_ni
  ni=individuo(1, 3)+dni;
 if ni<ni_min & r>soglia
   ni=ni_min;  end
 if ni>ni_max & r>soglia
   ni=ni_max;  end
  vettore_estratti(1, 3)=0;
 elseif c<y & y<=d
  dG=(-1+2*rand(1))*var_G
  G=individuo(1, 4)+dG;
 if G<G_min & r>soglia
   G=G_min;  end
 if G>G_max & r>soglia
   G=G_max;  end
  vettore_estratti(1, 4)=0;
 end
end
E1=E1*1000;E1=abs(round(E1)/1000); E2=E2*1000;E2=abs(round(E2)/1000);
ni=abs(round(ni*1000)/1000); G=G*1000;G=abs(round(G)/1000);
fileName=['C:\SUPPORT\ANALISI', int2str(canale), '\materiale', int2str(canale), '.bdf'];
matcard_2(fileName, E1, E2, ni, G);
fileName2=['erase /q /a:a ', 'C:\SUPPORT\ANALISI', int2str(canale), '\SIMULAZIONE\', '*.*'];
dos(fileName2);
fileName3=['C:\SUPPORT\ANALISI', int2str(canale), '\nastran.bat >null'];
dos(fileName3);


function[indici] = index_selection(Pop_matr, indici_processati)
%parents index selection for crossover
int=[0.5 0.5];
 while int
  p=rand(1);
  if p<=0.5
   a=1+(round((size(Pop_matr, 1))/3)-1)*rand(1); indice_a=round(a);
  elseif p>0.5 & p<=0.8
   a=(1+round((size(Pop_matr,1))/3))+(size(Pop_matr,1)-round((2*size(Pop_matr,1))/3)-
1)*rand(1);
   indice_a=round(a);
  else
   a=(round((2*size(Pop_matr,1))/3))+(size(Pop_matr,1)-round((2*size(Pop_matr, 1))/3))*rand(1);
   indice_a=round(a);
  end
  p1=rand(1);
  if p1<=0.5
   b=1+(round((size(Pop_matr, 1))/3)-1)*rand(1); indice_b=round(b);
  elseif p1>0.5 & p1<=0.8
   b=(1+round((size(Pop_matr,1))/3))+(size(Pop_matr,1)-round((2*size(Pop_matr,1))/3)-
1)*rand(1);
   indice_b=round(b);
  else
   b=(round((2*size(Pop_matr,1))/3))+(size(Pop_matr,1)-round((2*size(Pop_matr,1))/3))*rand(1);
   indice_b=round(b);
  end
  if indice_a==indice_b
   if indice_a >=2, indice_b=indice_a-1;
    else indice_b=indice_a+1; end
  end
  int=intersect(indici_processati, [indice_a, indice_b], 'rows');
 end
```

```
indici=[indice_a, indice_b];
```

function [mnew, snew] = Media_new(Pop, costante, mp, sp);
% average and standard deviation evaluation for ARGA implementation
```
dimPop=size(Pop, 1)
sample=Pop(1:dimPop/2, :);
msample=mean(sample(:, costante));
ssample=std(sample(:, costante));
mnew=mp+.5*(msample-mp);
snew=abs(sp+.5*(ssample-sp));
```

Batch file *"Nastan.bat"*:
```
c:\msc\bin\nastranw.exe jid=support\laminato_simmetrico.dat out=support\SIMULAZIONE
```

In order to use the ARGA in the dynamic characterization the "crea_individuo" has been modified while, in order to read the natural frequencies from the Nastran output file, the "get_frequency" function has been developed. In the following the code of the two procedure used are reported.

function [individuo] = crea_individuo(vettore_analisi, canale, esatti)
%read the results of the FEA in "canale" folder and evaluate the fitness
```
fileName=['C:\SUPPORT\ANALISI', int2str(canale), '\SIMULAZIONE\Laminato_simmetrico',
int2str(canale), '.f06'];
[Numerical_Freq] = get_frequency (fileName);
val =sqrt(sum(((Numerical _Freq-esatti)./ esatti).^2)); % fitness evaluation
E1p=vettore_analisi(2);
E2p=vettore_analisi(3);
nip=vettore_analisi(4);
Gp=vettore_analisi(5);
load('costanti')
perc_E1=(E1p-E1)/E1;
perc_E2=(E2p-E2)/E2;
perc_ni=(nip-ni)/ni;
perc_G=(Gp-G)/G;
individuo=[E1p E2p nip Gp val perc_E1 perc_E2 perc_ni perc_G vettore_analisi(6)
vettore_analisi(7) vettore_analisi(8)];
```

function [v_freq]=get_frequency(fileName)
% read frequencies from "fileName" Output file.
```
freq=4;
v_freq=zeros(freq,1);
fid=fopen(fileName,'r');
stop=1;  indice=1;
while (feof(fid)==0&stop)
    tline=fgetl(fid);
    if strcmp(tline,'     MODE     EXTRACTION     EIGENVALUE     RADIANS
CYCLES     GENERALIZED     GENERALIZED')
        tline=fgetl(fid);
        for i=1:freq%3
            tline=fgetl(fid);
          r=parse(tline);
          t=[r(5,1) r(5,2) r(5,3) r(5,4) r(5,5) r(5,6) r(5,7) r(5,8) r(5,9) r(5,10) r(5,11) r(5,12)];
           freq=str2double(t);
           v_freq(indice,1)=freq;
          indice=indice+1;
        end
        break
```

```
    end

end
fclose('all');
```

APPENDIX C: INTERPOLATION PROCEDURE

In order to assess the direct procedure for determining the elastic properties of isotropic rectangular plates an interpolation tables function has been carried out. The code makes use of calibrated tables to carry out the Young's modulus and Poisson's ratio by the definition of the aspect ratio (*a/b*), the mass, the thickness and the frequencies of the rectangular plates. In order to have an automatic characterization procedure, the following function has been used inside the Matlab code showed in Appendix A. In this way, it is possible to have a tool to characterise the rectangular samples in a very fast way.

```
function [E1_1, E1_2, E1_3, E1_4, E2_1, E2_2, E2_3, E2_4, E3_1, E3_2, E3_3, E3_4, ni1, ni2,
ni3, ErrorVector, ratio_vector] = calcoloCostanti(f1, f2, f3, f4, mass, thickness, width, ab)
ErrorVector=[1 1 1]; %it is used to verify the frequency ratio
ni_rif=0.32;  %it is used in the plates with a/b ratio equal to 1.5 or 2.0
load('tabelle.mat'); %load the tables obtained by means of FEA calculations
switch ab
  case 1,      A_origin=ab_1;   'ab= 1'
  case 1.5,    A_origin=ab_1_5; 'ab= 1.5'
  case 2,      A_origin=ab_2;   'ab= 2'
  case 2.5,    A_origin=ab_2_5; 'ab= 2.5'
  case 1.4973, A_origin=A_n2;   'piastra N2'
  case 1.9924, A_origin=A_n3;   'piastra N3'
  case 2.4709, A_origin=A_n4;   'piastra N4'
  case 1.4934, A_origin=A_n6;   'piastra N6'
  case 1.9852, A_origin=A_n7;   'piastra N7'
  case 2.4654, A_origin=A_n8;   'piastra N8'
end
vet_freq=[f1,f2,f3,f4]';
A=A_origin;
%%%%%%definition of the suitable frequency ratios %%%%%
%%% ab=1
if (ab>0.95 & ab<1.05);
   ratio_vector=[3,1,3,2,4,3]';ordine_lambda_freq=[1,2,3,4];
   segno_6=+1; segno_7=+1;segno_8=-1;
end
%%% ab=1.5
if (ab<1.6 & ab>1.4 );
   segno_6=+1; segno_7=-1;   segno_8=+1;
   if  ni_rif<0.12
      ratio_vector=[3,1,4,1,3,2]';
      ordine_lambda_freq=[1,2,3,4];
   else
      ratio_vector=[4,2,3,2,4,1]';
      ordine_lambda_freq=[2,1,4,3];
```

```
      end
end
%%%%  ab=2
if (ab<2.2 & ab>1.8 );
    segno_6=-1; segno_7=-1;   segno_8=+1;
    if  ni_rif<0.23
       ratio_vector=[2,1,4,1,3,2]';
        ordine_lambda_freq=[1,2,3,4];
    else
       ratio_vector=[2,1,3,1,4,2]';
       ordine_lambda_freq=[1,2,4,3];
    end
end
%%%% ab=2.5
if (ab>2.3 & ab<2.7);
    ratio_vector=[2,1,4,1,3,2]'; ordine_lambda_freq=[1,2,3,4];
    segno_6=-1; segno_7=-1;   segno_8=+1;
end
%%%%%%%%%%%%%%%%%%%%%%%%%%%%%%%%%%%%%%%%%%%%%%%
fr1_1=vet_freq(ratio_vector(1));  fr1_2=vet_freq(ratio_vector(2));
fr2_1=vet_freq(ratio_vector(3));  fr2_2=vet_freq(ratio_vector(4));
fr3_1=vet_freq(ratio_vector(5));  fr3_2=vet_freq(ratio_vector(6));
KnownValue1=fr1_1/fr1_2;
KnownValue2=fr2_1/fr2_2;
KnownValue3=fr3_1/fr3_2;  %1.0607
%%%%%% find Poisson's ratio (from the first frequency ratio) %%%%%%%%%%
A=A_origin;
ColNota=6; ColIncognita=1; KnownValue=KnownValue1;
if KnownValue>max(A(:,ColNota)) | KnownValue<min(A(:,ColNota));
   ErrorVector(1,1)=0;('range 1 Superato'),
   KnownValue=mean([max(A(:,ColNota)),min(A(:,ColNota))]);
end
ia=find( segno_6*A(:,ColNota)>segno_6*KnownValue );ia=ia(1,1);
%%%interpolation to find  v_hk from f_hk
x1=A(ia,ColNota); y1=A(ia,ColIncognita); x2=A(ia-1,ColNota);
y2=A(ia-1,ColIncognita); x=KnownValue;    y=(y1-y2)/(x2-x1)*(x2-x)+y2;
ni1=y;
%%%find E_h and E_k
%%find L_1 by interpolation
ColNota=1; ColIncognita=(find(ordine_lambda_freq==1))+1; KnownValue=ni1;
x1=A(ia,ColNota); y1=A(ia,ColIncognita); x2=A(ia-1,ColNota);
y2=A(ia-1,ColIncognita); x=KnownValue;    y=(y1-y2)/(x2-x1)*(x2-x)+y2;
L1=y;
E1_1=48/pi^2*(f1/L1)^2*(mass*width^2*(1-ni1^2))/thickness^3*1e-9*ab;
%%find L_2 by interpolation
ColNota=1; ColIncognita=(find(ordine_lambda_freq==2))+1; KnownValue=ni1;
x1=A(ia,ColNota); y1=A(ia,ColIncognita); x2=A(ia-1,ColNota);
y2=A(ia-1,ColIncognita); x=KnownValue;    y=(y1-y2)/(x2-x1)*(x2-x)+y2;
L2=y;
E1_2=48/pi^2*(f2/L2)^2*(mass*width^2*(1-ni1^2))/thickness^3*1e-9*ab;
%%find L_3 by interpolation
ColNota=1; ColIncognita=(find(ordine_lambda_freq==3))+1; KnownValue=ni1;
x1=A(ia,ColNota); y1=A(ia,ColIncognita); x2=A(ia-1,ColNota);
y2=A(ia-1,ColIncognita); x=KnownValue;    y=(y1-y2)/(x2-x1)*(x2-x)+y2;
L3=y;
E1_3=48/pi^2*(f3/L3)^2*(mass*width^2*(1-ni1^2))/thickness^3*1e-9*ab;
%%find L_4 by interpolation
ColNota=1; ColIncognita=(find(ordine_lambda_freq==4))+1; KnownValue=ni1;
x1=A(ia,ColNota); y1=A(ia,ColIncognita); x2=A(ia-1,ColNota);
y2=A(ia-1,ColIncognita); x=KnownValue;    y=(y1-y2)/(x2-x1)*(x2-x)+y2;
L4=y;
```

173

```
E1_4=48/pi^2*(f4/L4)^2*(mass*width^2*(1-ni1^2))/thickness^3*1e-9*ab;
```
%%%%% find Poisson's ratio (from the second frequency ratio) %%%%%%%%%
```
ColNota=7; ColIncognita=1; KnownValue=KnownValue2;
if KnownValue>max(A(:,ColNota)) | KnownValue<min(A(:,ColNota));
   ErrorVector(1,2)=0; ('range 2 Superato'),
   KnownValue=mean([max(A(:,ColNota)),min(A(:,ColNota))]);
end
ia=find( segno_7*A(:,ColNota)>segno_7*KnownValue ); ia=ia(1,1);
```
%%%interpolation to find v_{ij} from f_{ij}
```
x1=A(ia,ColNota); y1=A(ia,ColIncognita); x2=A(ia-1,ColNota);
y2=A(ia-1,ColIncognita); x=KnownValue;    y=(y1-y2)/(x2-x1)*(x2-x)+y2;
ni2=y;
```
%%%find E_i and E_j
```
ni_new=ni2;
```
%find L1 by interpolation
```
ColNota=1; ColIncognita=(find(ordine_lambda_freq==1))+1; KnownValue=ni_new;
x1=A(ia,ColNota); y1=A(ia,ColIncognita); x2=A(ia-1,ColNota);
y2=A(ia-1,ColIncognita); x=KnownValue;    y=(y1-y2)/(x2-x1)*(x2-x)+y2;
L1=y;
E2_1=48/pi^2*(f1/L1)^2*(mass*width^2*(1-ni_new^2))/thickness^3*1e-9*ab;
```
%%find L_2 by interpolation
```
ColNota=1; ColIncognita=(find(ordine_lambda_freq==2))+1; KnownValue=ni_new;
x1=A(ia,ColNota); y1=A(ia,ColIncognita); x2=A(ia-1,ColNota);
y2=A(ia-1,ColIncognita); x=KnownValue;    y=(y1-y2)/(x2-x1)*(x2-x)+y2;
L2=y;
E2_2=48/pi^2*(f2/L2)^2*(mass*width^2*(1-ni_new^2))/thickness^3*1e-9*ab;
```
%%find L_3 by interpolation
```
ColNota=1; ColIncognita=(find(ordine_lambda_freq==3))+1; KnownValue=ni_new;
x1=A(ia,ColNota); y1=A(ia,ColIncognita); x2=A(ia-1,ColNota);
y2=A(ia-1,ColIncognita); x=KnownValue;    y=(y1-y2)/(x2-x1)*(x2-x)+y2;
L3=y;
E2_3=48/pi^2*(f3/L3)^2*(mass*width^2*(1-ni_new^2))/thickness^3*1e-9*ab;
```
%%find L_4 by interpolation
```
ColNota=1; ColIncognita=(find(ordine_lambda_freq==4))+1; KnownValue=ni_new;
x1=A(ia,ColNota); y1=A(ia,ColIncognita); x2=A(ia-1,ColNota);
y2=A(ia-1,ColIncognita); x=KnownValue;    y=(y1-y2)/(x2-x1)*(x2-x)+y2;
L4=y;
E2_4=48/pi^2*(f4/L4)^2*(mass*width^2*(1-ni_new^2))/thickness^3*1e-9*ab;
```
%%%%% find Poisson's ratio (from the third frequency ratio) %%%%%%%%%
```
A=A_origin;
ColNota=8; ColIncognita=1; KnownValue=KnownValue3;
if KnownValue>max(A(:,ColNota)) | KnownValue<min(A(:,ColNota))
   ErrorVector(1,3)=0; ('range 3 Superato')
   KnownValue=mean([max(A(:,ColNota)),min(A(:,ColNota))]);
end
ia=find( segno_8*A(:,ColNota)>segno_8*KnownValue );ia=ia(1,1);
```
%%%interpolation to find v_{jk} from f_{jk}
```
x1=A(ia,ColNota); y1=A(ia,ColIncognita); x2=A(ia-1,ColNota);
y2=A(ia-1,ColIncognita); x=KnownValue; y=(y1-y2)/(x2-x1)*(x2-x)+y2;
ni3=y;
```
%%%Find E_j e E_k
```
ni_new=ni3;
```
%find L_1 by interpolation
```
ColNota=1; ColIncognita=(find(ordine_lambda_freq==1))+1; KnownValue=ni_new;
x1=A(ia,ColNota); y1=A(ia,ColIncognita); x2=A(ia-1,ColNota);
y2=A(ia-1,ColIncognita); x=KnownValue;    y=(y1-y2)/(x2-x1)*(x2-x)+y2;
L1=y;
E3_1=48/pi^2*(f1/L1)^2*(mass*width^2*(1-ni_new^2))/thickness^3*1e-9*ab;
```
%find L_2 by interpolation
```
ColNota=1; ColIncognita=(find(ordine_lambda_freq==2))+1; KnownValue=ni_new;
x1=A(ia,ColNota); y1=A(ia,ColIncognita); x2=A(ia-1,ColNota);
```

```
y2=A(ia-1,ColIncognita); x=KnownValue;    y=(y1-y2)/(x2-x1)*(x2-x)+y2;
L2=y;
E3_2=48/pi^2*(f2/L2)^2*(mass*width^2*(1-ni_new^2))/thickness^3*1e-9*ab;
```
%find L₃ by interpolation
```
ColNota=1; ColIncognita=(find(ordine_lambda_freq==3))+1; KnownValue=ni_new;
x1=A(ia,ColNota); y1=A(ia,ColIncognita); x2=A(ia-1,ColNota);
y2=A(ia-1,ColIncognita); x=KnownValue;    y=(y1-y2)/(x2-x1)*(x2-x)+y2;
L3=y;
E3_3=48/pi^2*(f3/L3)^2*(mass*width^2*(1-ni_new^2))/thickness^3*1e-9*ab;
```
%find L₄ by interpolation
```
ColNota=1; ColIncognita=(find(ordine_lambda_freq==4))+1; KnownValue=ni_new;
x1=A(ia,ColNota); y1=A(ia,ColIncognita); x2=A(ia-1,ColNota);
y2=A(ia-1,ColIncognita); x=KnownValue;    y=(y1-y2)/(x2-x1)*(x2-x)+y2;
L4=y;
E3_4=48/pi^2*(f4/L4)^2*(mass*width^2*(1-ni_new^2))/thickness^3*1e-9*ab;
```